The Dissertation Committee for IL NAM KIM Certifies that this is the approved version of the following dissertation:

OCEAN BIOGEOCHEMISTRY IN THE NORTHERN GULF OF MEXICO, THE EAST/JAPAN SEA, AND THE SOUTH PACIFIC WITH A FOCUS ON DENITRIFICATION

Committee:

Dong-Ha Min, Supervisor

Alison M. Macdonald

James W. McClelland

Wayne S. Gardner

Zhanfei Liu

OCEAN BIOGEOCHEMISTRY IN THE NORTHERN GULF OF MEXICO, THE EAST/JAPAN SEA, AND THE SOUTH PACIFIC WITH A FOCUS ON DENITRIFICATION

by

IL NAM KIM, B.S.; M.S.

Dissertation

Presented to the Faculty of the Graduate School of

The University of Texas at Austin

in Partial Fulfillment

of the Requirements

for the Degree of

Doctor of Philosophy

The University of Texas at Austin

May 2012

Dedication

I dedicate this dissertation to my family.

Acknowledgements

I would sincerely like to thank Dr. Dong-Ha Min (my dissertation advisor), Drs. Alison M. Macdonald, James W. McClelland, Wayne S. Gardner, and Zhanfei Liu (my committee members) for their valuable comments and time on this dissertation. I would like to thank Dr. Hedy Edmonds, as early committee member, for her valuable comments. Thanks to all the people who contributed to the Texas-Louisiana shelf-wide cruise program (for Chapter 2), the CREAMS II program (for Chapter 3), and the WOCE, BEAGLE, CO_2/CLIVAR Repeat Hydrography P06 programs (for Chapter 4). I would sincerely like to thank all UTMSI people (graduate students, staffs, and professors) for their help in many ways. Special thanks to Prof. Joan Holt for many thoughtful considerations. This dissertation work was supported by E.J. Lund Research Scholarship and UT Austin Graduate Student Continuing Fellowship. Finally, I would especially like to thank my family for their endless support.

OCEAN BIOGEOCHEMISTRY IN THE NORTHERN GULF OF MEXICO, THE EAST/JAPAN SEA, AND THE SOUTH PACIFIC WITH A FOCUS ON DENITRIFICATION

IL NAM KIM, Ph.D.

The University of Texas at Austin, 2012

Supervisor: Dong-Ha Min

Ocean nitrogen fixation and denitrification are crucial nitrogen source and sink mechanisms for the global ocean environment. While recent studies have reported that oceanic denitrification has increased over the last few decades, others have suggested that global ocean nitrogen fixation rates have been underestimated, and still others that anthropogenic perturbations have altered the global nitrogen cycle. This implies that the current estimates of the oceanic nitrogen inventory are incomplete and they need to be revised with more information. In addition, current denitrification estimates need to be reexamined due to their large associated uncertainties. Thus, I have conducted research estimating denitrification rates in three different locations: the northern Gulf of Mexico (GOM), the East/Japan Sea (EJS), and the South Pacific: from coastal to marginal to open ocean scale in different oceanographic conditions. Denitrification rates in the bottom layer (including bottom waters+sediments) at the shallow and often hypoxic northern GOM ranged from 103-544 μmol N m^{-2} d^{-1} (=1.4 to 7.4 Gg N mon^{-1} with area=$3.24x10^{10}m^2$), and were controlled not only by biogeochemical factors (i.e. organic matter supply and remineralization), but also by physical factors (i.e. stratification and relative contributions from different water masses). Despite high dissolved oxygen

concentrations, the significant decrease in nitrate concentrations below the expected levels, low N/P ratio (<12.4), and deep nitrite peak in the bottom layer indicate a presence of denitrification in EJS, confined at the Tatar Strait and the Ulleung Basin areas. The estimated denitrification rates range from 0.3 to 33.2 μmol N m^{-2} d^{-1}, and was comparable to the directly measured denitrification rates from sediment samples. The high-quality repeat hydrographic datasets observed at 32°S of the South Pacific Ocean offer an opportunity to estimate water column denitrification rates on a basin-scale in the open ocean away from the Eastern Tropical Pacific oxygen minimum zones. The mean water column denitrification rates in the oxygen minimum layer of P06 line (32°S) were estimated to range between 7.1 and 18.5 μmol N m^{-2} d^{-1}. The results imply that, although very small at any particular site, once integrated over a basin-scale, the open ocean water column denitrification can be a significant component of the oceanic nitrogen budget. Denitrification is subject to seasonal, decadal and possibly climate scale variations. While it is commonly estimated at the oxygen minimum zones or sediments, denitrification is not merely confined to such regions only, and small amounts of denitrification occur in other oceanic parts. Once integrated, it may be quantitatively significant for the world's oceans. Denitrification is playing a significant role in local, regional, and global ocean scales. In the future, we need to consider variability of denitrification in coastal regions, and to investigate denitrification in unexpected and unexplored regions, in order to improve our knowledge on global oceanic mass balance.

Table of Contents

List of Tables

List of Figures

Chapter 1: Introduction

Nitrogen (N) is an essential element for the growth of primary producers in the ocean environments. Excessive input of nitrogen into coastal regions frequently drives harmful algal blooms resulting from coastal eutrophication (Diaz and Rosenberg, 2008), while an insufficient supply of nitrogen, as a limiting-nutrient, decreases primary production (Falkowski, 1997). Complicated by its relatively short residence time and complex biogeochemical cycles (McElroy, 1983), knowledge of the availability of nitrogen is important in determining the extent of primary production in the ocean environments. In addition, nitrogen availability has been linked indirectly to glacial-interglacial climate variability by controlling biological pump (Deutsch et al., 2004; Gruber, 2008). For all these reasons, establishing the nitrogen mass balance of the global oceans in terms of sources and sinks has been a long-term scientific goal (Gruber and Sarmiento, 1997; Codispoti et al., 2001; Deutsch et al., 2001; Karl et al., 2002; Codispoti, 2007; Deutsch et al., 2007).

A schematic budget of marine nitrogen cycle is shown in Fig. 1.1 (Gruber, 2008). Current estimates indicate that the sum of sinks in the nitrogen budgets is greater than the sum of the sources for the oceans (Gruber and Sarmiento, 1997; Codispoti et al., 2001). However, many questions still remain (Gruber, 2008). Denitrification ($NO_3^- \rightarrow NO_2^- \rightarrow N_2O/N_2$) is the most significant mechanism responsible for nitrogen loss in the ocean environments, even though recent measurements indicate that anaerobic ammonium oxidation (Anammox; $NO_2^- + NH_4^+ \rightarrow N_2O/N_2$) is also a quantitatively important sink (Brandes et al., 2007). The study of denitrification has been conducted over several decades, but our understanding continues to be refined. Various methods have been used to estimate denitrification rates, for instance, sediment incubation systems measuring N_2 (or N_2O) gas, ^{15}N isotope techniques, and numerous modeling approaches (Brandes et al., 2007). Although each method has advantages and disadvantages, since no extensive ocean-scale actual measurements are currently available, only modeling studies permit us

to estimate denitrification over large spatial scales and to project it for the future as well as the past.

Denitrification is generally classified as water column and benthic denitrification, depending upon the nitrate source driving the denitrification process. Water column denitrification is driven by nitrate remineralized in the water column, usually under very low dissolved oxygen conditions. Benthic denitrification occurs in the sediment using nitrate derived from both sediments and overlying waters (Fig. 1.2).

The hydrographic properties in the northern Gulf of Mexico (GOM), a shallow coastal ocean on the inner continental shelf, have been observed regularly over the last 20 years. The hypoxic zone ($O_2 \leq 2$ mg L^{-1}) has increased in size (~1000 km^2 during 1985-1992 to ~15000 km^2 during 1993-2000) remarkably due to the increased anthropogenic influences (Rabalais et al., 2002). Thus, the northern GOM provides a great opportunity to model temporal variations in denitrification rates using an analysis with the time-series data. Such studies performed today may be used as a priori reference information for comparison after catastrophic events, such as the post-event environmental assessment of the "Deep Water Horizon" oil spill accident in May 2010.

The East/Japan Sea (EJS) is a semi-enclosed marginal sea in the mid latitude of the western North Pacific Ocean, which exhibits many dynamics resembling the open oceans including deep-water formation, eddies, subpolar front, and gyre-like circulations (Talley et al., 2006). Denitrification has not been considered as a significant process in the EJS, because EJS is well oxygenated throughout the water column (>190 μmol kg^{-1}). The concept of conventional denitrification may conflict with the EJS's environment. The main causes of the lower N/P ratio in EJS despite the high oxygen environment are yet to be understood in EJS. However, indirect and direct evidence supporting the possibility of denitrification in the EJS has grown from recent observations (Talley et al., 2001; Yanagi, 2002; Lee et al., 2007; Tischenko et al., 2007; Jeong et al., 2009; Kim et al., 2010). Therefore, analyzing this issue qualitatively and quantitatively is important to understand the nitrogen cycle in EJS.

The South Pacific Ocean is an important channel to supply dissolved oxygen (i.e. recently ventilated water parcels) into the deep/bottom layer of the North Pacific Ocean, because no deep water formation occurs in the North Pacific Ocean (Wijffels et al., 2001). The magnitude of denitrification in the open oceans is expected to be significantly lower than that at the oxygen minimum zones (OMZs) in the eastern tropical margins. For this reason, the denitrification process has not generally been quantified for the open ocean basin-scale except for the OMZs. Recently, potential magnitude of denitrification in the open ocean was estimated using the N^* method (Gruber and Sarmiento, 1997), but specific denitrification rates were not estimated. So, quantitative denitrification rates in a large scale are still poorly understood. Macroscopic aggregates of detritus (a.k.a. marine snow) are ubiquitous in the pelagic water column in the world oceans (Alldredge and Silver, 1988), although their density is quite low in open oceans. Marine snows may form reducing microzones within detrital aggregates despite highly oxygenated water column (Alldredge and Cohen, 1987; Shanks and Reeder, 1993; Ploug et al., 1997; Wolgast et al., 1998). It is speculated that the reducing microzone environments may provide a platform for open-ocean scale water column denitrification. Recent studies reported that denitrification has increased over the last few decades (Codispoti, 2007; Gruber, 2008; Deutsch and Weber, 2012). To gain accurate nitrogen budgets between sinks and source in the future, more information on denitrification in the open ocean is essential.

In the currently study, I used hydrographic datasets obtained from various ocean cruises to estimate denitrification rates. The hydrographic properties are determined not only by physical mixing, but also by biogeochemical processes (Anderson and Sarmiento, 1994). I utilized the extended Optimum Multi-Parameter (OMP) analysis as a main data analysis tool to study such conditions quantitatively. Hupe and Karstensen, (2000) applied the extended OMP analysis to estimate physical mixing and biogeochemical changes in the Arabian Sea, and demonstrated that it can quantify the amount of denitrification with the hydrographic data (Fig. 1.3). Although this technique has limitation in the number of source water types for the analysis can utilize and needs accurate source water type definitions, this technique is the so far most appropriate way

for my dissertation study investigating various spatial scales from coastal to marginal to open ocean with the hydrographic data. To estimate rates based on the denitrification amount calculated by the extended OMP analysis, I would need additional time information. I utilized mean study period (the northern GOM), relative age (the EJS), and transit time distribution (the South Pacific Ocean) for the rate calculations.

The main purpose of this dissertation is to estimate denitrification rates at three different study regions (the northern GOM, the EJS, and the South Pacific) with the extended OMP analysis illustrating respective spatial scales from coastal to marginal to open oceans. The dissertation is composed of five chapters: Introduction (Ch. 1), denitrification in the northern GOM (Ch. 2), denitrification in EJS (Ch. 3), denitrification in the South Pacific Ocean (Ch. 4), and Summary (Ch. 5). Chapter 2 addresses variability in summertime denitrification rates in the northern GOM. Through intensive profile analysis, Chapter 3 provides evidence for denitrification in EJS, despite the high dissolved oxygen environment, and quantifies the denitrification rates. Chapter 4 estimates mean water column denitrification rates in the subtropical South Pacific (~32°S) outside the Eastern Tropical Pacific OMZs. Chapter 5 summarizes the key findings of Chapters 2-4 and discusses their implications for the study of the global nitrogen inventory in the future.

REFERENCES

Alldredge, A.L., and M.W. Silver, 1988. Characteristics, dynamics and significance of marine snow. Progress in Oceanography, 20, 41-82.

Alldredge, A.L., and Y. Cohen, 1987. Can microscale chemical patches persist in the sea? Microelectrode study of marine snow, fecal pellets. Science, 235, 689-691.

Anderson, L.A., and J.L. Sarmiento, 1994. Redfield ratios of remineralization determined by nutrient data analysis. Global Biogeochemical Cycles, 8(1), 65-80.

Brandes, J.A., A.H. Devol, and C. Deutsch, 2007. New developments in the marine nitrogen cycle. Chemical Reviews, 107, 577-589.

Codispoti, L.A., 2007. An oceanic fixed nitrogen sink exceeding 400 Tg N a^{-1} vs the concept of homeostasis in the fixed-nitrogen inventory. Biogeosciences, 4, 233-253.

Codispoti, L.A., J.A. Brandes, J.P. Christensen, A.H. Devol, S.W.A. Naqvi, H.W. Paerl, and T. Yoshinari, 2001. The oceanic fixed nitrogen and nitrous oxide budgets: Moving targets as we enter the anthropocene?. Scientia Marina, 65, 85-105.

Deutsch C., N. Gruber, R.M. Key, and J. Sarmiento, 2001. Denitrification and N_2 fixation in the Pacific Ocean. Global Biogeochemical Cycles, 15, 483-506.

Deutsch, C., and T. Weber, 2012. Nutrient ratios as a tracer and driver of ocean biogeochemistry. The Annual Review of Marine Science, 4, 113-141.

Deutsch, C., D.M. Sigman, R.C. Thunell, A.N. Meckler, and G.H. Haug, 2004. Isotopic constraints on glacial/interglacial changes in the oceanic nitrogen budget. Global Biogeochemical Cycles, 18, GB4012, doi:10.1029/2003GB002189.

Deutsch, C., J.L. Sarmiento, D.M. Sigman, N. Gruber, and J.P. Dunne, 2007. Spatial coupling of nitrogen inputs and losses in the ocean. Nature, 445, 163-167.

Diaz, R.J., and R. Rosenberg, 2008. Spreading dead zones and consequences for marine ecosystems. Science, 321, 926-929.

Falkowski, P.G., 1997. Evolution of the nitrogen cycle and its influence on the biological sequestration of CO_2 in the ocean, Nature, 272-275.

Gruber, N., 2008. The marine nitrogen cycle: Overview of distributions and processes, In: Nitrogen in the marine environment, 2nd edition, edited by D.G. Capone, D.A. Bronk, M.R. Mulholland, and E.J. Carpenter, Elsevier, Amsterdam, 1-50.

Gruber, N., and J.L. Sarmiento, 1997. Global patterns of marine nitrogen fixation and denitrification, Global Biogeochemical Cycles, 11(2), 235-266.

Hupe, A., and J. Karstensen, 2000. Redfield stoichiometry in Arabian Sea subsurface waters. Global Biogeochemical Cycles, 14(1), 357-372.

Jeong, J.H., D.S. Kim, T.H. Lee, and S. An, 2009. High remineralization and denitrification activity in the shelf sediments of Dok Island, East Sea. The Sea, 14(2), 80-89.

Karl, D., A. Michaels, B. Bergman, D. Capone, E. Carpenter, R. Letelier, F. Lipschultz, H. Paerl, D. Sigman, and L. Stal, 2002. Dinitrogen fixation in the world's oceans. Biogeochemistry, 57, 47-98.

Kim, K., K.-R. Kim, D. Min, Y. Volkov, J.-H. Yoon, and M. Takematsu, 2001. Warming and Structural Changes in the East Sea (Japan Sea): A clue to future changes in Global Oceans?. Geophysical Research Letters, 28, 3293-3296.

Kim, T.-H. Y.-W. Lee, and G. Kim, 2010. Hydrographically mediated patterns of photosynthetic pigments in the East/Japan Sea: Low N:P ratios and cyanobacterial dominance. Journal of Marine Systems, 82, 72-79.

Lee, T., I.-N. Kim, D.-J. Kang, and D. Kim, 2007. Implications of deep nitrite in the Ulleung Basin. The Sea, 12(3), 239-243.

McElroy, M.B., 1983. Marine biological controls on atmospheric CO_2 and climate. Nature, 302, 328-329.

Ploug, H., M. Kühl, B. Buchholz-Cleven, B.B. Jørgensen, 1997. Anoxic aggregates-an ephemeral phenomenon in the pelagic environment?. Aquatic Microbial Ecology, 13, 285-294.

Rabalais, N.N., R.E. Turner, and D. Scavia, 2002. Beyond science into policy: Gulf of Mexico hypoxia and the Mississippi River. BioScience, 52(2), 129-142.

Shanks, A.L., and M.L. Reeder, 1993. Reducing microzones and sulfide production in marine snow. Marine Ecology Progress Series, 96, 43-47.

Talley L.D., P.Ya. Tishchenko, G. Mitchell, D.-J. Kang, D.-H. Min, A. Nedashkovskii, D. Masten, and P. Robbins, 2001. Nitrite in a deep, oxygenated environment the Japan/East Sea and Ulleung Basin. CREAMS 2001, Honolulu.

Talley, L.D., D.-H. Min, V.B. Lobanov, V.A. Luchin, V.I. Ponomarev, A.N. Salyuk, A.Y. Shcherbina, P.Y. Tishchenko, and I. Zhabin, 2006. Japan/East Sea water masses and their relation to the sea's circulation, Oceanography, 19(3), 32-49.

Tishchenko, P.Ya., L.D. Talley, V.B. Labanov, A.P. Nedashkovskii, G.Yu. Pavlova, and S.G. Sagalaev, 2007. The influence of geochemical processes in the near-bottom layer on the hydrochemical characteristics of the waters of the Sea of Japan. Oceanology, 47(3), 350-359.

Wijffels, S.E., J.M. Toole, and R. Davis, 2001. Revisiting the South Pacific subtropical circulation: A synthesis of World Ocean Circulation Experiment observations along 32°S. Journal of Geophysical Research, 106, 19481-19513.

Wolgast, D.M., A.F. Carlucci, and J.E. Bauer, 1998. Nitrate respiration associated with detrital aggregates in aerobic bottom waters of the abyssal NE Pacific. Deep-Sea Research II 45, 881-892.

Yanagi, T., 2002. Water, salt, phosphorus and nitrogen budgets of the Japan Sea. Journal of Oceanography, 58, 797-804.

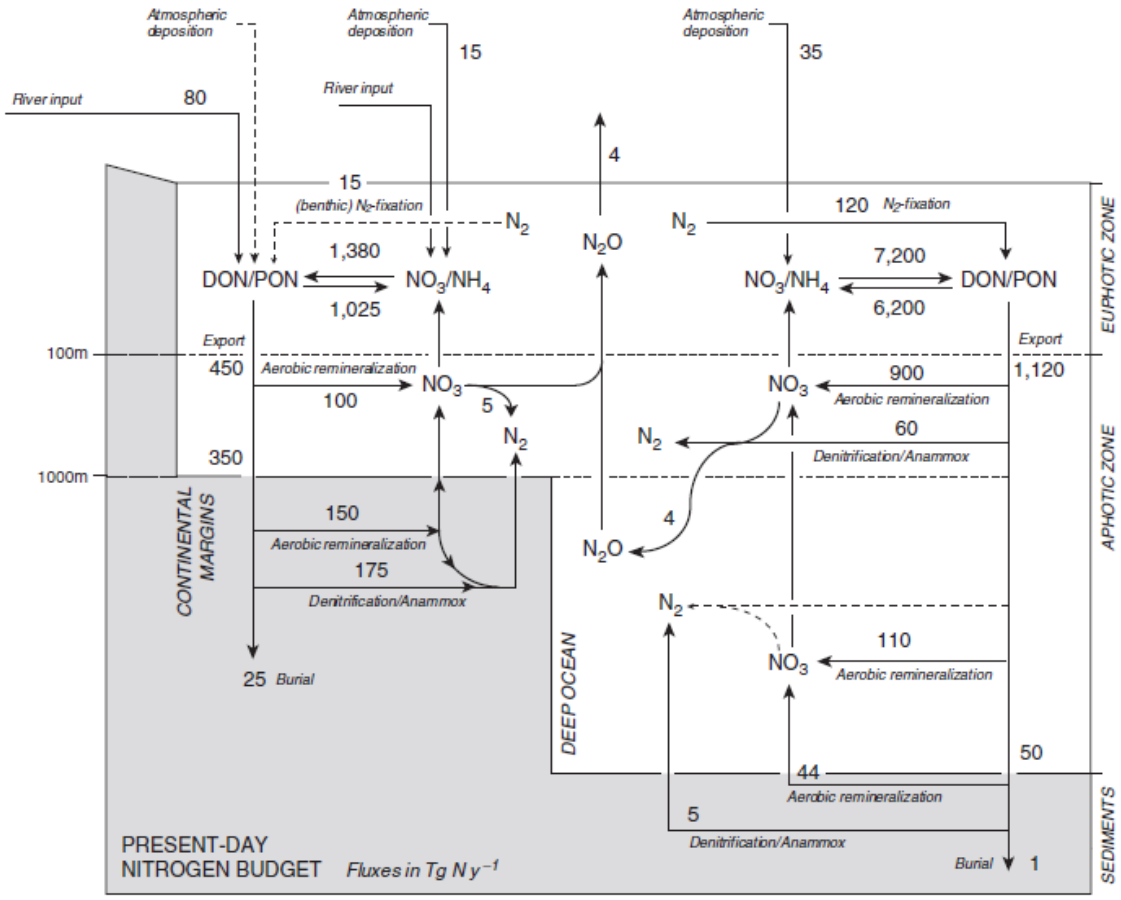

Figure 1.1: A schematic of marine nitrogen cycle with budget (adopted from Fig. 1.14 of Gruber, 2008).

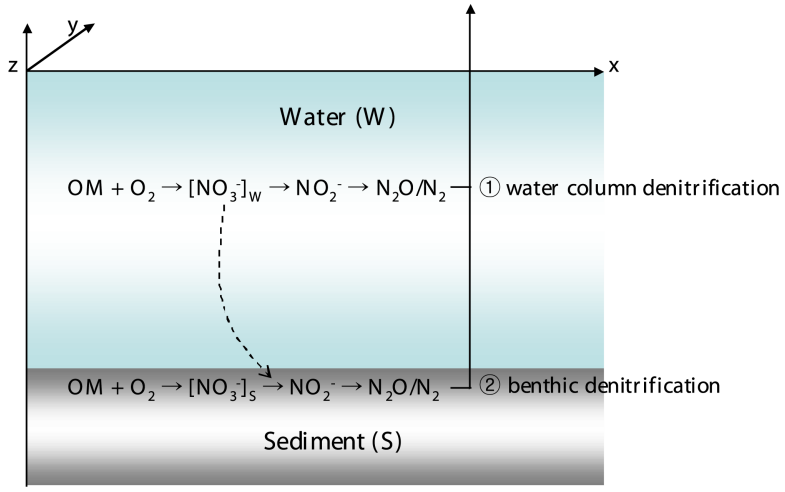

Figure 1.2: General classification of denitrification (water column and benthic) process in the ocean environment. OM- organic matter.

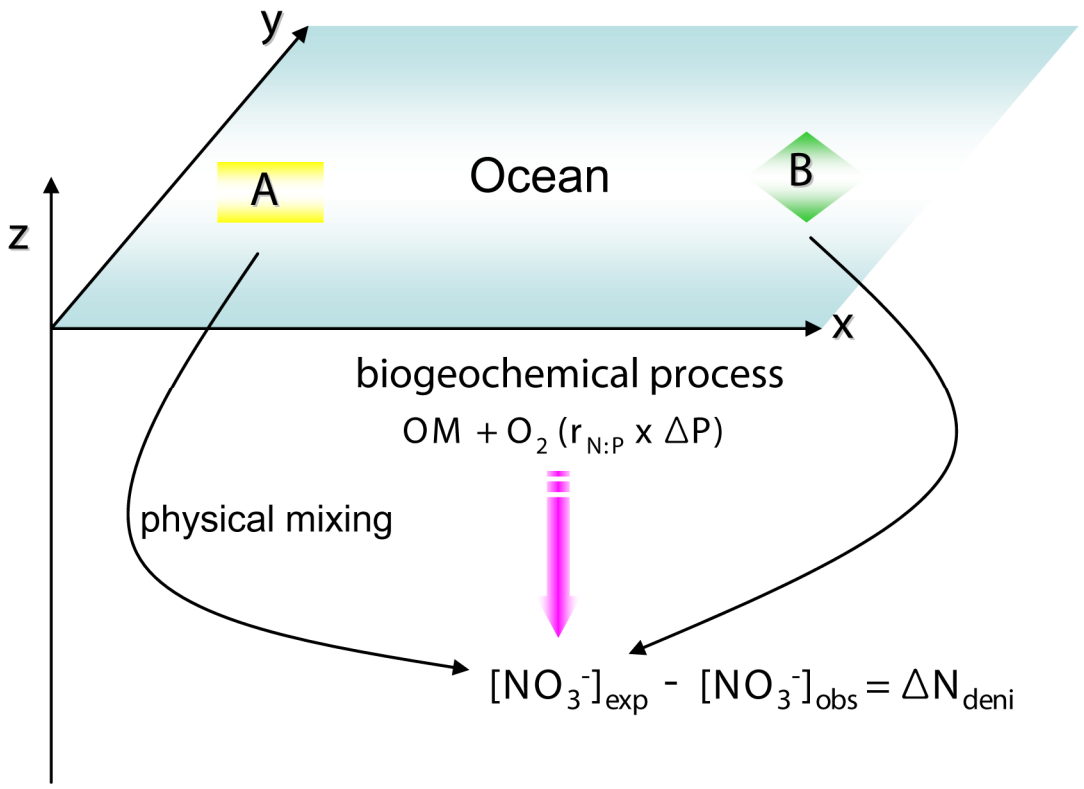

Figure 1.3: Schematic of estimating denitrification from the extended OMP analysis. The amount of denitrification (ΔN_{deni}) is computed from the difference between expected nitrate ($[NO_3^-]_{exp}$) and observed nitrate ($[NO_3^-]_{obs}$). During nitrification, nitrogen loss by N_2O production is occurred. However, this amount is substantially tiny, so I assume that the difference between $[NO_3^-]_{exp}$ and $[NO_3^-]_{obs}$ is explained by denitrification. The estimated nitrate is determined by physical mixing (i.e. advected nitrate from different water formation regions, such as 'A' and 'B') and biogeochemical processes (i.e. remineralized nitrate by decomposing organic matters (OM) through microbial respirations). The remineralized nitrate can be expressed by the Redfield ratio ($r_{N:P}$) multiplied by remineralized phosphate (ΔP).

Chapter 2: Physical and biogeochemical controls on temporal variability of summertime denitrification rates in the northern Gulf of Mexico

1. INTRODUCTION

The northern Gulf of Mexico (GOM) is known for frequent hypoxic water conditions in the sub-surface coastal waters with very low dissolved oxygen concentration ($O_2 \leq 2$ mg L^{-1} or ~63 µmol L^{-1}) and often referred to as the "Dead Zone". Hypoxia frequently develops during the summertime by combination of high biological production and strong stratification in the coastal waters (Wiseman et al., 1997). The area of the Dead Zone has increased remarkably during recent decades due to increased coastal eutrophication (Rabalais et al., 2002). The recent "Deepwater Horizon" oil spill event that occurred in the northern GOM has raised concern for potential development of more extensive hypoxia in the region. Under such conditions, denitrification could potentially play a more active role in biogeochemical cycles in the northern GOM and it needs to be better quantified. It may also be an important link to N_2O production in the northern GOM for longer-term perspective (Walker et al., 2010).

Denitrification is a dissimilatory process in which bacteria use nitrate as electron acceptor instead of oxygen under low oxygen conditions. Nitrate (NO_3^-) is typically reduced to nitrite (NO_2^-), and then to nitrous oxide and dinitrogen (N_2O and N_2) during the process. In the ocean environment, denitrification is directly related to modern climate change through N_2O production, which is a strong greenhouse gas (Nevison and Holland, 1997; Nevison et al., 2003; Naqvi et al., 2010), and indirectly to glacial-interglacial climate change via regulation of the nitrogen availability in the ocean, which can enhance the biological pump along with iron fertilization (McElroy, 1983; Altabet et al., 1995; Ganeshram et al., 1995; Falkowski, 1997; Ganeshram et al., 2000; Ganeshram et al., 2002).

Only a few denitrification studies have been published for this area despite the significance of the process. Denitrification rates in the northern GOM were estimated indirectly from sediment samples at 21-44 µmol N m^{-2} h^{-1} by Gardner et al. (1993) from

the difference between decrease of net organic nitrogen concentration and increase of inorganic nitrogen (NH_4^+, NO_3^-, and NO_2^-) concentrations in July 1990, and estimated directly at 91-462 (149±58-406±55) μmol N m^{-2} h^{-1} from 7 different sediment samples in July 1999 by Childs et al., (2002, 2003). The error in estimates of Childs et al. (2002) was reported in Table 1 of Childs et al. (2003). The results from these 2 groups are significantly different from each other. Considering the generally high level of variability of coastal oceans, it is difficult to determine whether these diverse estimates are at norm or anomalies, without the information on temporal variation.

To address these issues, the main goals of this study are (1) to estimate the denitrification rates in the inner continental shelf area of the northern GOM by using the long-term hydrographic data (1985-2007) and the extended Optimum Multi-Parameter (OMP) analysis, (2) to model the temporal variation of denitrification rates, and (3) to determine probable factors causing temporal variation in denitrification rates in the northern GOM.

2. DATA

Summertime Texas-Louisiana shelf-wide cruise data were obtained from http://www.nodc.noaa.gov (1985-1987, 1991-1993, and 1998-2007 periods) and http://www.aoml.noaa.gov/ocd/necop/ (1994-1997). The selected study area is a broad continental shelf (bottom depth<100m) with two large river systems, the Mississippi and Atchafalaya Rivers (Fig. 2.1). The parameters used for the extended OMP analysis were latitude, longitude, depth, temperature (T), salinity (S), dissolved oxygen (DO), nitrate+nitrite (N), phosphate (P), and silicate (Si). Nutrient measurements were made at only two depths during the original hydrographic surveys: near surface (ca. 1m from surface) and near bottom (ca. 1m from the bottom). The surface and bottom T, S, and DO data are selected at the depths of nutrient measurements to use the data from the same depths in the extended OMP analysis.

3. THE EXTENDED OPTIMUM MULTI-PARAMETER (OMP) ANALYSIS

The magnitudes and changes of ocean properties are determined by physical mixing and biogeochemical processes (Anderson and Sarmiento, 1994). Extended OMP analysis is a useful way to quantify such conditions. The basic OMP analysis was originally developed to analyze physical mixing processes (Tomczak and Large, 1989). Redfield ratios were later added in the calculations to analyze the influences of basic biogeochemical processes, and this version is called the "extended OMP analysis" (Karstensen and Tomczak, 1998). Extended OMP analysis was further improved to estimate the biogeochemical changes in remineralization, denitrification, and carbonate dissolution (Hupe and Karstensen, 2000). The extended OMP analysis is essentially an inverse method based on an over-determined linear system that has copious solutions for the unknown variables (i.e. number of equations is more than number of unknown variables). However, the solutions can be found by a non-negative least squares method (NNLS) (Tomczak and Large, 1989). The matrix structure of the extended OMP analysis used here is expressed as:

$$\underbrace{\begin{vmatrix} T_1 & + \cdots + & T_4 & + & 0 & + & 0 \\ S_1 & + \cdots + & S_4 & + & 0 & + & 0 \\ DO_1 & + \cdots + & DO_4 & - & r_{O2/P} & + & 0 \\ P_1 & + \cdots + & P_4 & + & 1 & + & r_\alpha \\ N_1 & + \cdots + & N_4 & + & r_{N/P} & - & 1 \\ Si_1 & + \cdots + & Si_4 & + & r_{Si/P} & + & 0 \\ 1 & + \cdots + & 1 & + & 0 & + & 0 \end{vmatrix}}_{A} \times \underbrace{\begin{vmatrix} x_1 \\ x_2 \\ x_3 \\ x_4 \\ \Delta P_{remi} \\ \Delta N_{deni} \end{vmatrix}}_{x} - \underbrace{\begin{vmatrix} T_{obs} \\ S_{obs} \\ DO_{obs} \\ P_{obs} \\ N_{obs} \\ Si_{obs} \\ 1 \end{vmatrix}}_{d} = \underbrace{\begin{vmatrix} R_T \\ R_S \\ R_{DO} \\ R_P \\ R_N \\ R_{Si} \\ R_{MC} \end{vmatrix}}_{R} \quad (1)$$

where, the matrix **A** is defined by the physicochemical characteristics of water masses, the Redfield ratios ($r_{O2/P}$, $r_{N/P}$, and $r_{Si/P}$), and r_α (1/104) to estimate the amount of phosphate remineralized by denitrification (Gruber and Sarmiento, 1997; Hupe and Karstensen, 2000), the column **x** is composed of relative mixing ratios of x_i among water masses, the amount of remineralized phosphate (ΔP_{remi}), and the amount of denitrification (ΔN_{deni}), the next column d contains observation data for the physicochemical properties, and the last column **R** represents residuals from the extended OMP calculation for each

parameter. The last row of the matrix consisting of "1" constrains mass conservation among the source water masses ($\sum_{i=1}^{n} x_i = 1$). The computations of the extended OMP analysis are carried out by (1) defining the physicochemical characteristics of source water types (or end-member types) to form the matrix **A**, (2) assigning the Redfield ratios ($r_{N:P:Si:-O2}$) to the matrix **A**, (3) estimating the weights of each parameter, and (4) finding the non-negative solutions for x_i, ΔP_{remi}, and ΔN_{deni} by minimizing the residual. An extended OMP program written in MATLAB^{TM} was used in the analysis (http://www.ldeo.columbia.edu/~jkarsten/omp_std/).

Four different end-members are defined (Table 2.1), and 4 different Redfield ratio cases are considered (Table 2.2). More detailed information on physicochemical characteristics of end-members, assignment of Redfield ratios, weights for each parameter, validation for the extended OMP analysis, and limitations for the extended OMP analysis is described below (Sections 3.1-3.5).

3.1 Physicochemical characteristics of end-members

Temperature and salinity data collected in the Texas-Louisiana shelf region during the July 1985-2007 period, except for July 1988-1990, were used to investigate physical properties of waters on a T-S diagram (Fig. 2.2). Based on the data distribution pattern, three different end-members are assumed to participate in mixing process in the study area: low temperature and high salinity waters, high temperature and high salinity waters, and high temperature and low salinity waters. Geographical locations and temperature and salinity properties based on T-S diagram used to define the physicochemical characteristics of end-members are as follows (Fig. 2.3). Low temperature and high salinity waters are ranged from 18≤T≤19 and 35.2≤S≤37.5 on the T-S diagram. I adopted mean values of physicochemical properties of two stations that satisfy these conditions as characteristics of end-member 1 (Fig. 2.3a). End-member 1 is at salinity maximum (Fig. 2.2). Salinity maximum waters are the Gulf Water (GW; 36.4≤S≤36.5) in the western GOM and the Subtropical Underwater (SUW; S>36.5) in the

eastern GOM (Morrison et al., 1983; Vidal et al., 1994). End-member 1 is geographically close to the GW, but the salinity characteristic (S=36.7) is greater than that of GW. SUW enters the western GOM with the Loop Current (Jochens and DiMarco, 2008). The temperature and density of end-member 1 (T=18.6 and σ_t=26.4) appears similar to those of Eighteen Degree Water (EDW) from the Sargasso Sea, but EDW is distinct with its oxygen maximum (3.6-3.8 ml l^{-1} or 161-170 μmol L^{-1}) and lower salinity at about 36.3 (Morrison and Nowlin, 1977). The water properties of EDW, except for temperature, do not fit those of end-member 1. End-member 1 thus was defined as SUW. High temperature and high salinity waters (29≤T≤30 and 35≤S≤37 on the T-S diagram), end-member 2, are distributed widely in the study area (Fig. 2.3b). The mixture of Mississippi and Atchafalaya discharge waters and inner shelf waters spreads as the Texas-Louisiana Coastal Current (TLCC) (Wiseman and Kelly, 1994; Jarosz and Murray, 2005). TLCC occupies large part of the study area, and flows seasonally along the Texas-Louisiana coast. Thus, it refers to end-member 2 as the Texas-Louisiana Coastal Water (TLCW). Two large rivers contribute fresh surface waters in the study area; the Mississippi River (~70%), and the Atchafalaya River (~30%) (Dagg and Breed, 2003). These two rivers were distinguished by their geographic locations. The nutrient concentrations of the Mississippi River water are substantially higher than those of Atchafalaya River water (Pakulski et al., 2000). The physicochemical characteristics of end-member 3, Atchafalaya Discharge water (ADW), are defined by S≤5 and longitude: west of 91°W. Several stations near the mouth of Atchafalaya River inshore of 20m isobath belong to this group (Fig. 2.3c). Although the physical properties are similar among the selected stations, their chemical properties (N, P, and Si) are distinct. Temperature, salinity, and oxygen characteristics of ADW were defined by averaging data from the different stations (Fig. 2.3c). The characteristics of nitrate+nitrite (N), phosphate (P), and silicate (Si) of ADW were selected from a station at the mouth of Atchafalaya River (square symbol in Fig. 2.3c), where N, P, and Si concentrations are highest among the stations. Two stations at the mouth of the Mississippi River mouth were selected for the end-member 4, the Mississippi Discharge Water (MDW), with S≤5 and longitude: east of 90°

W conditions (Fig. 2.3d). Only the nutrient concentrations were originally measured at the mouth of Mississippi River during the Texas-Louisiana shelf-wide cruises with no physical property measurements (Table 2.3). Thus, the temperature, salinity, and oxygen characteristics of MDW were defined by averaging those two stations' data shown in Fig. 2.3d, and its chemical characteristics (N, P, and Si) were selected from the mean values shown in Table 2.3. Note that the salinity characteristics of ADW and MDW are assumed as zero at the river mouths. The defined characteristics of end-members used in the extended OMP analysis are summarized in Table 2.1.

3.2 Assignment of Redfield ratios

Extended OMP analysis accounts for the effects of biogeochemical processes by using Redfield ratios. In general, Redfield ratios are estimated through linear regression analysis with nutrient data. The dataset showed, however, wide scatters of P and N, so appropriate numbers could not be defined with the regression analysis. Therefore, 4 different cases of different Redfield ratios were considered: (1) the traditional Redfield ratios (Redfield et al., 1963), $r_{N:P:-O2}$=16:1:138, (2) slightly revised Redfield ratios, $r_{N:P:-O2}$=16:1:150 (Anderson, 1995), (3) a simple average N:P ratio of individual samples in the study area, $r_{N:P:-O2}$=11:1:138, and (4) a simple average N:P ratio in the study area with slightly different $r_{P:-O2}$, $r_{N:P:-O2}$=11:1:150. The silicates regenerated in the water column are the result of remineralization and dissolution (Park, 1967; Kido and Nishimura, 1973). The part of remineralization is represented by the ratio of Si/P, and the dissolution part is placed on the column vector x as an unknown variable. The extended OMP analysis is based on over-determined system with more known equations (number of rows) than unknown variables (number of columns). So the addition of a new unknown variable to the column vector x makes it an even-determined system of equal number of equations and the unknown variables. In addition, the two processes are difficult to distinguish in the shallow coastal water environment. Thus, the ratio of Si/P is assumed to represent the mixed results of remineralization and dissolution. The Si/P ratio of 15 was

used for the cases 1 and 2 (Redfield et al., 1963), and 16 for the cases 3 and 4, that were previously estimated in the northern GOM (Justic et al., 1995).

3.3 Weights for each parameter

The parameters for the extended OMP analysis contain different precisions and accuracies from each other. Appropriate weights can be assigned to each parameter to consider this matter (Tomczak and Large, 1989):

$$W_j = \frac{\sigma_j^2}{\delta_{j\max}} \tag{2}$$

where, σ_j^2 is the variance of parameter j calculated from the physicochemical characteristics of end-members defined, and δ_{jmax} is the largest among the variances of parameters estimated in the source regions for each end-member. Since it cannot have the information on δ_{jmax}, a different weight equation previously applied to a marginal sea system (Kim and Lee, 2004) was used. The weight equation is written as:

$$W_j = \frac{\sigma_j}{accuracy_j} \tag{3}$$

where, σ_j is the standard deviation of parameter j calculated from the physicochemical characteristics of end-members defined. It allows each parameter j to distinguish end-members (Leffanue and Tomczak, 2004). The $accuracy_j$ is defined as the measurement error of parameter *j*. The weights used for the extended OMP analysis are summarized in Table 2.4.

3.4 Validation of the extended OMP analysis

The extended OMP analysis is based on over-determined system, which means that there can be multiple copious solutions, but it ultimately finds a best solution by minimizing the residuals. The residuals provide a way to evaluate determination of number of end-members and the validation of solutions (Tomczak and Large, 1989). The residuals of mass conservation (R_{MC}), for example, are calculated as follows:

$$R_{MC}(\%) = \left(\sum_{i=1}^{4} x_i - 1 \right) \times 100 \quad (4)$$

The salinity distinguishes the end-members (ADW and MDW vs. TLCW vs. SUW) clearly in the study area. The plot of Salinity vs. R_{MC} is used to determine which waters have high residuals. The residuals increase slightly near the salinity of 36, which is a mixture of TLCW and SUW, but overall the residuals are well constrained within ~2% (Fig. 2.4). Poor choices of end-members or their characteristics would have resulted in larger residuals.

3.5 Limitations for the extended OMP analysis

The extended OMP analysis can be used with any hydrographic data (Tomczak and Large, 1989), and it requires good definitions of physicochemical characteristics of end-members at their source regions. In general, however, it is difficult to define pure end-members in coastal oceans due to high spatiotemporal variability, lack of source water information, and insufficient long-term hydrographic data. The 4 different end-members (i.e. ADW, MDW, TLCW, and SUW) and their physicochemical characteristics were defined with the data obtained in the study area (Table 2.1). Although the currently defined characteristics of end-members do not completely fulfill the needs to be defined at the actual source regions, since the observations were conducted in the same area of the northern GOM for the July season over 20-year of period, the characteristics defined with the long-term data can represent the system within particular space and time.

The end-member characteristics of ADW and MDW were defined near the mouth of Atchafalaya and Mississippi Rivers (Fig. 2.3c and d), of TLCW in the shallow inner shelf area, and of SUW south of the Mississippi River delta where a branch of SUW approaches onshore along with the Loop Current (LC) or Loop Current Eddies (LCEs). SUW enters GOM through the Yucatan Channel along with LC as a shallow salinity maximum (Jochens and DiMarco, 2008), after it is formed by subduction in subtropical Atlantic Ocean (O'Connor et al., 2005).

It is assumed that the currently defined end-member properties can represent the source water contributions for the study area although they may not be the actual source waters at the original formation areas. Therefore, SUW contribution in the extended OMP analysis is indeed a contribution of the 'modified' SUW in the northern GOM, as it cannot account for the property changes between the formation area and the study area for SUW.

The end-member definitions are significantly important in the extended OMP analysis, because the solutions can be underestimated or overestimated if wrong information on them is used for the extended OMP analysis. Although the end-member characteristics were defined with the long-term hydrographic data and the residuals of mass conservation were within ~2%, there might be still potential error in terms of the definitions of end-member characteristics.

Considering the limitations above, I conclude that the end-member characteristics and the results (x_i, ΔP, and ΔN) from the extended OMP analysis are valid within the study area and July of summer season only. In addition, I assume that the effect of wintertime source water conditions is insignificant during the summertime since the study area is shallow (<100m) and does not show the bottom topography that may entrap significant waters with wintertime signatures (Fig. 2.1).

4. RESULTS AND DISCUSSIONS

4.1 Temporal variation of bottom water mixing ratios among end-members

The composition of the bottom waters (i.e. mixing ratios for individual end-members) in the study area exhibits significant temporal variability over time (Fig. 2.5). The contributions from SUW and TLCW dominate the composition of the bottom water (>90%), whereas the contributions from the River inflows (ADW and MDW) are insignificant in the bottom water (Fig. 2.5). Since the 4 Redfield ratios used in the analysis do not differ greatly, only results of cases 1 ($r_{N:P:Si:-O2}$=16:1:15:138) and 3 ($r_{N:P:Si:-O2}$=11:1:16:138) are shown in Fig. 2.5. The results of cases 2 and 4 are shown in Table

2.5, along with the estimated mixing ratios with individual cases. The mixing ratios of SUW and TLCW show little variation with time until 1997. Since then, the SUW fraction for the bottom water has decreased gradually, whereas the TLCW fraction has increased with time, indicating that the bottom water composition in the study area can change substantially with time. TLCW has dominated the bottom water composition in the study area during the 2000's.

The water temperature characteristic helps distinguish SUW (colder) from TLCW (warmer) (Table 2.1). The mean temperatures of the surface and the bottom waters have increased significantly during the study period (Fig. 2.6). Since the datasets are mere snapshots obtained only in July time at a highly variable and dynamic coastal ocean environment, one cannot relate this phenomenon to climate change. However, the bottom waters have been occupied predominantly by warmer TLCW in the recent period is likely related to large-scale circulation processes in GOM. The potential effects of bottom water compositional changes to denitrification rates are explored below.

4.2 Estimation of denitrification rates

Denitrification likely occurs in suboxic ($O_2 \leq 4.5$ μmol $L^{-1} \approx 0.1$ ml $L^{-1} \approx 0.2$ mg L^{-1}) condition (Naqvi et al., 2010). Significant denitrification ($\Delta N_{deni} > 0$) and suboxia were found only in the bottom waters in the study area. However, denitrification signals estimated from the extended OMP analysis derived from bottom waters cannot be distinguished from those derived from sediments. The thickness of the bottom layer (ΔH) is 1m on average (Fig. 2.7). Here it is assumed that denitrification is occurring in a bottom layer that includes both bottom waters and sediments. All the water properties are assumed to be vertically uniform in this layer (Fig. 2.7). The unit of denitrification estimated by the extended OMP analysis (eqn. 1) is given as concentration, μmol L^{-1} (or, mmol m^{-3}). Time and volume (m^3) data are necessary to transform the concentration unit to a rate. I estimate the denitrification rates only for the study area (mean area; $\overline{A}$); that is approximately 3.24×10^{10} m^2. I also assume that the denitrification rate is constant during July time period (ΔT). Since there is no information on significance of anaerobic

ammonium oxidation (Anammox) and dissimilatory nitrate reduction to ammonium (DNRA) in nitrogen loss in the study area (Dagg et al., 2007), I also assume that denitrification (ΔN_{deni}) alone is a major nitrogen sink in the study area. With the above assumptions, the denitrification rate can be expresses as:

$$deni.\ rate\ \left(Gg\ N\ mon^{-1}\right) = \overline{\Delta N}_{deni}\left(\frac{mmol\ N}{m^3}\right) \times \frac{14g\ N}{1mol} \times \overline{A}\left(m^2\right) \times \Delta H(m) \times \Delta T\left(mon\right)^{-1} \quad (5)$$

where, $\overline{\Delta N}_{deni}$ is the mean denitrification within the study area, and G denotes Giga or 10^{-9}. The $\overline{\Delta N}_{deni}$ is 6±3 mmol N m^{-3}, and the mean denitrification rate is 3±2 Gg N mon^{-1}.

4.3 Temporal variation of denitrification rates

The estimated denitrification rates show substantial variability with time in the study area (Fig. 2.8) in the ranges of 2±3 to 14±10 Gg N mon^{-1} and 1±3 to 5±4 Gg N mon^{-1} for the Redfield ratio cases of 1 and 3, respectively (Table 2.6). The denitrification rates had decreased gradually from 1985 to 1997. They increased with time from a minimum in July 1997 to 2007, but this trend was also characterized by high variation.

Two other previous estimates obtained in the similar area (Gardner et al., 1993; Childs et al., 2003) and the latitudinal mean denitrification rates (at 0°-20°N, 20°-45°N, and >45°N) in the North Atlantic continental shelf regions (Seitzinger and Giblin, 1996) are compared to the current estimates (Fig. 2.8). A denitrification rate recently measured in July 2008 at the same study area (~25 μmol N m^{-2} h^{-1} at 28.8°N/ 90.2°W; Gardner et al., 2010) is consistent with the current estimates (Fig. 2.8), even though data from just one station is available. The literature values are converted to the unit of Gg N mon^{-1} by multiplying $\overline{A} \approx 3.24 \times 10^{10} m^2$ for the study area. Overall, the estimated denitrification rates of the current study are similar to the mean denitrification rates of the latitudinal bands of 0-20°N and >45°N in the North Atlantic Ocean (Fig. 2.8). The previous estimates, indirectly estimated in July 1990 (7-14 Gg N mon^{-1}) (Gardner et al., 1993) and directly estimated in July 2008 (~8 Gg N mon^{-1}; Gardner et al., 2010) are comparable to

the current analysis within the given standard deviations, despite their slightly higher values (Fig. 2.8). Although the lower bound value (~30 Gg N mon^{-1}; Childs et al., 2003) in July 1999 resembles the estimates of this study, their upper bound value (~151 Gg N mon^{-1}) is much higher than the current estimates and the latitudinal mean denitrification rates of the North Atlantic continental shelf regions (Fig. 2.8). Childs et al., (2002) described sediment denitrification in the northern Gulf of Mexico, and their estimates (see their Table 1) were comparable to the indirectly and directly estimated values (Gardner et al., 1993; Gardner et al., 2010) and the modeled values from this study. However, later Childs et al., (2003) reported the erratum on their denitrification rates indicating an error in their previous calculation caused by the use of wrong gas constant, however denitrification rates calculated with the correct gas constant were not published. I suspect that their seemingly high denitrification rates are biased by this error. Furthermore, their upper bound value (~30 Gg N mon^{-1}) is much higher than other all literature values, so I suppose that their high value is an overestimate. To obtain accurately representative values of denitrification rates in this region, showing highly spatiotemporal variation, direct denitrification measurements with short time intervals are needed for the study area. The details of the estimated denitrification rates are summarized in Table 2.6.

4.4 The effect of water mass distributions on denitrification rates

Potential factors causing the low denitrification rates in July 1997 and high rates in July 2002 (Fig. 2.8) are considered. The distributions of water mass mixing ratios (as mean values of the cases 1-4) of SUW and TLCW for the bottom water are shown in Fig. 2.9, along with a contour line of DO=2mg L^{-1} (or ≈63μmol L^{-1}) as a demarcation of hypoxia in the area. A hypoxic condition developed in the study area in both years during July. On the other hand, the distributions of mixing ratios of SUW and TLCW were significantly different; SUW extended farther into the coast from offshore and TLCW was confined inshore within ~20m isobath in July 1997 (Figs. 2.9a and c), whereas the

SUW's contribution was weak and the TLCW's occupation was widespread in July 2002 (Figs. 2.9b and d).

The meso-scale sea surface height anomalies (http://argo.colorado.edu/~realtime/gsfc_gom-real-time_ssh/) showed that an anticyclonic (clockwise circulation) warm core eddy (89-92°W and 27-28.5°N) approached the southern boundary of the study area with an enhanced contribution of SUW in July 1997 (Figs. 2.9a and e). Although warm eddies were separated from the LC near the study area in July 2002, they were not as close to the study area as in July 1997 with lesser input of SUW (Figs. 2.9b and f). SUW, originates in the subtropical Atlantic Ocean, enters GOM through the Caribbean Sea following LC. It spreads further into the interior of GOM along with LCEs that are separated from the main LC. The influence of SUW to the study area would likely depend on the extension of LC and the distribution of LCEs.

Denitrification rate depends on nitrate availability from recycled ammonium produced via remineralization, and may correlate with the organic matter supply in the water column. The enhanced presence of colder and saltier SUW in July 1997 presumably generated a stronger stratification of the water column with a steep vertical density gradient, and this pattern can reduce the supply of organic matter to the bottom layer in the study area. In addition, oligotrophic SUW contains lower nutrient concentrations. The bottom water N concentration (NO_3^-+NO_2^-) was much higher in July 2002 than that in July 1997 (Fig. 2.10). Therefore, the magnitude of SUW extension may influence the denitrification rate of bottom waters in the study area.

4.5 Correlations of denitrification rate with remineralization vs. water mass composition

Relationships among denitrification rate, amount of remineralized organic carbon, and water mass mixing ratios were analyzed to examine relationships between biogeochemical and physical factors. The amounts of denitrification (ΔN_{deni}) and remineralized phosphate (ΔP_{remi}), averaged from the cases 1-4 (Tables 2.6-7), were estimated by the extended OMP method. The amount of remineralized organic carbon for

the rate of organic matter supply into the bottom layer is estimated from ΔP_{remi} x 106 ($r_{C:P}$) assuming that the amount of remineralized phosphate is positively correlated with the supply rate of organic matter following the Redfield ratios. The denitrification rate and the amount of remineralized carbon showed a significant positive correlation (R=0.79) (Fig. 2.11a). The correlations between the denitrification rate and SUW (Fig. 2.11b), vs. TLCW (Fig. 2.11c) were significantly negative (R=-0.57) and positive (R=0.51), respectively. The mean mixing ratio of SUW in the study area was higher in July 1997 than in July 2002 (Fig. 2.11b and Table 2.5), while the amount of remineralized carbon was much lower in July 1997 (≈8 μmol L^{-1}) than that in July 2002 (≈103 μmol L^{-1}) (Fig. 2.11a and Table 2.7).

The mean mixing ratio of SUW was lower again in July 2005 like in July 2002 (Fig. 2.11b and Table 2.5), but the denitrification rate (=4±2 Gg N mon^{-1}) in July 2005 was not similar to that in July 2002 (=7±4 Gg N mon^{-1}) (Fig. 2.11b and Table 2.6). This result may have resulted from the lower amount of remineralized carbon in July 2005 (≈35 μmol L^{-1}) than in July 2002 (≈103 μmol L^{-1}) (Fig. 2.11a and Table 2.7). Perhaps the supply of organic matters into the bottom layer was relatively higher in July 2002 than in July 2005.

In summary, denitrification rates were low in July 1997, because SUW was dominant in the bottom waters with low remineralized carbon. The enhanced vertical density gradient might have impeded an input of organic matter into the bottom layer (i.e. negative connection between the biogeochemical factor: lower remineralization and the physical factor: enhanced stratification). On the other hand, the extent of SUW was limited and the amount of remineralized carbon was high in July 2002. The increased remineralization and reduced stratification might have caused higher denitrification rates (i.e. positive connection between the biogeochemical factor: increased remineralization and the physical factor: weakened stratification). The results of this study therefore indicate that the magnitude of denitrification rate does not necessarily correlate with the size of hypoxia in the study area. Hypoxia can develop broadly in the study area by physical (stratification) and/or biogeochemical (remineralization) factors, but

denitrification is determined by a rather competitive relationship between physical (stratification) and biogeochemical (remineralization) factors.

5. CONCLUSIONS

The magnitude and temporal variation of denitrification rates at the hypoxic area of the northern GOM during July 1985-2007 are presented (except for July 1988-1990), estimated by the extended OMP analysis. The denitrification rates estimated at the bottom waters ranged from 1-7 Gg N mon^{-1} (for July and for the mean study area of $3.24x10^{10}$ m^2). The denitrification rates have decreased gradually from 1985 to 1997, and increased during the 1998-2007 period. The composition of bottom waters on the Texas-Louisiana inner shelf has changed since ~1997, with the increase of TLCW and decrease of SUW. This change may have influenced denitrification rates at the bottom water layer in the study area. The denitrification rates in the northern GOM were controlled not only by organic matter supply (biogeochemical factor: remineralization), but also by the relative contributions from different water masses (physical factor: stratification).

REFERENCES

Altabet, M.A., R. Francols, D.W. Murray, and W.L. Prell, 1995. Climate-related variations in denitrification in the Arabian Sea from sediment $^{15}N/^{14}N$ ratios. Nature, 506-508.

Anderson, L.A., 1995. On the hydrogen and oxygen content of marine phytoplankton. Deep-Sea Research I, 42, 1675-1680.

Anderson, L.A., and J.L. Sarmiento, 1994. Redfield ratios of remineralization determined by nutrient data analysis. Global Biogeochemical Cycles, 8(1), 65-80.

Childs, C.R., N.N. Rabalais, R.E. Turner, and L.M. Proctor, 2002, Sediment denitrification in the Gulf of Mexico zone of hypoxia. Marine Ecology Progress Series, 240, 285-290.

Childs, C.R., N.N. Rabalais, R.E. Turner, and L.M. Proctor, 2003. Sediment denitrification in the Gulf of Mexico zone of hypoxia (Erratum). Marine Ecology Progress Series, 274, 310.

Dagg, M.J., and G.A. Breed, 2003. Biological effects of Mississippi River nitrogen on the northern Gulf of Mexico-a review and synthesis. Journal of Marine Systems, 43, 133-152.

Falkowski, P.G., 1997. Evolution of the nitrogen cycle and its influence on the biological sequestration of CO_2 in the ocean. Nature, 272-275.

Ganeshram, R.S., T.F. Pedersen, S.E. Calvert, and J.W. Murray, 1995. Large changes in oceanic nutrient inventories from glacier to interglacial periods. Nature, 755-758.

Ganeshram, R.S., T.F. Pedersen, S.E. Calvert, G.W. McNeill, and M.R. Fontugne, 2000. Glacial-interglacial variability in denitrification in the world's oceans: Causes and consequences. Paleoceanography, 15(4), 361-376.

Ganeshram, R.S., T.F. Pedersen, S.E. Calvert, S.E. Calvert, and R. Francois, 2002. Reduced nitrogen fixation in the glacial ocean inferred from changes in marine nitrogen and phosphorus inventories. Nature, 415, 156-159.

Gardner, W.S., E.E. Briones, and E.C. Kaegi, 1993. Ammonium excretion by benthic invertebrates and sediment-water nitrogen flux in the Gulf of Mexico near the Mississippi River outflow. Estuaries, 16(4), 799-808.

Gardner, W.S., M.J. McCarthy, and L. Xiao, 2010. Denitrification as a mechanism causing nitrogen limitation of microbial activities at the sediment water interface in the hypoxic region of the eutrophic northern Gulf of Mexico. 2010 Gulf Estuarine Research Society (GERS) Meeting, Port Aransas, TX.

Gruber, N., and J.L. Sarmiento, 1997. Global patterns of marine nitrogen fixation and denitrification. Global Biogeochemical Cycles, 11(2), 235-266.

Hupe, A., and J. Karstensen, 2000. Redfield stoichiometry in Arabian Sea subsurface waters. Global Biogeochemical Cycles, 14(1) 357-372.

Jarosz, E., and S.P. Murray, 2005. Velocity and transport characteristics of the Louisiana-Texas Coastal Current; Circulation in the Gulf of Mexico: Observations and Models. Geophysical Monograph Series 161, 143-156.

Jochens, A.E., S.F. DiMarco, 2008. Physical oceanographic conditions in the deepwater Gulf of Mexico in summer 2000-2002. Deep-Sea Research II, 55, 2541-2554.

Justic, D., N.N. Rabalais, and R.E. Turner, 1995. Stoichiometric nutrient balance and origin of coastal eutrophication. Marine Pollution Bulletin, 30(1), 41-46.

Karstensen, J., and M. Tomczak, 1998. Age determination of mixed water masses using CFC and oxygen data. Journal of Geophysical Research, 103, 18599-18609.

Kido K. and M. Nishimura. 1973. Regeneration of silicate in the ocean. Journal of the Oceanographical Society of Japan. **29**, 185-192.

Kim, I.-N., and T. Lee, 2004. Summer hydrographic features of the East Sea analyzed by the Optimum Multiparameter method. Ocean and Polar Research, 26(4), 581-594.

Leffanue, H., and M. Tomczak, 2004. Using OMP analysis to observe temporal variability in water mass distribution. Journal of Marine Systems, 48, 3-14.

McElroy, M.B., 1983. Marine biological controls on atmospheric CO_2 and climate. Nature, 302, 328-329.

Morrison, J.M., and W.D. Nowlin, Jr., 1977. Repeated nutrient oxygen and density sections through the Loop Current. Journal of Marine Research, 35, 105-128.

Morrison, J.M., W.J. Merrell, R.M. Key, and T.C. Key, 1983. Property distributions and deep chemical measurements within the Western Gulf of Mexico. Journal of Geophysical Research, 88, 2601-2608.

Naqvi, S.W.A., H.W. Bange, L. Farias, P.M.S. Monteiro, M.I. Scranton, and J. Zhang, 2010. Marine hypoxia/anoxia as a source of CH_4 and N_2O. Biogeosciences, 7, 2159-2190.

Nevison, C., and E. Holland, 1997. A reexamination of the impact of anthropogenically fixed nitrogen on atmospheric N_2O and the stratospheric O_3 layer. Journal of Geophysical Research, 102, 25519-25536.

Nevison, C., J.H. Butler, and J.W. Elkins, 2003. Global distribution of N2O and the $\triangle N_2O$-AOU yield in the subsurface ocean. Global Biogeochemical Cycles, 17(4), 1119, doi:10.1029/2003GB002068.

O'Connor, B.M., R.A. Fine, and D.B. Olson, 2005. A global comparison of subtropical underwater formation rates. Deep Sea Research I, 52, 1569-1590.

Pakulski, J.D., R. Benner, T. Whitledge, R. Amon, B. Eadie, L. Cifuentes, J. Ammerman, and D. Stockwell, 2000. Microbial metabolism and nutrient cycling in the Mississippi and Atchafalaya River plumes. Estuarine, Coastal and Shelf Science, 50, 173-184.

Park, K., 1967. Nutrient regeneration and preformed nutrients off Oregon. Limnology and Oceanography, 12, 353-357.

Rabalais, N.N., R.E. Turner, and D. Scavia, 2002. Beyond science into policy: Gulf of Mexico hypoxia and the Mississippi River. BioScience, 52(2), 129-142.

Redfield, A.C., B.H. Ketchum, and F.A. Richards, 1963. The influence of organism on the composition of sea water. The Sea, 2, 26-77.

Seitzinger, S.P., and A.E. Giblin, 1996. Estimating denitrification in North Atlantic continental shelf sediments. Biogeochemistry, 35, 235-260.

Tomczak, M., and D.G.B. Large, 1989. Optimum Multiparameter analysis of mixing in the thermocline of the Eastern Indian Ocean. Journal of Geophysical Research, 94, 16141-16149.

Vidal, V.M.V., F.V. Vidal, A.F. Hernandez, E. Meza, and L. Zambrano, 1994. Winter water mass distributions in the Western Gulf of Mexico affected by a colliding anticyclonic ring. Journal of Oceanography, 50, 559-588.

Walker, J.T., C.A. Stow, and C. Geron, 2010. Nitrous oxide emissions from the Gulf of Mexico hypoxic zone. Environmental Science & Technology, 44, 1617-1623.

Wiseman, Wm.J., and F.J. Kelly, 1994. Salinity variability within the Louisiana coastal current during the 1982 flood season. Estuaries, 17, 732-739.

Wiseman, Wm.J., N.N. Rabalais, R.E. Turner, S.P. Dinnel, and A. MacNaughton, 1997. Seasonal and interannual variability within the Louisiana coastal current: stratification and hypoxia. Journal of Marine Systems, 12, 237-248.

Table 2.1: Summertime physicochemical characteristics of four mixing end-members defined in the northern Gulf of Mexico used for the extended OMP analysis.

Parameter	End-members			
	SUW (HS&LT)	TLCW (HS&HT)	ADW (LS)	MDW (LS)
T (℃)	18.6±0.3	29.6±0.4	31.1±0.6	29.4±1
S (psu)	36.7±0.1	35.3±0.2	0±0	0±0
DO (μmol L^{-1})	101±21	151±59	259±40	249±29
P (μmol L^{-1})	0.3±0.1	0.6±0.5	1±0	4±1
N (μmol L^{-1})	7±2	3±5	31±0	127±35
Si (μmol L^{-1})	11±3	14±7	91±0	113±41

H(L)S: high(low) salinity, H(L)T: high(low) temperature

SUW: Subtropical Underwater, TLCW: Texas-Louisiana Coastal Water,

ADW: Atchafalaya Discharge Water, MDW: Mississippi Discharge Water

Table 2.2: Four cases of different Redfield ratios ($r_{N:P:Si:-O2}$) used for the extended OMP analysis.

Parameter	Redfield ratios (N:P:Si:-O_2) Case			
	1	2	3	4
N	16	16	11	11
P	1	1	1	1
Si	15	15	16	16
O_2	138	150	138	150

Table 2.3: Observed N and P concentrations at the mouth of the Mississippi River for July, 1993-2007.

Year	NO2+NO3 ($\mu mol\ L^{-1}$)	PO4 ($\mu mol\ L^{-1}$)	Si ($\mu mol\ L^{-1}$)
1993	150	5.5	168
1994	101	4.2	104
1995	95	2.9	117
1996	222	4.3	108
1998	151	3.4	129
1999	117	3.6	120
2000	136	3.4	127
2001	119	5.0	139
2002	157	1.0	63
2003	94	2.9	61
2004	113	3.5	168
2005	121	3.6	99
2006	96	3.0	28
2007	99	3.6	150
mean±std	127±35	4±1	113±41

Table 2.4: Estimated weight values for each parameter for the extended OMP analysis calculated using equation 3.

T (℃)	S (psu)	DO (μmol L^{-1})	NO2+NO3 (μmol L^{-1})	PO4 (μmol L^{-1})	Si (μmol L^{-1})
3	100	1	25	7	7

Table 2.5: Summertime mean mixing ratios estimated by the extended OMP analysis in the northern GOM.

Year (July)	Subtropical Underwater (%)				
	Case 1 (16:1:15:-138)	Case 2 (16:1:15:-150)	Case 3 (11:1:16:-138)	Case 4 (11:1:16:-150)	Cases 1-4 mean±std
1985	48±27	47±27	47±27	47±27	47±0.1
1986	32±22	31±22	32±23	32±23	32±0.4
1987	35±22	35±22	35±23	35±23	35±0.2
1988	ND	ND	ND	ND	ND
1989	ND	ND	ND	ND	ND
1990	ND	ND	ND	ND	ND
1991	44±22	44±22	47±24	47±24	46±2
1992	43±26	43±26	43±26	43±26	43±0.1
1993	47±25	47±25	50±24	49±24	48±1
1994	41±23	41±23	42±23	42±23	41±0.3
1995	36±18	36±18	37±19	37±19	37±0.4
1996	48±26	48±26	49±26	49±26	49±1
1997	51±22	51±22	52±23	52±23	51±0.3
1998	45±32	45±32	45±32	44±32	45±0.2
1999	34±23	34±23	37±25	36±25	35±2
2000	33±30	33±30	35±32	35±32	34±1
2001	37±22	37±23	38±23	38±23	37±1
2002	18±13	17±13	17±13	17±13	17±0.3
2003	37±25	37±25	36±25	37±24	36±0.1
2004	31±24	31±24	31±24	31±24	31±0.3
2005	17±14	16±14	17±14	16±14	17±0.1
2006	30±25	30±25	31±26	30±26	30±0.1
2007	29±20	29±20	30±23	30±23	30±1

(Table 2.5 continued)

Year (July)	Texas-Louisiana Coastal Water (%)				
	Case 1 (16:1:15:-138)	Case 2 (16:1:15:-150)	Case 3 (11:1:16:-138)	Case 4 (11:1:16:-150)	Cases 1-4 mean±std
1985	46±22	46±22	46±22	46±22	46±0.2
1986	60±17	61±17	60±18	60±18	60±0.4
1987	58±18	58±18	58±18	58±18	58±0.3
1988	ND	ND	ND	ND	ND
1989	ND	ND	ND	ND	ND
1990	ND	ND	ND	ND	ND
1991	50±18	50±28	47±21	47±21	48±2
1992	51±21	51±21	51±21	51±20	51±0.1
1993	47±20	47±20	44±20	44±20	45±2
1994	54±19	54±19	53±19	54±19	54±0.3
1995	60±16	60±16	59±16	59±16	59±0.4
1996	47±22	47±22	46±22	47±22	47±1
1997	44±19	44±19	44±19	44±19	44±0.3
1998	48±27	49±27	49±27	49±27	49±0.2
1999	60±19	61±19	57±21	58±22	59±2
2000	66±29	66±29	64±31	64±31	65±1
2001	58±19	58±19	56±20	57±20	57±1
2002	77±11	77±11	77±11	77±11	77±0.3
2003	58±20	58±20	58±20	58±20	58±0.1
2004	64±20	64±20	64±20	64±20	64±0.3
2005	76±10	76±10	76±10	76±10	76±0.1
2006	66±22	66±22	66±22	66±22	66±0.1
2007	66±18	67±18	65±21	65±21	66±1

(Table 2.5 continued)

Year (July)	Atchafalaya Discharge Water (%)				
	Case 1 (16:1:15:-138)	Case 2 (16:1:15:-150)	Case 3 (11:1:16:-138)	Case 4 (11:1:16:-150)	Cases 1-4 mean±std
1985	5±7	5±7	5±7	5±7	5±0
1986	6±9	6±9	6±8	6±9	6±0.2
1987	4±7	4±7	4±7	4±7	4±0.1
1988	ND	ND	ND	ND	ND
1989	ND	ND	ND	ND	ND
1990	ND	ND	ND	ND	ND
1991	4±7	4±7	4±7	4±7	4±0
1992	6±8	6±8	6±8	6±8	6±0
1993	5±8	5±8	5±8	5±8	5±0.1
1994	4±6	4±6	4±6	4±6	4±0.1
1995	4±5	4±5	4±5	4±5	4±0.1
1996	4±6	4±6	4±6	4±6	4±0
1997	5±5	5±5	5±5	5±5	5±0
1998	6±7	6±7	6±7	5±7	6±0.1
1999	4±6	4±7	3±6	3±6	4±0.3
2000	1±2	1±2	1±2	1±2	1±0
2001	4±6	4±6	4±6	4±6	4±0.1
2002	4±6	4±6	4±6	3±6	4±0.1
2003	4±7	4±7	4±7	4±7	4±0.1
2004	5±6	4±6	4±6	4±6	4±0.2
2005	7±7	7±7	6±7	6±7	6±0.2
2006	3±6	3±6	3±6	3±6	3±0
2007	5±9	4±9	4±9	4±9	4±0

(Table 2.5 continued)

Year (July)	Mississippi Discharge Water (%)				
	Case 1 (16:1:15:-138)	Case 2 (16:1:15:-150)	Case 3 (11:1:16:-138)	Case 4 (11:1:16:-150)	Cases 1-4 mean±std
1985	2±4	2±4	2±4	2±4	2±0
1986	2±4	2±4	3±4	3±4	2±0.2
1987	3±4	3±4	3±4	3±4	3±0.1
1988	ND	ND	ND	ND	ND
1989	ND	ND	ND	ND	ND
1990	ND	ND	ND	ND	ND
1991	3±4	3±4	3±4	3±4	3±0.2
1992	0.4±2	0.4±2	0.4±3	0.4±2	0.4±0
1993	2±4	2±4	2±4	2±4	2±0.1
1994	1±4	1±4	1±4	1±4	1±0.1
1995	1±2	1±2	1±2	1±2	1±0.1
1996	1±2	1±2	1±2	1±2	1±0.1
1997	1±1	1±1	1±1	1±1	1±0
1998	1±3	1±3	1±3	1±3	1±0.1
1999	2±3	2±3	3±3	3±3	3±0.4
2000	1±1	1±1	1±1	1±1	1±0.1
2001	1±2	1±2	2±2	2±2	1±0.2
2002	2±3	2±3	2±3	3±3	2±0.1
2003	2±3	2±3	2±3	2±3	2±0.1
2004	1±2	1±3	1±3	1±3	1±0.2
2005	2±3	2±3	2±3	2±3	2±0.2
2006	1±3	1±3	1±3	1±3	1±0
2007	1±2	1±2	1±2	1±2	1±0.1

Table 2.6: Summertime mean denitrification rates estimated by the extended OMP analysis in the northern GOM.

Year (July)	Denitrification rate (Gg N mon^{-1})					Ref.
	Case 1 (16:1:15:-138)	Case 2 (16:1:15:-150)	Case 3 (11:1:16:-138)	Case 4 (11:1:16:-150)	Cases 1-4 mean±std	
1985	7±7	4±4	3±3	3±3	4±2	
1986	8±10	4±5	3±4	3±4	5±3	
1987	5±5	3±3	2±2	2±2	3±2	
1988	ND	ND	ND	ND	ND	
1989	ND	ND	ND	ND	ND	
1990	ND	ND	ND	ND	ND	Gardner et al.(1993): 7-14
1991	4±7	2±4	1±3	1±3	2±1	
1992	7±5	3±3	3±2	3±2	4±2	
1993	4±6	2±3	2±2	2±2	2±1	
1994	4±4	2±2	2±2	2±2	2±1	
1995	3±4	2±2	1±2	1±2	2±1	
1996	3±4	1±2	1±2	1±2	2±1	
1997	2±3	1±2	1±1	1±1	1±1	
1998	9±11	5±5	4±4	4±4	5±3	
1999	5±11	2±5	2±4	2±4	3±1	Childs et al.(2003): 30-151
2000	3±4	2±2	1±1	1±1	2±1	
2001	4±7	2±4	1±3	1±3	2±1	
2002	14±10	7±5	5±4	5±4	7±4	Seitzinger and Giblin (1996) 0°-20°N: 19 20°-45°N: 35 >45°N: 12
2003	8±3	4±2	3±2	3±2	5±2	
2004	10±9	5±5	4±4	4±4	6±3	
2005	7±5	4±2	3±2	3±2	4±2	
2006	7±7	3±4	2±3	2±3	4±2	
2007	6±7	3±4	2±3	2±3	3±2	
2008	ND	ND	ND	ND	ND	Gardner et al. (2010): 8

Table 2.7: Summertime mean remineralized carbon amount estimated by the extended OMP analysis in the northern GOM.

Year (July)	Remineralized Carbon (μmol kg^{-1}) = remineralized phosphate (ΔP_{remi}) x 106 ($r_{C:P}$)				
	Case 1 (16:1:15:-138)	Case 2 (16:1:15:-150)	Case 3 (11:1:16:-138)	Case 4 (11:1:16:-150)	Cases 1-4 mean±std
1985	44±66	43±65	45±67	44±66	44±1
1986	66±68	66±67	68±70	67±67	67±2
1987	26±35	26±35	26±36	26±35	26±1
1988	ND	ND	ND	ND	ND
1989	ND	ND	ND	ND	ND
1990	ND	ND	ND	ND	ND
1991	48±57	48±56	49±59	48±58	48±1
1992	17±36	17±36	18±37	17±37	17±1
1993	58±66	57±65	61±69	60±69	59±2
1994	38±45	38±44	40±47	39±46	39±2
1995	25±40	25±39	26±42	26±42	26±2
1996	22±34	22±33	23±35	23±35	22±1
1997	8±16	8±16	8±17	8±17	8±1
1998	59±74	58±72	60±76	59±74	59±2
1999	65±68	65±67	67±71	66±70	66±2
2000	36±45	35±44	38±47	37±47	37±1
2001	41±50	41±50	43±52	42±52	42±1
2002	103±61	102±60	105±63	104±62	103±1
2003	41±32	40±31	41±33	40±32	41±1
2004	84±64	85±63	88±66	86±65	87±2
2005	35±31	35±31	35±33	35±32	35±1
2006	53±52	53±51	55±53	55±52	54±1
2007	59±77	58±77	63±85	62±84	60±6

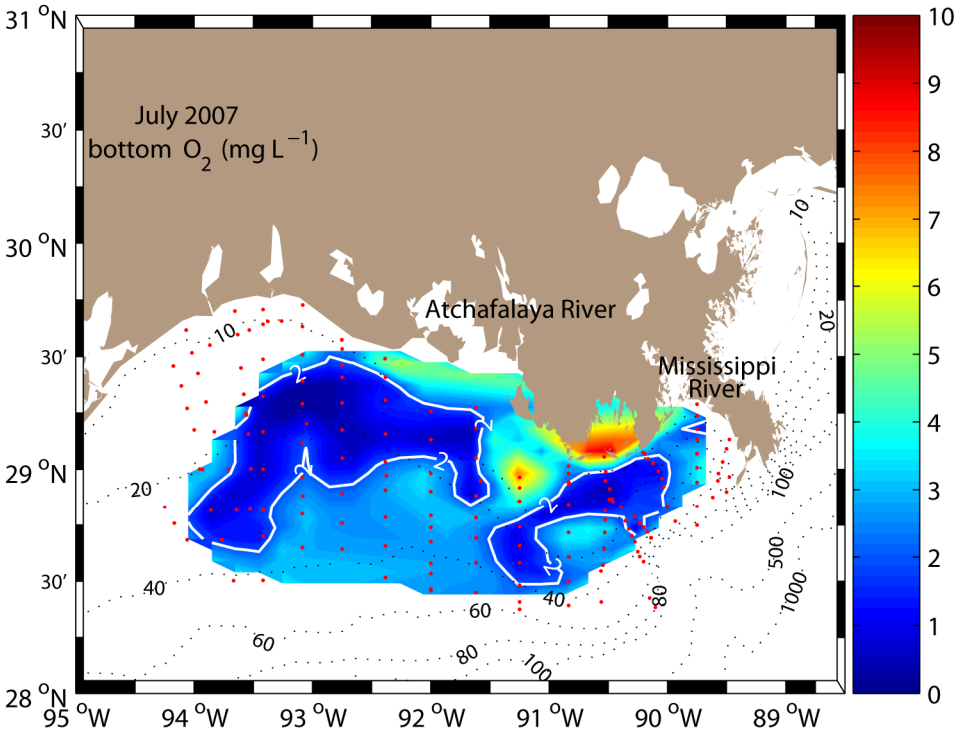

Figure 2.1: Study area map. Texas-Louisiana shelf-wide cruises were conducted regularly by LUMCON (The Louisiana Universities Marine Consortium) since July 1985. The bottom water dissolved oxygen distribution observed in July 2007 is shown with all sampling station locations (dots) for the July 1985-2007 period, except for July 1988-1990.

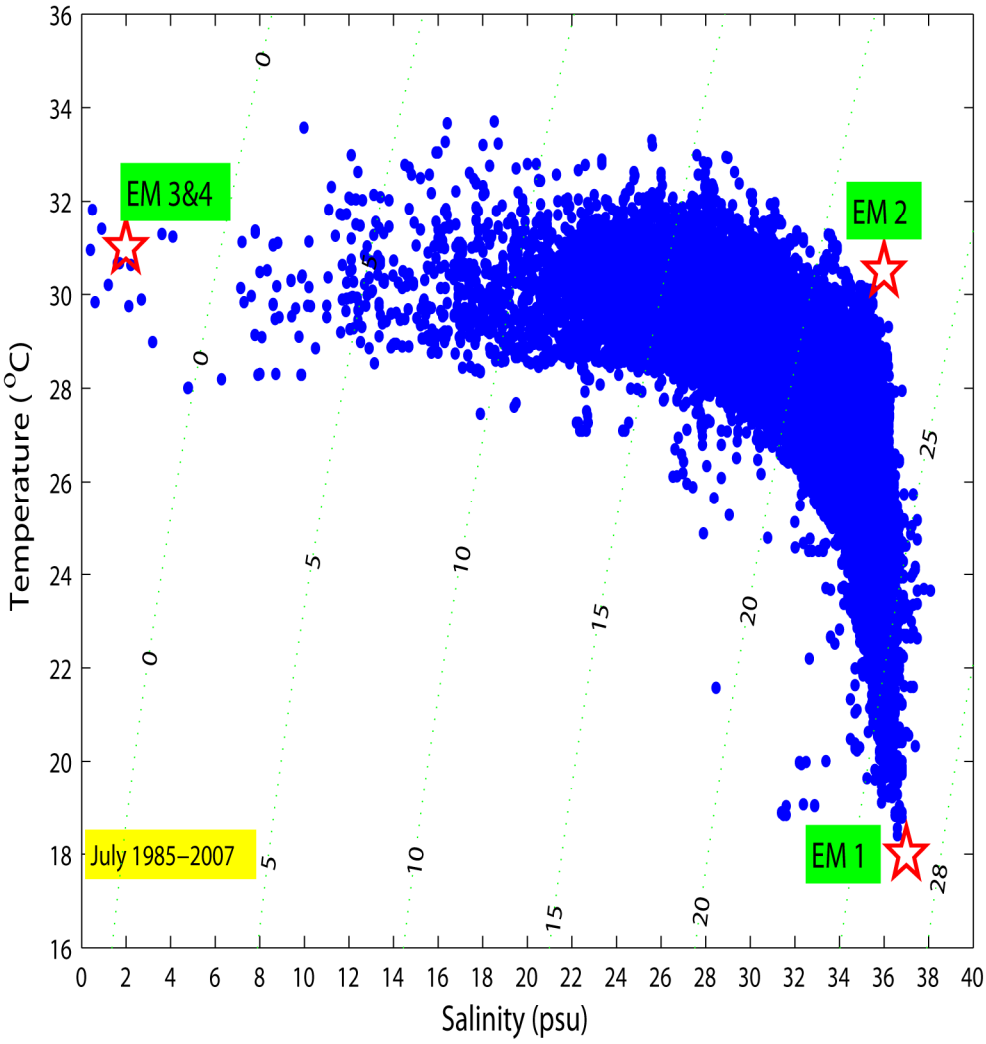

Figure 2.2: A temperature-salinity diagram for the study area in GOM during the study period (July of 1985-2007; except for July 1988-1990). The end-members (stars) and distributions of their physical characteristics are shown in the diagram.

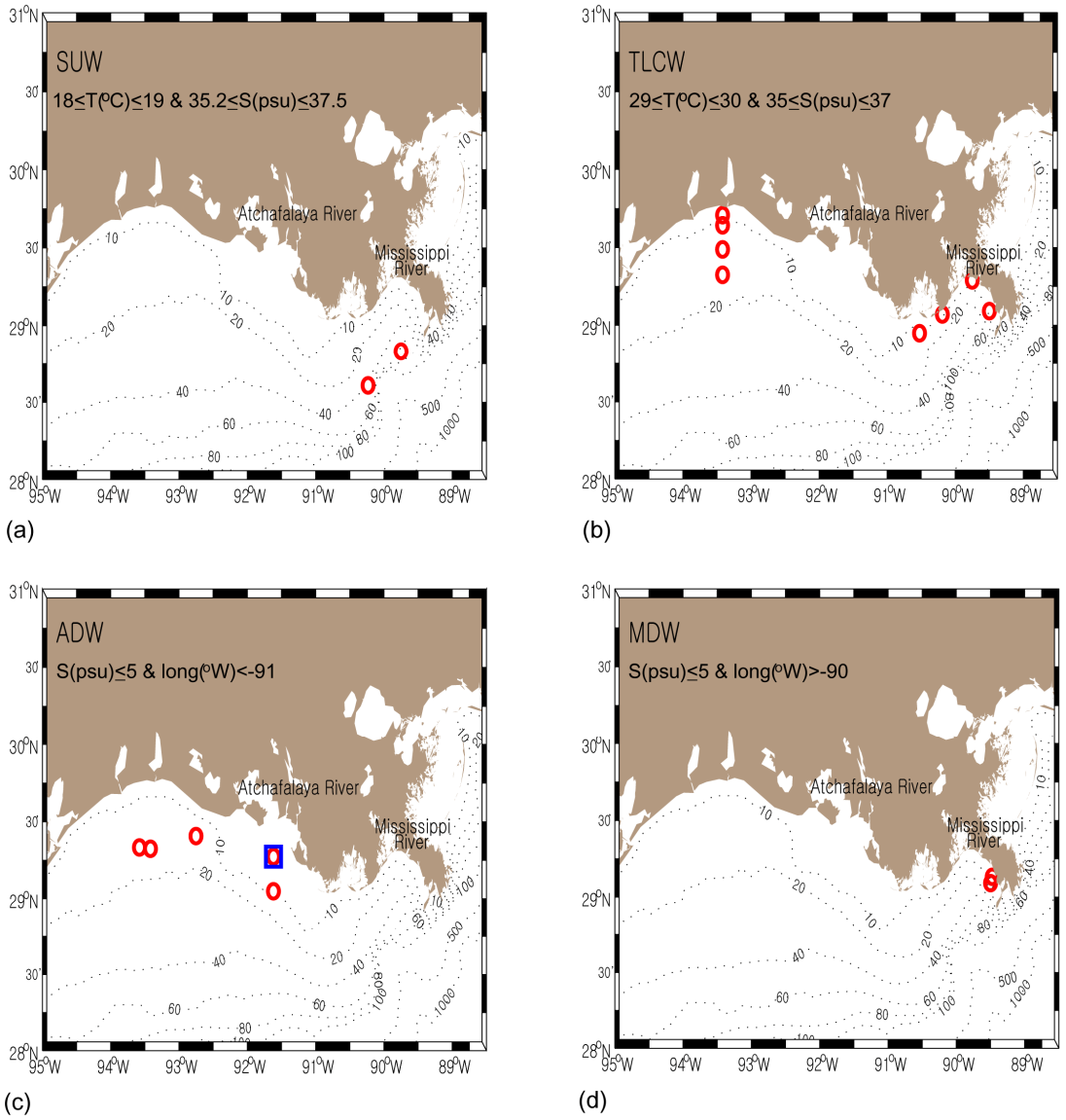

Figure 2.3: Hydrographic stations (circles) used to determine physicochemical characteristics of 4 end-members. (a) Subtropical Underwater (SUW), (b) Texas-Louisiana Coastal Water (TLCW), (c) Atchafalaya Discharge Water (ADW), (d) Mississippi Discharge Water (MDW). The square station in (c) was selected to define the nutrient characteristics of ADW.

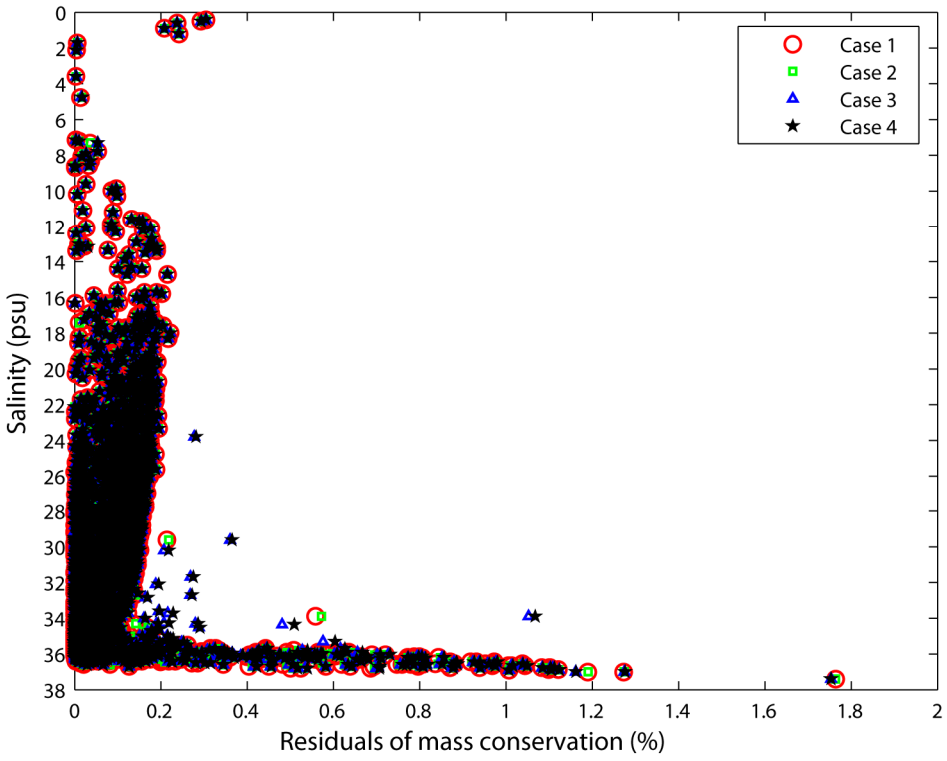

Figure 2.4: The plot of salinity vs. residuals of mass conservation for 4 Redfield ratio cases. The pattern shows how the solutions follow the constraint of mass conservation, $\sum_{i=1}^{n} x_i = 1$. The residuals are slightly increasing near 36 psu of salinity, but overall they are well confined within ~2%.

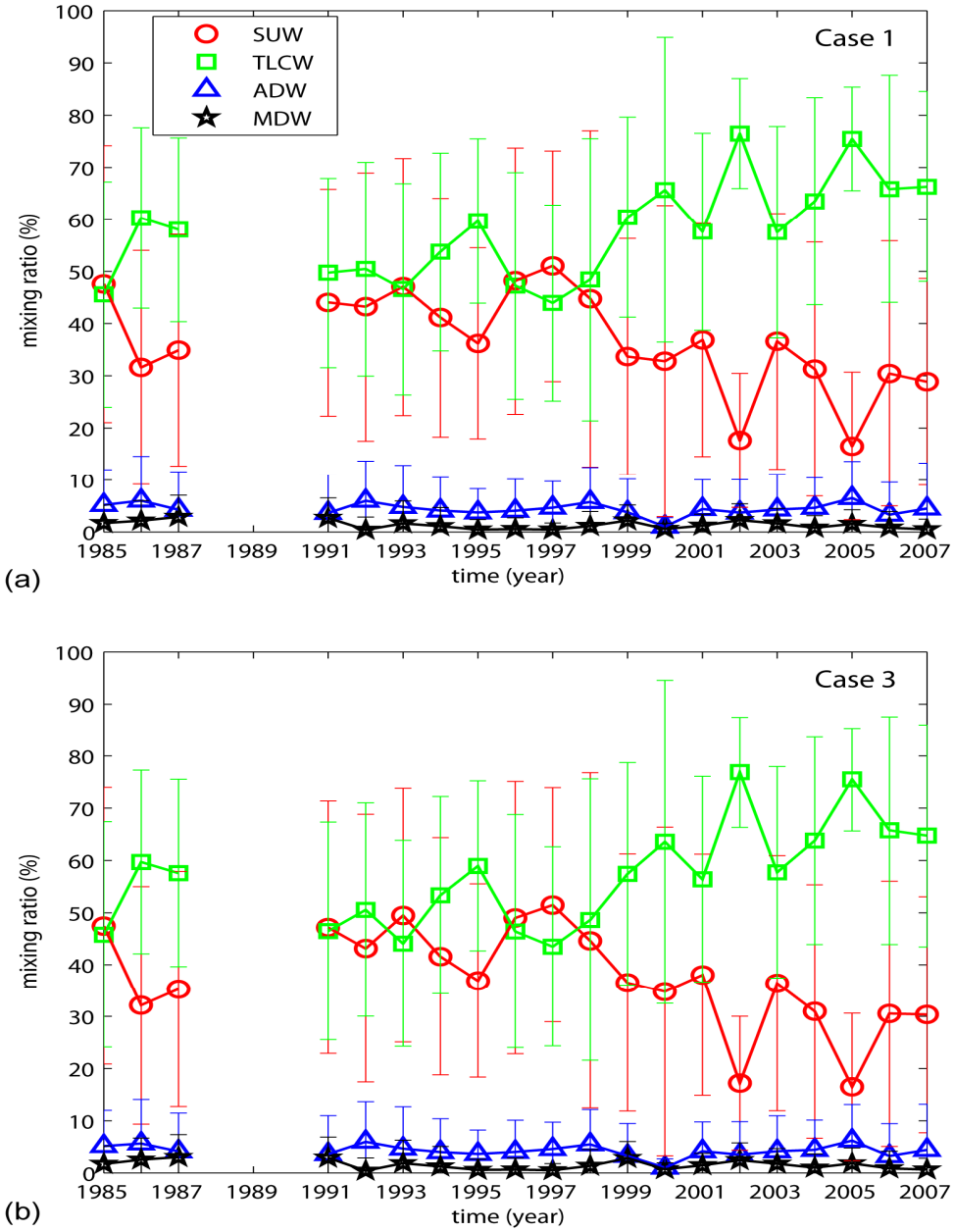

Figure 2.5: The temporal variability of mean mixing ratios among the Subtropical Underwater (SUW), Texas-Louisiana Coastal Water (TLCW), Atchafalaya Discharge Water (ADW), and Mississippi Discharge Water (MDW) in the study area. (a) Mixing ratios with Case 1 ($r_{N:P:Si:-O2}$=16:1:15:138), and (b) with Case 3 ($r_{N:P:Si:-O2}$=11:1:16:138). Error bars represent standard deviation (Table 2.5).

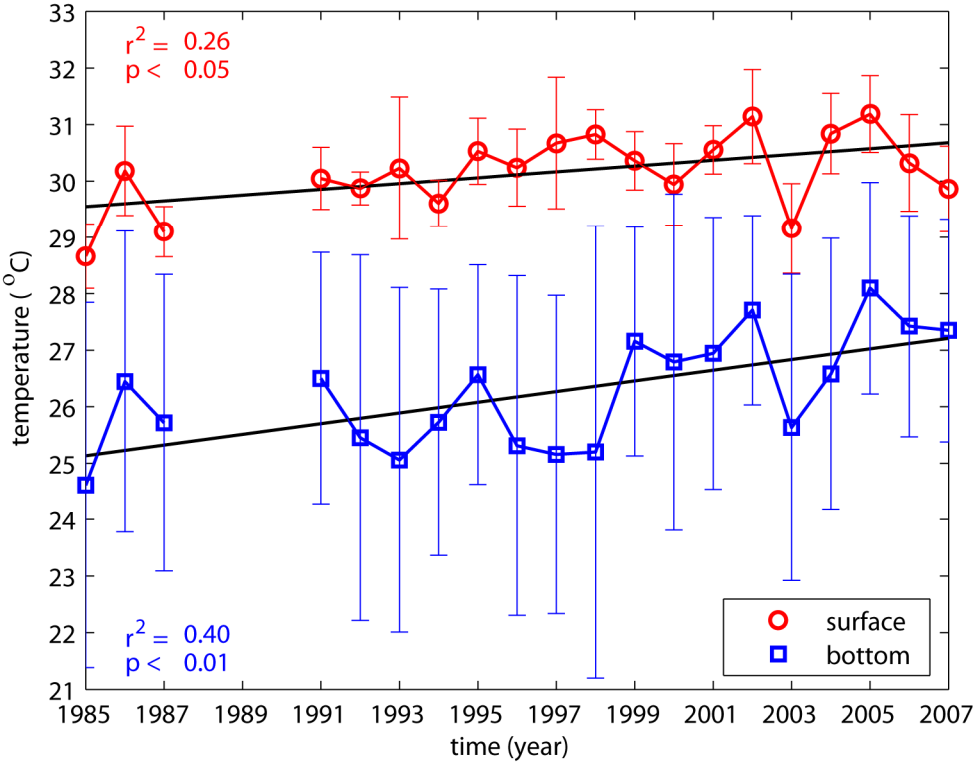

Figure 2.6: The changes of surface and bottom temperatures in the study area of northern GOM between 1985 and 2007 (except for 1988-1990). Error bars represent standard deviation. *P* values were calculated by *t*-test (n=20).

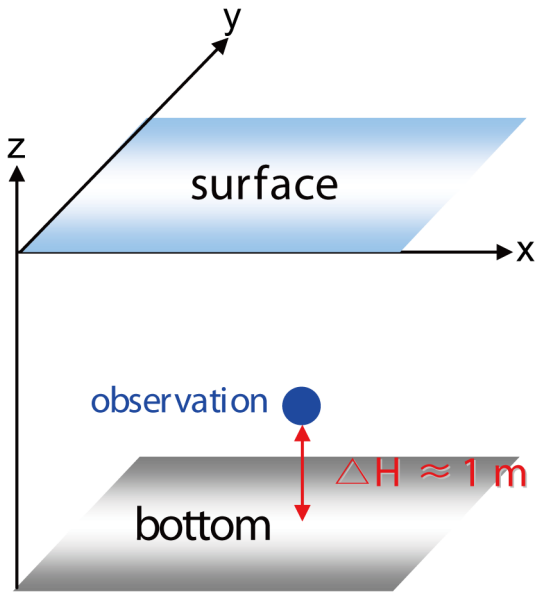

Figure 2.7: Illustration of the component of ΔH, assuming that denitrification is occurring within this bottom layer including bottom waters and sediments. ΔH is approximately 1m on average.

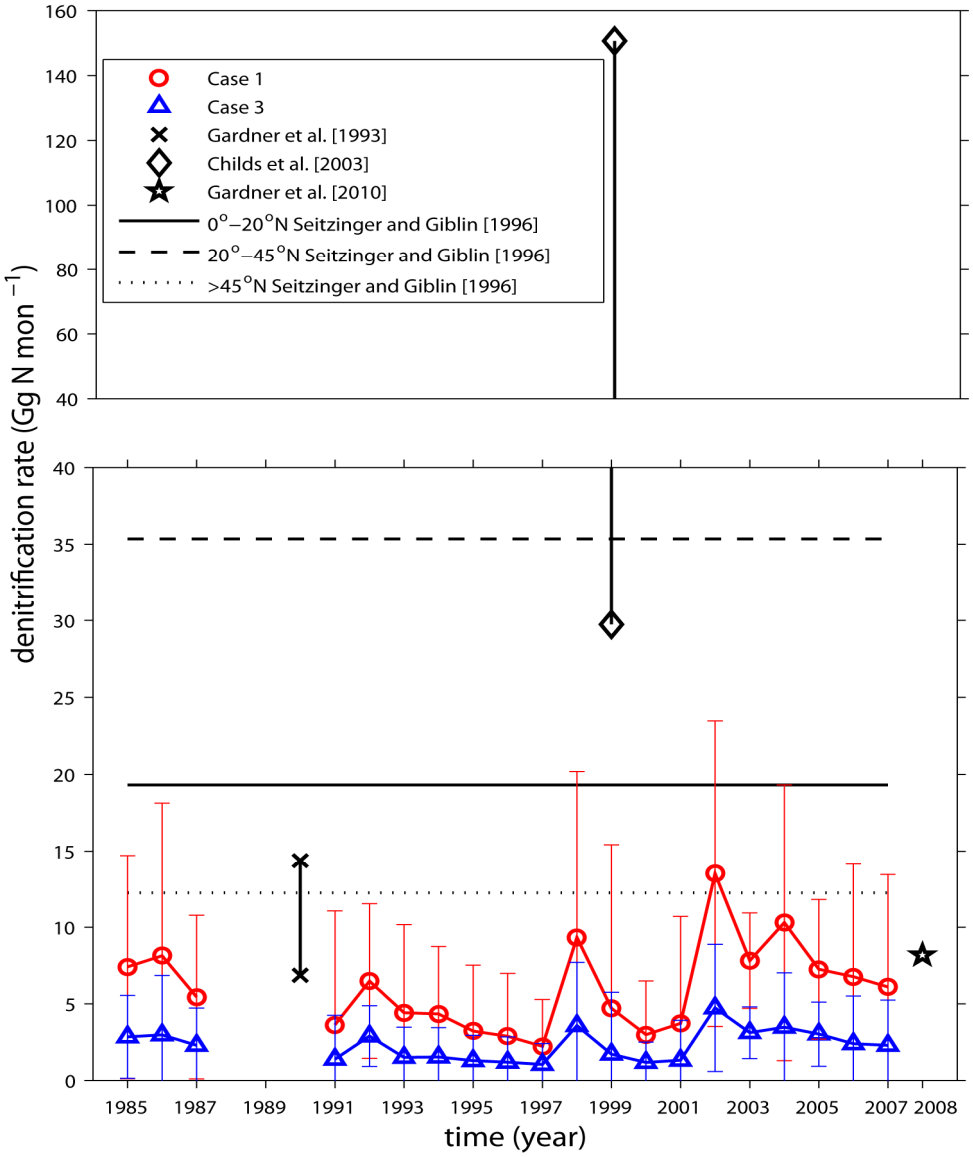

Figure 2.8: The temporal variability of mean denitrification rates (Gg N mon^{-1}) in the study area. Different symbols indicate the denitrification rates with Case 1 (circle), the denitrification rates with Case 3 (triangle), and three other previous estimates in the study area (cross for Gardner et al., 1993, diamond for Childs et al., 2003, and star for Gardner et al., 2010). Different line styles represent the latitudinal mean denitrification rates at 0°-20°N (solid line), 20°-45°N (broken solid line), and >45°N (dotted line), respectively, in the North Atlantic continental shelf regions (Seitzinger and Giblin, 1996). Error bars represent standard deviation (Table 2.6).

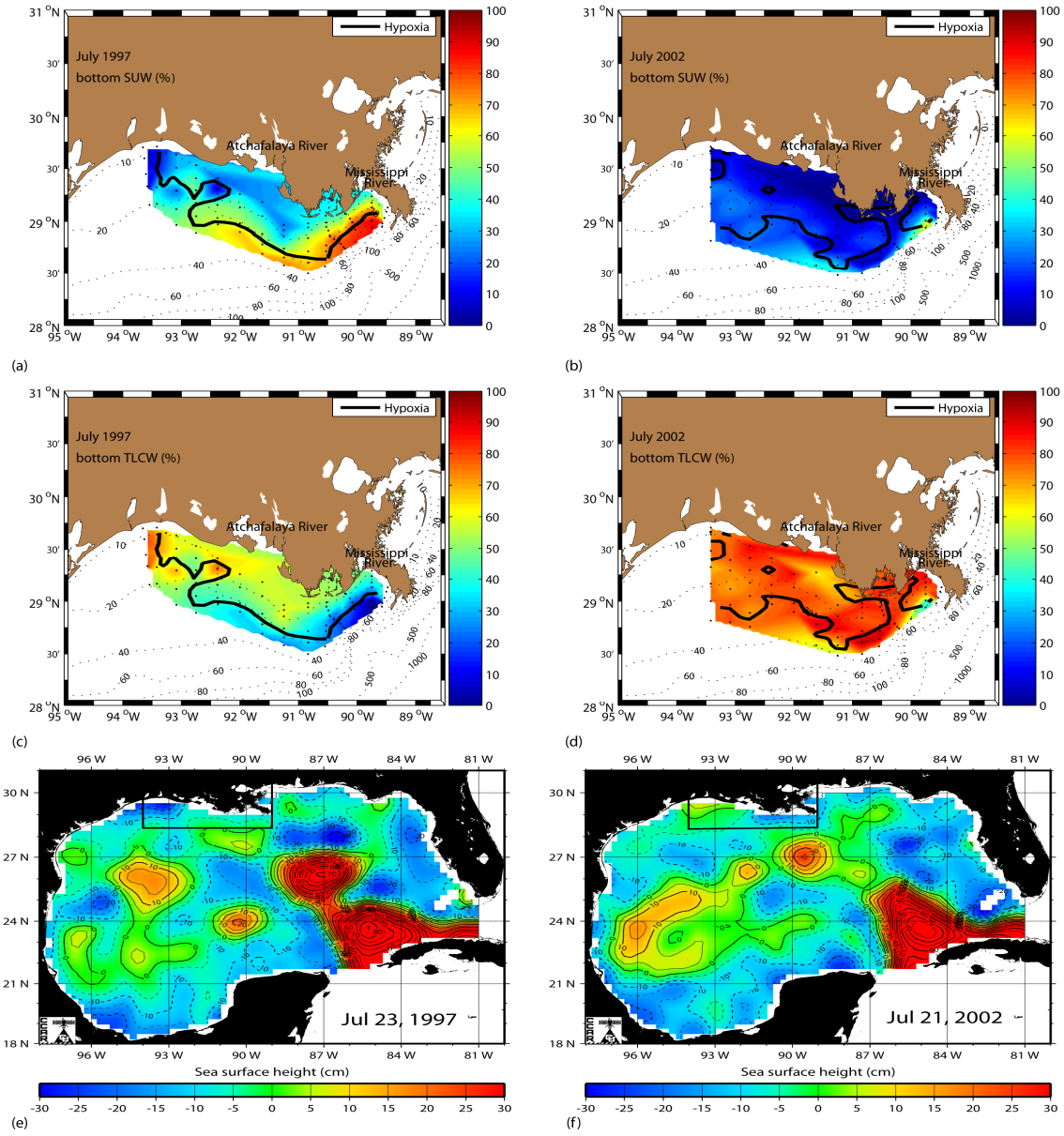

Figure 2.9: Maps of bottom water mixing ratios (Note that the mean values averaged from the cases 1-4 are used) of TLCW and SUW and the larger-scale sea surface height anomalies. (a) The distribution of bottom water mixing ratios of SUW at the bottom in July 1997, (b) in July 2002, (c) The distribution of bottom water mixing ratios of TLCW in July 1997, (d) in July 2002, (e) The map of sea surface height anomalies in July 1997, and (f) in July 2002. While hypoxia (DO≤2mg L^{-1}) was well developed in both time periods (black solid line), the magnitude of denitrification rate was nearly opposite (color contours).

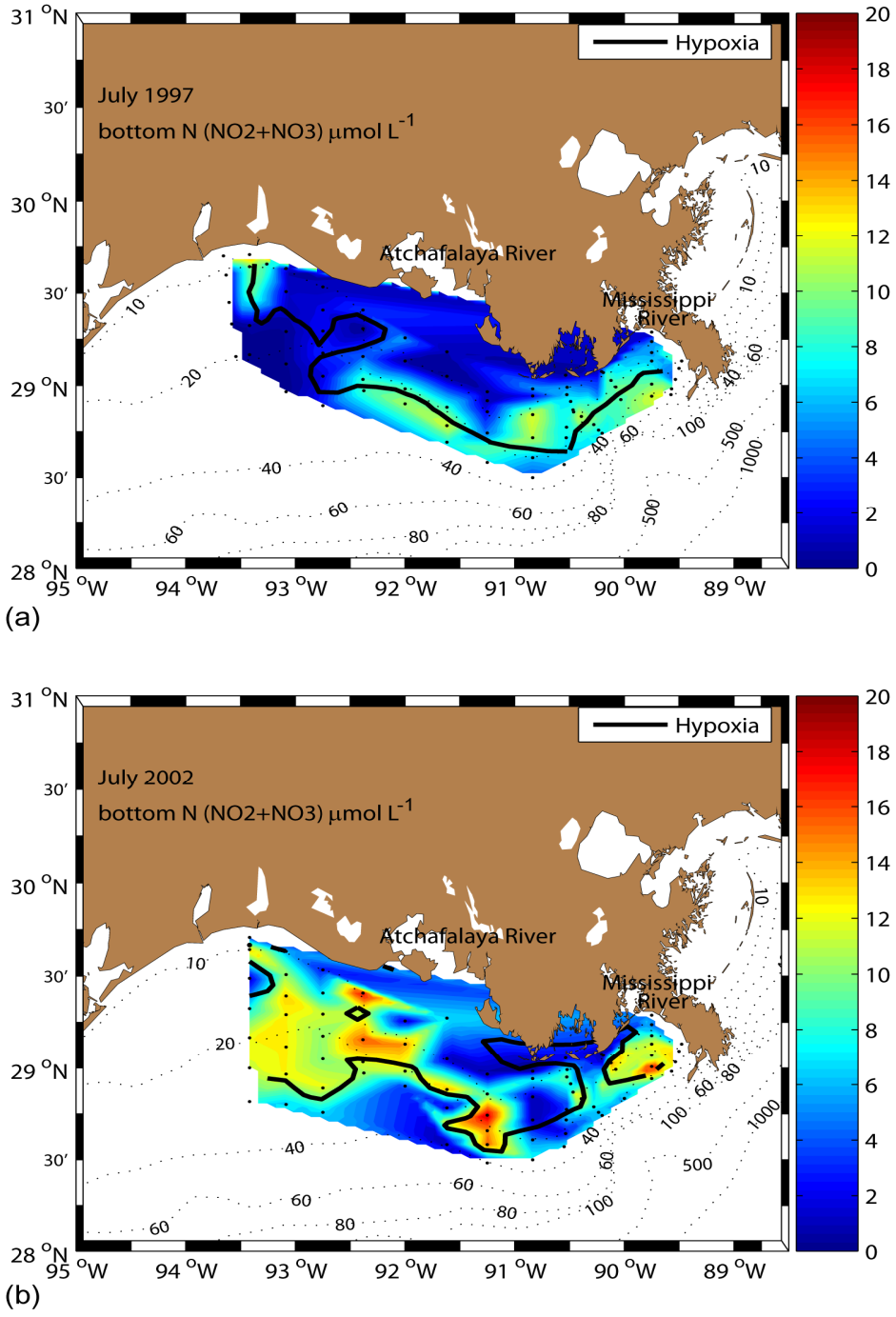

Figure 2.10: The bottom water N (NO2+NO3) concentration distributions in (a) In July 1997, and (b) in July 2002. The thick solid line delineates the boundary of hypoxic condition (i.e. dead zone).

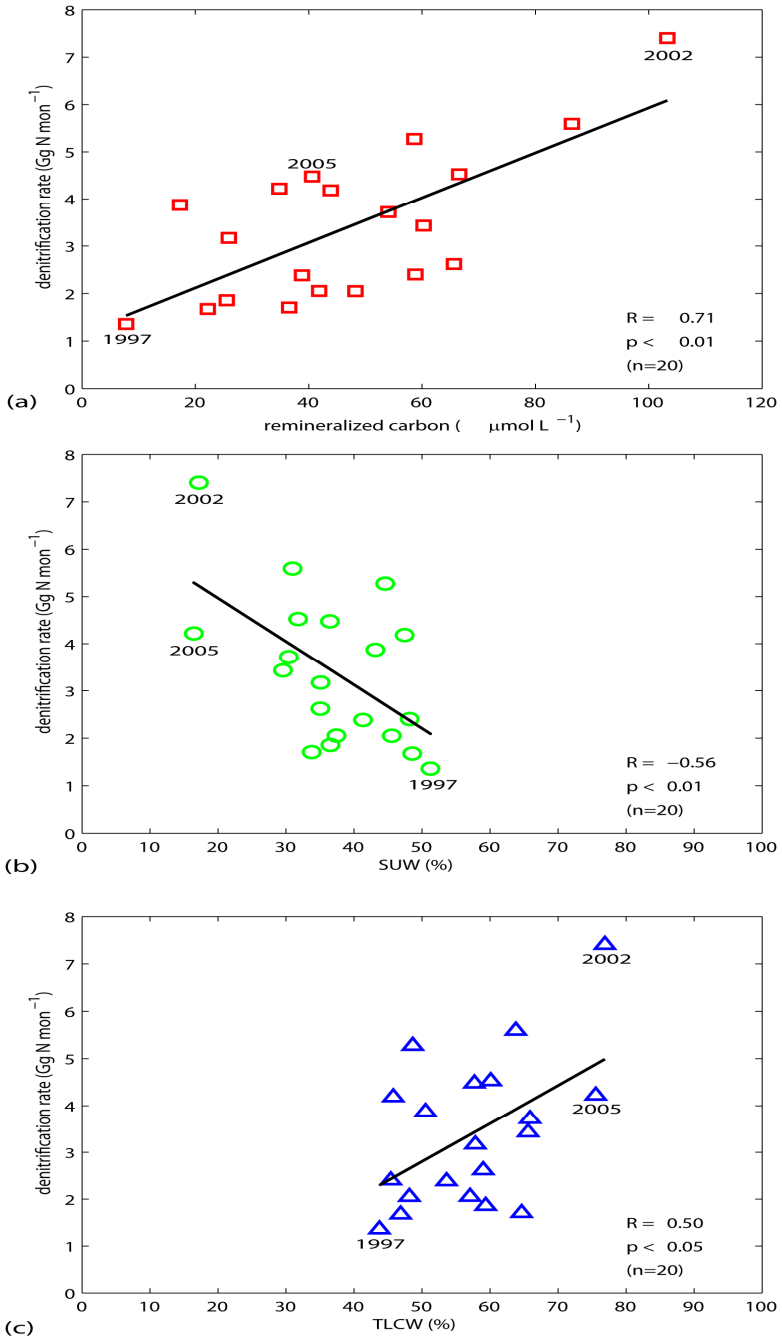

Figure 2.11: Relationships between denitrification rate (Gg N mon^{-1}) and (a) the amount of remineralized carbon (µmol L^{-1}), (b) mixing ratios of SUW (%), and (c) mixing ratios of TLCW (%), with corresponding correlation coefficients (R). The mean values are averaged from the cases 1-4 (Tables 2.5-7). *P* values were calculated by *t*-test (n=20).

Chapter 3: Implication of deep nitrate deficit observed in the highly oxygenated East/Japan Sea

1. INTRODUCTION

Denitrification is a process mediated microbiologically that reduces nitrate to nitrite to nitrous oxide and dinitrogen ($NO_3^- \rightarrow NO_2^- \rightarrow N_2O/N_2$) to decompose organic matters in the absence of oxygen. Denitrification occurs under low oxygen conditions in the environment because nitrate is used as the electron acceptor instead of oxygen (Hulth et al., 2005; Brandes et al., 2007; Naqvi et al., 2010). Denitrification removes nitrate from the water deviating the nitrate to phosphate (N/P) ratio to below the traditional Redfield ratio of 16 (Hupe and Karstensen, 2000). The East/Japan Sea (EJS) is a marginal sea, with a maximum depth close to 4,000m, adjacent to the western North Pacific Ocean (Chang et al., 2004). It exhibits many open ocean-like features including deep-water formation (Talley et al., 2006). Denitrification was not considered as a significant process affecting the nitrogen cycle in EJS, because the sea is well oxygenated throughout the water column (>190 μmol kg^{-1} at minimum).

The global average N/P ratio of 14.5 in the oceanic water column lies below the traditional Redfield ratio of 16, indicating potential nitrogen removal via denitrification (Deutsch and Weber, 2012). The EJS also shows peculiarly low N/P ratio (9.8 to 14.70) compared to the traditional Redfield ratio (Table 3.1), but its driving mechanism is not yet understood clearly. However, recent studies suggest the possibility of denitrification in EJS. Deep nitrite signals occurred near the bottom in the deep basins of EJS (Talley et al., 2001; Lee et al., 2007). The basin-wide mean denitrification rates were estimated at 1.5×10^{10} g N d^{-1} from nitrogen mass balance calculations (Yanagi, 2002) and at 0.9×10^{10} g N d^{-1} from organic matter mass balance (Tishchenko, et al., 2007). Direct measurements of denitrification rates from sediments yielded 14.1-75.3 μmol N m^{-2} d^{-1} at the shelf of Dok-Island in the Ulleung Basin (Jeong et al., 2009). Cyanobacteria, which are capable of nitrogen fixation in the marine system, cover 10-50% of the phytoplankton

community in the surface layer of EJS. Their presence may reflect compensation to supply nitrogen against the loss of nitrogen from denitrification (Kim et al., 2010c).

Most of these studies just mention denitrification (Kim et al., 2010c; Yanagi, 2002), or the sedimentary denitrification (Lee et al., 2007; Jeong et al., 2009; Talley et al., 2001; Tishchenko et al., 2007) in EJS only briefly and not in detail. In general, sedimentary denitrification occurs if oxygen is depleted in the sediments, even if water column oxygen concentrations near the sediment-water interface are high. Previous estimates of denitrification rates were derived for the whole water column of EJS (Tishchenko et al., 2007; Yanagi, 2002), except for one study of denitrification rates from sediment (Jeong et al., 2009).

Denitrification is generally classified as water column and benthic denitrification, depending on the source of nitrate. Water column denitrification is driven by the nitrate remineralized in the water column, and benthic denitrification is driven by nitrate both from the sediments and the overlying waters. These reactions typically occur under very low oxygen conditions where nitrate becomes the next available electron acceptor for the process. We found deep secondary nitrite peaks in the EJS (Fig. 3.2), but it is uncertain whether the signals come from bottom water or sediment. I therefore hypothesize that denitrification is occurring within a thick bottom water layer including the sediment surface (See ΔH in Fig. 3.6d-f) at certain local areas, such as the Ulleung Basin and near the Tatar Strait, instead of over the entire EJS. My questions are; "What evidence supports the occurrence of denitrification in the bottom layer?" and "What mechanisms drive the process?".

The main goals of this study are to (1) present evidence indicating denitrification in the Ulleung Basin and the Tatar Strait regions through qualitative and quantitative data analysis, (2) estimate denitrification rates from the extended Optimum Multi-Parameter (OMP) analysis and the nitrate profile analysis using the relationship of Redfield ratios, and (3) speculate about possible mechanisms supporting this denitrification pattern.

2. DATA

Basin-wide hydrographic observations were made in the summer of 1999 by two expeditions, covering the whole EJS, except for the North Korean territorial waters (Fig. 3.1). The expeditions were conducted via the Circulation Research of East Asian Marginal Seas II (CREAMS II) program, as a collaborative research effort among the United States, Russia, and South Korea. More specific cruise information is available in Talley et al. (2004), and the data used for the current analysis was obtained from http://sam.ucsd.edu/onr_data/hydrography.html. Here, latitude, longitude, pressure, potential temperature (PT), salinity (S), dissolved oxygen (DO), nitrate (N), phosphate (P), silicate (Si), total alkalinity (Talk), and dissolved inorganic carbon (DIC) were used for the analysis. Note that the DIC values were calculated from total alkalinity and total pH through the CO2SYS program (Van Heuven et al., 2009). Only the data below 300dbar were analyzed to minimize any influence of seasonal variation. The bottom depths at individual stations were obtained from information of the CTD casting depth and its height above the bottom (i.e. water-sediment interface). The deep EJS was divided into the Japan Basin (JB), the Ulleung Basin (UB), and the Yamato Basin (YB). JB was divided into the Western Japan Basin (WJB) and the Eastern Japan Basin (EJB) with a boundary along 135°E, for a more convenient analysis presentation (Fig. 3.1).

3. RESULTS AND DISCUSSIONS

3.1 Evidence indicating the occurrence of denitrification in the bottom layer

3.1.1 The N/P ratio of EJS

The N/P ratio of EJS based on the 1999 data was estimated at 12.4±0.1 (Fig. 3.3a), which is lower than the traditional Redfield ratio of 16. This result could indicate a large-scale denitrification in the sea. No direct evidence, however, is yet available to support that conclusion. Some nutrient data deviate from the fitted regression line at

higher concentration ranges (Fig. 3.3b), and provide evidence that nitrate was depleted by denitrification under certain conditions in EJS.

The low DO feature is well developed in EJB near TtS between 500 and 1100dbar depth, and in UB between 1100 and 2200dbar depth, both near the bottom (Fig. 3.4a). Nitrite (NO_2^-) is an intermediate nitrogen product occurring in nitrification ($NH_4^+ \rightarrow NO_2^- \rightarrow NO_3^-$), denitrification ($NO_3^- \rightarrow NO_2^- \rightarrow N_2O/N_2$), or dissimilatory nitrate reduction to ammonium (DNRA; $NO_3^- \rightarrow NO_2^- \rightarrow NH_4^+$), and it is a useful indicator to distinguish oxidative vs. reductive pathways in the nitrogen cycle (Lomas and Lipschultz, 2006). Generally, a primary nitrite peak is produced by nitrification in the shallow euphotic layer, and nitrite below this depth may accumulate by either denitrification or DNRA (Kelso et al., 1997). However, DNRA occurs primarily in estuarine and coastal sediments under anaerobic conditions (Kaspar, 1983; Binnerup et al., 1992; Brandes et al., 2007), and its end product, NH_4^+, is eventually converted to nitrate via nitrification ($NH_4^+ \rightarrow NO_2^- \rightarrow NO_3^-$). This process, in the long run, conserves nitrogen sources (Burgin and Hamilton, 2007), and its quantitative significance in deep waters is unknown (Zehr and Kudela, 2011). Most nitrite concentrations higher than 0.01 μmol kg^{-1} were detected in the same areas in the two basins (Fig. 3.4b). Therefore, nitrite accumulation in the bottom layer of EJS may be derived from denitrification. A N/P ratio minimum may develop significantly at the low oxygen content layer as a result of nitrate loss (Fig. 3.4c). Collectively, the features shown in Fig. 3.4 support the presence of denitrification in the bottom waters of EJS.

3.1.2 Detailed analysis of vertical property distribution

Remineralization processes in the water column increase nitrate concentration with depth as sinking organic matter is decomposed with consumption of DO. On the other hand, denitrification decreases nitrate concentration and produces nitrite. Two stations (Stas. 10 and 121) in UB and one station (Sta. 129) in EJB near TtS were selected as representative examples representing the most clear denitrification signals among the stations with $[NO_2^-]$>0.01 μmol kg^{-1} (Fig. 3.2). The vertical profiles of DO, nitrate,

phosphate, nitrite, and N/P ratio data at these stations (Stas. 10, 121, and 129) were analyzed. The profiles at both areas show decreases of DO and nitrate, increase of phosphate, lower N/P ratio, and detectable nitrite, simultaneously suggesting denitrification.

Stas. 10 and 121 are located in the mid to lower part of the continental slope of UB, respectively (Fig. 3.5a). The DO decreases sharply toward the bottom depth at Stas. 10 (1380dbar) and 121 (1894dbar) over few hundred meters of depth (Figs. 3.5c and e). The phosphate concentration increases toward the bottom, while nitrate concentration decreases slightly near the bottom (Figs. 3.5d and f). A deep nitrite peak (Figs. 3.5c and e) and local N/P ratio lower than the basin average (Fig. 3.5b) are apparent at the bottom layer. Sta. 129 is located on the upper part of the continental slope in EJB near TtS with a relatively shallow bottom depth (609dbar) (Fig. 3.5a). The profiles at the Sta. 129 show similar patterns to those of Stas. 10 and 121 (Figs. 3.5b and g-h).

3.2 Estimation of denitrification rates

The N^* (=N - 16P + 2.9 μmol kg^{-1}) method can estimate large-scale denitrification using hydrographic data (Gruber and Sarmiento, 1997; Deutsch et al., 2001). If the N^* method is applied in EJS, the whole water column below 300dbar shows negative N^* values, indicating prevailing denitrification in EJS. Considering well-oxygenated water column (O_2>190 μmol kg^{-1}) of EJS and evidences addressed at Section 3.1, the N^* method may overestimate denitrification in EJS. Thus, the denitrification rates were estimated with the nitrate profile analysis using the relationship of Redfield ratios and the extended OMP analysis.

3.2.1 The nitrate profile analysis using the relationship of Redfield ratios

The observed respective nitrate concentrations are a sum of the preformed nitrate and the remineralized nitrate (eqn. 1). The preformed nitrate (~11 μmol kg^{-1}) at the cold surface water is transported into the interior of EJS along with its deep water formation

(Kim et al., 1992). The bottom layer may have a nitrate sink due to denitrification (Fig. 3.6). The observed nitrate then can be expressed as:

$$[NO_3]_{obs}^{z-1} = [NO_3]_{pre}^{z-1} + [NO_3]_{remi}^{z-1} \quad (1)$$

and

$$[NO_3]_{obs}^{z} = [NO_3]_{pre}^{z} + [NO_3]_{remi}^{z} - [NO_3]_{deni}^{z} \quad (2)$$

where, the superscripts z-1 and z are the upper and lower boundary depths of denitrification, and the subscripts *obs*, *pre*, *remi*, and *deni* are for the observed, preformed, remineralized, and denitrified nitrate concentrations, respectively. The depth pairs for z-1 and z for Stas. 10, 121, and 129 are 1314 and 1375dbar, 1784 and 1886dbar, and 508 and 602dbar, respectively. If it is assumed that the preformed nitrate concentrations are same at the two depths (i.e. $[NO_3]_{pre}^{z-1} = [NO_3]_{pre}^{z}$), the amount of denitrification can be estimated by (Eq. 2 – Eq. 1):

$$[NO_3]_{deni}^{z} = \left([NO_3]_{obs}^{z-1} - [NO_3]_{obs}^{z}\right) + \left([NO_3]_{remi}^{z} - [NO_3]_{remi}^{z-1}\right) \quad (3)$$

The remineralized nitrate can be substituted by the oxygen consumption or phosphate production as follows:

$$[NO_3]_{deni}^{z} = \left([NO_3]_{obs}^{z-1} - [NO_3]_{obs}^{z}\right) + r_{N/-O2} \times \left([AOU]_{f(T,S)}^{z} - [AOU]_{f(T,S)}^{z-1}\right) \quad (4)$$

or

$$[NO_3]_{deni}^{z} = \left([NO_3]_{obs}^{z-1} - [NO_3]_{obs}^{z}\right) + r_{N/P} \times \left([PO_4]_{obs}^{z} - [PO_4]_{obs}^{z-1}\right) \quad (5)$$

where, $[AOU]_{f(T,S)}$ is the apparent oxygen utilization (AOU), which is the difference between the observed DO and the saturated DO calculated as a function of temperature and salinity. Surface water oxygen concentration is assumed to be at equilibrium with the atmosphere. Both the observed (12.4/118 and 12.4/1) and traditional (16/138 and 16/1) Redfield ratios for $r_{N/-O2}$ and $r_{N/P}$ were used in the analysis.

The estimated denitrification was ca. 0.4–0.9 μmol N kg^{-1} at 1375dbar at Sta. 10, 0.4-0.6 μmol N kg^{-1} at 1886dbar at Sta. 121, and 0.8-1.5 μmol N kg^{-1} at 602dbar at Sta. 129, respectively (Figs. 3.6a-c). Sta. 129 located in EJS near TtS showed slightly higher

amount of denitrification. From the difference between the observed and expected nitrate (=ΔN) above the bottom, the estimated relative age difference (=Δage) between the upper and lower boundary of the area (=ΔH), and the triangular area (=1/2·ΔN·ΔH) between the two, the denitrification rate can be estimated (Figs. 3.6d-f). The expected ($=[NO_3]^{\tau}_{obs}+[NO_3]^{\tau}_{deni}$) and observed nitrate concentrations are extrapolated linearly to the bottom depth (Figs. 3.6d-f). The relative age, defined by AOU (μmol kg^{-1}) divided by the oxygen utilization rate (OUR; μmol kg^{-1} yr^{-1}), is one way to obtain the information on the time scale of accumulating denitrification signals in the bottom layer (Poole and Tomczak, 1999; Karstensen et al., 2008; Kim et al., 2010a). It is assumed that the relative age increases with depth and horizontal advection is small in these two regions. The OUR as a function of depth (z) in the basins can be parameterized as OUR (z) = $6.592e^{-0.0011\cdot Z}$ at UB and $10.680e^{-0.00138\cdot Z}$ at EJB (Kim et al., 2010b). When the UB's OUR values (Stas. 10 and 121) are transformed to oxygen consumption flux in the bottom layer (i.e. $0.85-1.60\frac{\mu mol\ N}{kg\cdot yr}\times\rho\left(\frac{kg}{m^3}\right)\times\Delta H(m)=0.26-0.30\frac{mmol\ N}{m^2\cdot d}$), they are compatible with previous values (Kang et al., 2011): 0.24-0.30 mmol O_2 m^{-2} d^{-1} with ΔH = 80-100m at UB. The denitrification rate is then estimated as:

$$deni.\ rate=\frac{1}{2}\times\Delta N\left(\frac{\mu mol\ N}{kg}\right)\times\rho\left(\frac{kg}{m^3}\right)\times\Delta H(m)/\Delta age(yr) \qquad (6)$$

where, ρ is seawater density. The estimated denitrification rates and the components (i.e. ΔN, ΔH, and Δage) are summarized in Table 3.2. The estimated denitrification rates near the bottom are approximately 17.5-33.2 μmol N m^{-2} d^{-1} at Sta. 129 on the upper part of the continental slope, 4.2-9.1 μmol N m^{-2} d^{-1} at Sta. 10 on the mid part of the continental slope, and 2.8-4.4 μmol N m^{-2} d^{-1} at Sta. 121 on the lower part of the continental slope (Table 3.2). It implies that there might be a spatial gradient of denitrification rates along the continental slope (upper-mid-lower). More samples along the continental slope should be examined in future studies.

3.2.2 The extended OMP analysis

Generally, the measurements of ocean parameters are determined by physical mixing combined with biogeochemical processes (Anderson and Sarmiento, 1994). The extended OMP analysis provides one way to consider physical mixing and biogeochemical processes together. Since that time, the basic OMP analysis was developed (Tomczak and Large 1989), and the current format of the extended OMP analysis was improved, The extended OMP analysis quantified the amount of water column denitrification in the Arabian Sea (Hupe and Karstensen, 2000). The matrix form of extended OMP analysis is written as:

$$\begin{bmatrix} PT_1 & + \cdots + & PT_4 & + & 0 & + & 0 & + & 0 \\ S_1 & + \cdots + & S_4 & + & 0 & + & 0 & + & 0 \\ DO_1 & + \cdots + & DO_4 & - & r_{O2/P} & + & 0 & + & 0 \\ P_1 & + \cdots + & P_4 & + & 1 & + & r_D & + & 0 \\ N_1 & + \cdots + & N_4 & + & r_{N/P} & - & 1 & + & 0 \\ Si_1 & + \cdots + & Si_4 & + & r_{Si/P} & + & 0 & + & 0 \\ TALK_1 & + \cdots + & TALK_4 & - & r_{N/P} & + & 1 & + & 2 \\ DIC_1 & + \cdots + & DIC_4 & + & r_{Corg/P} & + & r_D r_{Cirg/P} & + & 1 \\ 1 & + \cdots + & 1 & + & 0 & + & 0 & + & 0 \end{bmatrix} \times \begin{bmatrix} x_1 \\ x_2 \\ x_3 \\ x_4 \\ \Delta P_{remi} \\ \Delta N_{deni} \\ \Delta C_{inorg} \end{bmatrix} - \begin{bmatrix} PT_{obs} \\ S_{obs} \\ DO_{obs} \\ P_{obs} \\ N_{obs} \\ Si_{obs} \\ TALK_{obs} \\ DIC_{obs} \\ 1 \end{bmatrix} = \begin{bmatrix} R_{PT} \\ R_S \\ R_{DO} \\ R_P \\ R_N \\ R_{Si} \\ R_{TALK} \\ R_{DIC} \\ R_{MC} \end{bmatrix}$$

$$\boldsymbol{A} \qquad \boldsymbol{x} \quad \boldsymbol{X} \quad - \quad \boldsymbol{b} \quad = \boldsymbol{R} \quad (7)$$

where, the matrix **A** is defined as the physicochemical characteristics of the source water types, the column $\boldsymbol{X}$ is composed of mixing ratios (x_i) among source water masses, the amount of remineralized phosphate (ΔP_{remi}), the amount of denitrification (ΔN_{deni}), the amount of inorganic carbonate dissolution (ΔC_{inorg}), the column **b** is the observations, and the column **R** is the residuals of parameters. The last row that consists of '1' is to constrain the mass conservation ($\sum x_i$=1). The ratios of $r_{C:Si:N:P:-O2}$ indicate the Redfield ratios, and r_D is a ratio to express the amount of phosphate produced by denitrification and is given as 1/104 (Gruber and Sarmiento, 1997; Hupe and Karstensen, 2000). The extended OMP analysis is based on an over-determined system, so the non-negative solutions (x_i, ΔP_{remi}, ΔN_{deni}, and ΔC_{inorg}) are defined by minimizing residuals.

3.2.2.1 Modification of the silicate equation in the extended OMP analysis

The silicate equation in the extended OMP analysis can be represented as follows:

$$Si_{obs} + R_{Si} = \sum_{i=1}^{n} x_i \cdot Si_i + r_{Si/P} \cdot \Delta P \quad (8)$$

where, Si_{obs} is the observed silicate, R_{si} is the silicate residual, and $\sum_{i=1}^{n} x_i \cdot Si_i$ is the combination of mixing ratios (x_i) and silicate characteristics of source water types defined (Si_i) (Hupe and Karstensen 2000). The $r_{Si/P} \cdot \Delta P$ can be expressed as the result of silicate dissolution. However, the observed silicate in the water column is determined by three components including physical mixing ($\sum_{i=1}^{n} x_i \cdot Si_i$), remineralization, and dissolution (Park, 1967; Kido and Nishimura, 1973). Thus, the effect of remineralization was not considered. As shown in Fig. 3.7, two slopes are obvious. The first slope ranges approximately from 0.75 (at 300dbar) to 1.75 (at ~900dbar) of phosphate concentrations (μmol kg^{-1}), and the second one ranges from ca. 1.75 (at ~900dbar) to ca. 2.2 (at ~3700dbar). When P vs. Si is fitted with a linear regression, the determination coefficient (r^2) is substantially poor (Fig. 3.7b). So, the silicate equation in the extended OMP analysis is revised as:

$$Si_{obs} + R_{Si} = \sum_{i=1}^{n} x_i \cdot Si_i + r_{Si/P} \cdot \Delta P + \Delta Si_{inorg} \quad (9)$$

The silicate remineralization is expressed as $r_{Si/P(\approx 28)} \cdot \Delta P$ (Fig. 3.7a), and the silicate dissolution (ΔSi_{inorg}) is placed on the column **X** as an additional unknown variable.

3.2.2.2 Modification of the total alkalinity equation in the extended OMP analysis

The total alkalinity equation is influenced by physical mixing ($\sum_{i=1}^{n} x_i \cdot TALK_i$), remineralization ($r_{N/P} \cdot \Delta P_{remi}$), denitrification ($\Delta N_{deni}$), and carbonate dissolution ($2\Delta C_{inorg}$), as shown in equation (1). Initially only the effect of nitrate by remineralization ($r_{N/P} \cdot \Delta P_{remi}$) was considered as a negative ion on the total alkalinity equation (Hupe and

Karstensen 2000). Although the remineralized phosphate (ΔP_{remi}) is quantitatively small, the ΔP_{remi} also affects the total alkalinity as one of negative ions (Zeebe and Wolf-Gladrow, 2001). In addition, denitrification regenerates some phosphate from organic matters (Gruber and Sarmiento, 1997) as follows:

$$C_{106}H_{175}O_{42}N_{16}P + 104NO_3^- \rightarrow 4CO_2 + 102HCO_3^- + 60N_2 + 36H_2O + HPO_4^{2-} \quad (10)$$

Therefore, the total alkalinity equation is revised here as follows:

$$TALK_{obs} + R_{TALK} = \sum_{i=1}^{n} x_i \cdot TALK_i - (r_{N:P} + 1) \cdot \Delta P + (1 - r_d) \cdot \Delta N_{deni} + 2\Delta C_{inorg} \quad (11)$$

The extended OMP analysis is then given as:

$$\begin{bmatrix} PT_1 & + \cdots + & PT_4 & + & 0 & + & 0 & + & 0 & + & 0 \\ S_1 & + \cdots + & S_4 & + & 0 & + & 0 & + & 0 & + & 0 \\ DO_1 & + \cdots + & DO_4 & - & r_{O2/P} & + & 0 & + & 0 & + & 0 \\ P_1 & + \cdots + & P_4 & + & 1 & + & r_D & + & 0 & + & 0 \\ N_1 & + \cdots + & N_4 & + & r_{N/P} & - & 1 & + & 0 & + & 0 \\ Si_1 & + \cdots + & Si_4 & + & r_{Si/P} & + & 0 & + & 0 & + & 1 \\ TALK_1 & + \cdots + & TALK_4 & - & (r_{N/P} + 1) & + & (1 - r_D) & + & 2 & + & 0 \\ DIC_1 & + \cdots + & DIC_4 & + & r_{Corg/P} & + & r_D r_{Corg/P} & + & 1 & + & 0 \\ 1 & + \cdots + & 1 & + & 0 & + & 0 & + & 0 & + & 0 \end{bmatrix} \times \begin{bmatrix} x_1 \\ x_2 \\ x_3 \\ x_4 \\ \Delta P_{remi} \\ \Delta N_{deni} \\ \Delta C_{inorg} \\ \Delta Si_{inorg} \end{bmatrix} - \begin{bmatrix} PT_{obs} \\ S_{obs} \\ DO_{obs} \\ P_{obs} \\ N_{obs} \\ Si_{obs} \\ TALK_{obs} \\ DIC_{obs} \\ 1 \end{bmatrix} = \begin{bmatrix} R_{PT} \\ R_S \\ R_{DO} \\ R_P \\ R_N \\ R_{Si} \\ R_{TALK} \\ R_{DIC} \\ R_{MC} \end{bmatrix} \quad (12)$$

3.2.2.3 Physicochemical characteristics of source water types

The physicochemical characteristics of eight different source water types can be defined by using geographical locations and water properties such as temperature, salinity, and DO, i.e.: (1) North Korea Surface Water (NKSW), (2) East Korean Coastal Water (EKCW), (3) Modified Tsushima Surface Water (MTSW), (4) Tatar Surface Cold Water (TSCW), (5) Tsushima Middle Water (TMW), (6) Liman Cold Water (LCW), (7) East Sea Intermediate Water (ESIW), and (8) East Sea Proper Water (ESPW). The source water types (1)-(4) are surface water, (5)-(7) are intermediate water, and (7) and (8) are deep water (Kim and Lee 2004). Because only the data collected deeper than 300dbar is considered, only TMW, LCW, ESIW, and ESPW are included among eight different

source water types used in the extended OMP analysis. The physicochemical characteristics of source water types are summarized in Table 3.3.

3.2.2.4 Redfield ratios and weights used for the extended OMP analysis

The calculations of biogeochemical processes in the extended OMP analysis are based on the relationship of Redfield ratios ($r_{C:Si:N:P:-O2}$). The traditional Redfield ratios, $r_{C:N:P:-O2}$=106:16:1:-138, have been used widely (Redfield et al., 1963). These ratios are common in the worlds' open oceans, but substantial regional differences occur among different ocean basins and depths. Recent observations indicate that the traditional Redfield ratios need to be revised slightly. For example, the traditional Redfield ratios was reexamined through a non-linear approach in deep oceans (>400m), and a revision of $r_{C:N:P:-O2}$=117±14:16±1:1:-170 was suggested (Anderson and Sarmiento 1994). Subsequently, The mean organic matter composition of marine phytoplankton was reanalyzed, and the Redfield ratio revised to $r_{C:N:P:-O2}$=106:16:1:150±10 (Anderson 1995). The EJS's Redfield ratios fitted by linear regression analysis (>300dbar) were estimated here as $r_{C:N:P:-O2}$=103:12.4:1:118 (Fig. 3.8). To check the sensitivity according to the use of different Redfield ratios, four different cases are considered (Table 3.4): (Case 1) $r_{C:N:P:-O2}$=106:16:1:138, (Case 2) $r_{C:N:P:-O2}$=117±14:16±1:1:170, (Case 3) $r_{C:N:P:-O2}$=117:16:1:170, and (Case 4) $r_{C:N:P:-O2}$=103:12.4:1:118. The ratio of $r_{Si:P}$=28 estimated in the EJS (Fig. 3.7a) was used uniformly for Cases 1-4.

Since each parameter differs in accuracy and precision, the basic/extended OMP analysis assigns the weight values for each parameter. A weight equation as follows:

$$W_j = \frac{\sigma_j^2}{\delta_{j\max}} \tag{13}$$

where, σ_j^2 is the variance of parameter j calculated from the physicochemical characteristics of source water types, and δ_{jmax} is the largest one among the variances of parameters estimated in the source regions of source water types (Tomczak and Large 1989). A modified weight equation was suggested because of the limitation of data

availability in regions of source water types and insufficient information about exact their source regions (Kim and Lee 2004), that is:

$$W_j = \frac{\sigma_j}{accuracy_j} \quad (14)$$

where, σ_j is the standard deviation of parameter j calculated from the physicochemical characteristics of source water types, and $accuracy_j$ is the measurement error of parameter j. The weight values used for the extended OMP analysis are summarized in Table 3.5. Note that the weight of DIC was assigned with the same value as that of TALK, because the DIC was estimated from total alkalinity and total pH.

3.2.2.5 Residuals of mass conservation

The last row that consists of '1' in the eq. 12 constrains the mass conservation ($\sum_{i=1}^{4} x_i = 1$). This constraint is used as a tracer to examine the validation of the results of extended OMP analysis (Tomczak and Large, 1989). The residuals of mass conservation (R_{MC}) are calculated as follows:

$$R_{MC}(\%) = \left(\sum_{i=1}^{4} x_i - 1 \right) \times 100 \quad (15)$$

A plot of potential density vs. residuals of mass conservation (Fig. 3.9) shows a slight increase in the residuals between 27.3 and 27.35 σ_θ, but overall the residuals (cases 1-4) are defined within ~2.5%.

3.2.2.6 Potential denitrification locations expected

The extended OMP analysis suggested that eight stations (10, 16, 17, 19, 118, 120, 126, and 129), intersected from Cases 1-4, collectively, were considered as the locations where denitrification ($\Delta N_{deni}>0$) may occur in EJS (Fig. 3.10). Six stations (10, 16, 17, 19, 118, and 120) were in the UB, and two stations (126 and 129) were near the TtS.

The extended OMP analysis did not reproduce the station of 121 (see 3.2.1) as the potential denitrification location, perhaps due to the variation of physicochemical properties in source regions and the limitation of data distribution covering the study area. Overall, the spatial distribution of denitrification estimated from the extended OMP analysis was similar to that from the nitrate profile analysis in which estimated denitrification was higher in the EJB than in the UB. The mean denitrification concentrations of the eight stations ranged from about 51±0.1 to 530±330 μmol N m^{-3} at the bottom layer (Table 3.6). The denitrification rates are estimated with the eight stations below Section 3.2.2.7.

3.2.2.7 Denitrification rates in the bottom layer

The extended OMP analysis provides the amount of denitrification with concentration. Length (m) and time (ΔT) information is needed to change concentration to rate. As shown in Fig. 3.11, denitrification is assumed to occur within the triangular area at the bottom ($=1/2 \cdot \Delta N_{deni} \cdot \Delta H$), and the time information (ΔT) between the upper and the lower boundary (ΔH) is estimated from the concept of relative age used in Section 3.2.1. The OUR estimated for UB ($OUR(z) = 6.592e^{-0.0011 \cdot Z}$) was used for the six stations (10, 16, 17, 19, 118, and 120), and the OUR for EJB ($OUR(z) = 10.680e^{-0.00138 \cdot Z}$) for the other two stations (126 and 129). The detailed approach is described in Section 3.2.1.

The denitrification rates estimated from the extended OMP analysis in the UB range from 0.3±0-3±1 μmol N m^{-2} d^{-1}, and that in the EJB range from 3±4-11±7 μmol N m^{-2} d^{-1} (Table 3.6). The denitrification rates estimated from the nitrate profile analysis and the extended OMP analysis ranged from about 0.3-33.2 μmol N m^{-2} d^{-1} (Tables 3.2 and 6).

3.3 Validation of the estimated denitrification rates

The denitrification rates estimated previously (Yanagi 2002; Tishchenko et al., 2007), 1.5 x 10^{10} g N d^{-1} and 0.9 x 10^{10} g N d^{-1}, respectively, are rather large. These values are compared to the estimates of this study through a simple rate transformation. The transformed value, for Yanagi (2002) for example, would be:

$$deni.\ rate_{(Yanagi,2002)} = 1.5\times10^{10}\frac{g\ N}{d}\times\frac{1mol\ N}{14g}/A = 1071.4\mu mol\ N\ m^{-2}d^{-1} \quad (16)$$

where, A (=1.008 x 10^{12} m^2) is the surface area of EJS. The transformed denitrification rates by Tishchenko et al., (2007) would be 661 μmol N m^{-2} d^{-1}. These values are 2-3 orders of magnitude larger than the values estimated from this study (0.3-33.2 μmol N m^{-2} d^{-1}). The denitrification rates at the hypoxic/anoxic seas, such as the Arabian Sea, the Black Sea, and the northern Gulf of Mexico, where denitrification rates are far greater, are 400-3780, 48-560, and 504-1056 μmol N m^{-2} d^{-1}, respectively (Gardner et al., 1993; McCarthy et al., 2007; Schwartz et al., 2009). The basin-wide estimates by Yanagi (2002) and Tishchenko et al., (2007) are similar to the values from the hypoxic/anoxic seas, even though EJS is oxygenated throughout the water column. Perhaps, the previous estimates are overestimated since the results (0.3-33.2 μmol N m^{-2} d^{-1}) are more comparable to the denitrification rates measured directly from sediments at the shelf of Dok Island in UB (14.1-75.3 μmol N m^{-2} d^{-1}) (Jeong et al., 2009).

3.4 Extended benthic denitrification to bottom waters vs. 'aerobic denitrification'

The results shown in Sections 3.1-3.3 supports the idea that denitrification occurs at certain areas in UB and EJB near TtS. However, the high oxygen content of the water column (>190 μmol kg^{-1}) in EJS for a conventional denitrification process to occur warrants caution in drawing a simple conclusion. I speculate two potential scenarios: (1) An upward extension of denitrifying bacterial activity in the sediments to the bottom waters via 'micro-reducing environments' caused by high deposition rates of organic matters along with recent warming and decrease in DO in the bottom layer, and (2) An

'aerobic denitrification', which utilizes both DO and nitrate in the deep water column of EJS, although this process has not been verified in an ocean system yet.

The UB is the most productive region in EJS due to a coupling of coastal upwelling and an active eddy feature (Lee and Kim, 2003; Hyun et al., 2009). The region near TtS is also a high primary production area due to the input of the Amur River (Tishchenko et al., 2007). Both regions are famous fishing grounds. These two regions would demand high oxygen consumption at the bottom due to high rates of supply and deposition of organic matters (Tishchenko et al., 2007; Lee et al., 2008). As inferred from extremely high sedimentation rates, accumulating sedimentary organic carbon contents up to ~4% (Cha et al., 2007; Lee et al., 2010), a 'micro reducing environment' may be formed in the bottom layer (Wolgast et al., 1998), enabling an upward extension of denitrifying bacterial activity from the sediments to the bottom waters above. Recent increases in atmospheric nitrogen deposition flux to EJS (Kim et al., 2011), warming of the water column (Gamo et al., 2001; Kim et al., 2001; Kim et al., 2004; Min and Kim, 2006), oxygen content decreases (Kim and Kim, 1996; Chen et al., 1999; Gamo, 1999; Kang et al., 2004), and high deposition rates of organic matters (Cha et al., 2007; Tishchenko et al., 2007; Lee et al., 2008; Hyun et al., 2010; Lee et al., 2010) might have created a favorable environment for denitrification in the bottom layer at the two basins in EJS in recent times.

An 'aerobic denitrification' is a newly found process in which certain bacteria (e.g. *Thiosphaera pantotropha* and *Pseudomonas stutzeri*) are able to use nitrate and DO simultaneously as electron acceptors in their respiration (Robertson and Kuenen, 1984a; Robertson et al., 1989; Robertson et al., 1995; Su et al., 2001). Both DO and nitrate decrease near the bottom at the current study sites (Fig. 3.4). Aerobic denitrification can occur in the 90% of DO saturation condition in culture experiments (Robertson and Kuenen, 1984b; Su et al., 2001). This implies aerobic denitrification may occur simultaneously with remineralization even in highly oxygenated water. Aerobic denitrification was reported for shallow intertidal waters in the German Wadden Sea (Gao et al., 2010). Sufficient supplies of organic matter and nitrate with high oxygen

consumption in UB and EJB near TtS might stimulate the aerobic denitrification, using nitrate and DO at the same time.

Although it is difficult to verify these speculations with the current data, this study poses important insights in the modern nitrogen cycle in EJS. We need to investigate benthic microbial environments at more slope and basin sites in EJS, and model the EJS's denitrification process. A model would help investigate how bottom water denitrification may contribute to a low water column N/P ratio in EJS.

4. CONCLUSIONS

Denitrification evidence was found in UB and EJB near TtS of EJS based on intensive analysis of N/P ratio, DO, nitrate, nitrite, and phosphate from the 1999 CREAMS II data. Decrease of nitrate concentrations, increase of phosphate concentrations, lower N/P ratio (<12.4), and deep nitrite peaks in the bottom layer are apparent in these two regions. The denitrification rates were estimated at 0.3-33.2 μmol N m^{-2} d^{-1} by the nitrate profile analysis and the extended OMP analysis, and were comparable to the denitrification rates measured directly from sediments. Although the detailed mechanisms of denitrification in the well-oxygenated EJS is still unclear, I speculate that the denitrifying bacterial activity might be active in the bottom waters via 'micro-reducing environment', or that 'aerobic denitrification' may possibly occur in the bottom waters of EJS. These speculations need to be examined in the future to improve understanding of EJS's nitrogen cycle.

REFERENCES

Anderson, L.A., 1995. On the hydrogen and oxygen content of marine phytoplankton. Deep-Sea Research I, 42, 1675-1680.

Anderson, L.A., and J.L. Sarmiento, 1994. Redfield ratios of remineralization determined by nutrient data analysis. Global Biogeochemical Cycles, 8(1), 65-80.

Binnerup, S.J. K. Jensen, N.P. Revsbech, M.H. Jensen, and J. Sørensen, 1992. Denitrification, dissimilatory reduction of nitrate to ammonium, and nitrification in a bioturbated estuarine sediments as measured with ^{15}N and microsensor techniques. Applied and Environmental Microbiology, 58(1), 303-313.

Brandes, J.A., A.H. Devol, and C. Deutsch, 2007. New developments in the marine nitrogen cycle. Chemical Reviews, 107(2), 577-589.

Burgin, A.J., and S.K. Hamilton, 2007. Have we overemphasized the role of denitrification in aquatic ecosystems? A review of nitrate removal pathways. Frontiers in Ecology and the Environment, 5(2), 89-96.

Cha, H.-J., M.S. Choi, C.-B. Lee, and D.-H. Shin, 2007. Geochemistry of surface sediments in the southwestern East/Japan Sea. Journal of Asian Earth Sciences, 29, 685-697.

Chae, Y.K., Y.H. Seung, and S.K. Kang, 2005. Mode change of deep water formation deduced from slow variation of thermal structure: one-dimensional model study. Ocean and Polar Research, 27(2), 115-123.

Chang, K.-I., W.J. Teague, S.J. Lyu, H.T. Perkins, D.-K. Lee, D.R. Watts, Y.-B. Kim, D.A. Mitchell, C.M. Lee, and K. Kim, 2004. Circulation and currents in the southwestern East/Japan Sea: Overview and review. Progress in Oceanography, 61, 105-156.

Chen, C.-T.A., A.S. Bychkov, S.L. Wang, and G.Yu. Pavlova, 1999. An anoxic Sea of Japan by the year 2200?. Marine Chemistry, 67, 249-265.

Chen, C.-T.A., G..-C. Gong, S.-L. Wang, and A.S. Bychkov, 1996. Redfield ratios and regeneration rates of particulate matter in the Sea of Japan as a model of closed system. Geophysical Research Letters, 23(14), 1785-1788.

Chung, C.S., J.H. Shim, Y.C. Park, and S.G. Park, 1989. Primary productivity and nitrogenous nutrient dynamics in the East Sea of Korea. The Sea, 24, 52-61.

Deutsch C., N. Gruber, R.M. Key, and J. Sarmiento, 2001. Denitrification and N_2 fixation in the Pacific Ocean. Global Biogeochemical Cycles, 15, 483-506.

Deutsch, C, and T. Weber, 2012. Nutrient ratios as a tracer and driver of ocean biogeochemistry. Annual Review of Marine Science, 4, 113-141.

Gao, H., F. Schreiber, G. Collins, M.M. Jensen, J.E. Kostka, G. Lavik, D.d. Beer, Zhou, H.-Y., M.M.M. Kuypers, 2010. Aerobic denitrification in permeable Wadden Sea sediments. The ISME Journal, 4, 417-426.

Gamo, T., 1999. Global warming may have slowed down the deep conveyor belt of a marginal sea of the northwestern Pacific: Japan Sea. Geophysical Research Letters, 26, 3137-3140.

Gamo, T., N. Momoshima, and S. Tolmacheyov, 2001. Recent upward shift of the deep convection system in the Japan Sea, as inferred from the geochemical tracers tritium, oxygen, and nutrients. Geophysical Research Letters, 28(21), 4143-4146.

Gardner, W.S., E.E. Briones, and E.C. Kaegi, 1993. Ammonium excretion by benthic invertebrates and sediment-water nitrogen flux in the Gulf of Mexico near the Mississippi River outflow. Estuaries, 16, 799-808.

Gruber, N., and J.L. Sarmiento, 1997. Global patterns of marine nitrogen fixation and denitrification. Global Biogeochemical cycles. 11(2), 235-266.

Hulth, S., R.C. Aller, D.E. Canfield, T. Dalsgaard, P. Engström, F. Gilbert, K. Sundbäck, and B. Thamdrup, 2005. Nitrogen removal in marine environments: recent findings and future research challenges. Marine Chemistry, 94, 125-145.

Hupe, A., and J. Karstensen, 2000. Redfield stoichiometry in Arabian Sea subsurface waters. Global Biogeochemical Cycles, 14(1), 357-372.

Hyun, J.-H., D. Kim, C.-W. Shin, J.-H. Noh, E.-J. Yang, J.-S. Mok, S.-H. Kim, H.-C. Kim, and S. Yoo, 2009. Enhanced phytoplankton and bacterioplankton production coupled to coastal upwelling and an anticyclonic eddy in the Ulleung Basin, East Sea. Aquatic Microbial Ecology, 54, 45-54.

Hyun, J.-H., J.-S. Mok, O.-R. You, D. Kim, and D.-L. Choi, 2010. Variations and controls of sulfate reduction in the continental slope and rise of the Ulleung Basin off the southeast Korean upwelling system in the East Sea. Geomicrobiology Journal, 27, 212-222.

Jeong, J.H., D.S. Kim, T.H. Lee, and S. An, 2009. High remineralization and denitrification activity in the shelf sediments of Dok Island, East Sea. The Sea, 14(2), 80-89.

Kang, D.-J., J.-Y. Kim, T. Lee, and K.-R. Kim, 2004. Will the East/Japan Sea become an anoxic sea in the next century?. Marine Chemistry, 91, 77-84.

Kang, D.-J., S. Park, Y.-G. Kim, K. Kim, and K.-R. Kim, 2003. A moving-boundary box model (MBBM) for oceans in change: An application to the East/Japan Sea. Geophysical Research Letters, 30(6), 1299, doi:10.1029/2002GL016486.

Kang, D.-J., Y.-B. Kim, and K.-R. Kim, 2011. Dissolved oxygen at the bottom boundary layer of the Ulleung Basin, East Sea. Ocean and Polar Research, 32(4). 439-448.

Karstensen, J., L. Stramma, and M. Visbeck, 2008. Oxygen minimum zones in the eastern tropical Atlantic and Pacific oceans. Progress in Oceanography, 77, 331-350.

Kaspar, H.F., 1983. Denitrification, nitrate reduction to ammonium, and inorganic nitrogen pools in intertidal sediments. Marine Biology, 74, 133-139.

Kelso, B.H.L., R.V. Smith, R.J. Laughlin, and S.D. Lennox, 1997. Dissimilatory nitrate reduction in anaerobic sediments leading to river nitrite accumulation. Applied and Environmental Microbiology, 63(12), 4679-4685.

Kido, K., and M. Nishimura, 1973. Regeneration of silicate in the Ocean. Journal of the Oceanographical Society of Japan, 29, 185-192.

Kim, I.-N., and T. Lee, 2004. Summer hydrographic features of the East Sea analyzed by the Optimum Multiparameter method. Ocean and Polar Research, 26(4), 581-594.

Kim, I.-N., D.-H. Min, and T. Lee, 2010b. Estimates of basin-specific oxygen utilization rates (OURs) in the East Sea (Sea of Japan). The Sea, 15(2), 86-96.

Kim, I.-N., D.-H. Min, D.H. Kim, and T. Lee, 2010a. Investigation of the physicochemical features and mixing of East/Japan Sea Intermediate Water: An isopycnic analysis approach. Journal of Marine Research, 68, 799-818.

Kim, J.-Y., D.-J. Kang, E, Kim, J.H. Cho, C.R. Lee, K.-R. Kim, and T. Lee, 2003. Biological pump in the East Sea estimated by a box model. The Sea, 8(3), 295-306.

Kim, K.-R., and K. Kim, 1996. What is happening in the East Sea (Japan Sea)?; Recent chemical observations during CREAMS 93-96. Journal of the Korean Society of Oceanography, 31(4), 164-172.

Kim, K., K.-R. Kim, D. Min, Y. Volkov, J.-H. Yoon, and M. Takematsu, 2001. Warming and Structural Changes in the East Sea(Japan Sea): A clue to future changes in Global Oceans?. Geophysical Research Letters, 28, 3293-3296.

Kim, K., K.-R. Kim, Y.-G. Kim, Y.-K. Cho, D.-J. Kang, M. Takematsu, and Y. Volkov, 2004. Water masses and decadal variability in the East Sea (Sea of Japan). Progress in Oceanography, 61, 157-174.

Kim, K.-R., T.S. Rhee, and K. Kim, 1992. A note on initial nitrate and initial phosphate as tracers for the origin of East Sea (Japan Sea) Proper Water, La mer, 30, 149-155.

Kim, T.-H. Y.-W. Lee, and G. Kim, 2010c. Hydrographically mediated patterns of photosynthetic pigments in the East/Japan Sea: Low N:P ratios and cyanobacterial dominance. Journal of Marine Systems, 82, 72-79.

Kim, T.-W., K. Lee, R.G. Najjar, H.-D. Jeong, and H.J. Jeong, 2011. Increasing N abundance in the marginal seas of the Northwestern Pacific Ocean due to atmospheric nitrogen deposition. Science, 334, 505-509.

Lee T, D. Kim, B.-K. Khim, and D.-L. Choi, 2010. Organic carbon cycling in Ulleung Basin sediments, East Sea. Ocean and Polar Research, 32(2), 145-156.

Lee, T. J.-H. Hyun, J.S. Mok, and D. Kim, 2008. Organic carbon accumulation and sulfate reduction rates in slope and basin sediments of the Ulleung Basin East/Japan Sea, Geo-Marine Letters, 28, 153-159.

Lee, T., and I.-N. Kim, 2003. Chemical imprints of the upwelled waters off the coast of the southern East Sea of Korea. Journal of the Korean Society of Oceanography, 38, 101-110.

Lee, T., I.-N. Kim, D.-J. Kang, and D. Kim, 2007. Implications of deep nitrite in the Ulleung Basin. The Sea, 12(3), 239-243.

Lomas, M.W., and F. Lipschultz, 2006. Forming the primary nitrite maximum: Nitrifiers or phytoplankton?, Limnology and Oceanography, 51(5), 2453-2467.

McCarthy, J.J. A. Yilmaz, Y. Coban-Yildiz, and J.L. Nevins, 2007. Nitrogen cycling in the offshore waters of the Black Sea. Estuarine, Coastal and Shelf Science. 74, 493-514.

Min, H.S., and C.-H. Kim, 2006. Water mass formation variability in the intermediate layer of the East Sea. Ocean Science Journal, 41(4), 255-260.

Moon, C.H., H.S. Yang, and K.W. Lee, 1996. Regeneration Processes of nutrients in the Polar Front Area of the East Sea I. Relationship between Water Mass and nutrient Distribution Pattern in Autumn. Journal of the Korean Fisheries Society, 29(4): 503-526.

Naqvi, S.W.A., H.W. Bange, L. Farias, P.M.S. Monteiro, M.I. Scranton, and J. Zhang, 2010. Marine hypoxia/anoxia as a source of CH_4 and N_2O. Biogeosciences, 7, 2159-2190.

Park, K., 1967. Nutrient regeneration and preformed nutrients off Oregon. Limnology and Oceanography, 12, 353-357.

Poole, R., and M. Tomczak, 1999. Optimum multiparameter analysis of the water mass structure in the Atlantic Ocean thermocline. Deep-Sea Research I, 46, 1895-1921.

Redfield, A.C., B.H. Ketchum, and F.A. Richards, 1963. The influence of organism on the composition of sea water, The sea, 2, 26-77.

Robertson, L.A., and J.G. Kuenen, 1984a. Aerobic denitrification – old wine in new bottles?. Antonie van Leeuwenhoek, 50, 525-544.

Robertson, L.A., and J.G. Kuenen, 1984b. Aerobic denitrification: a controversy revived. Archives of Microbiology, 139, 351-354.

Robertson, L.A., R. Cornelisse, P. De Vos, R. Hadioetomo, and J.G. Kuenen, 1989. Aerobic denitrification in various heterotrophic nitrifiers. Antonie van Leeuwenhoek., 56, 289-299.

Robertson, L.A., T. Dalsgaard, N.-P. Revsbech, and J.G. Kuenen, 1995. Confirmation of 'aerobic denitrification' in batch cultures, using gas chromatography and ^{15}N mass spectrometry. FEMS Microbiology Ecology, 18, 113-120.

Schwartz, M.C., C. Woulds, and G.L. Cowie, 2009. Sedimentary denitrification rates across the Arabian Sea oxygen minimum zone. Deep-Sea Research II, 56, 324-332.

Shim, J.H., S.R. Yang, and W.H. Lee, 1989. Phytohydrography and the vertical pattern of nitracline in the southern waters of the Korean East Sea in early spring. Journal of the Korean Society Oceanography, 24, 15-28.

Su, J.-J., B.-Y. Liu, and C.-Y. Liu, 2001. Comparison of aerobic denitrification under high oxygen atmosphere by Thiosphaera pantotropha ATCC 35512 and Pseudo monas stutzeri SU2 newly isolated from the activated sludge of a piggery wastewater treatment system. Journal of Applied Microbiology, 90, 457-462.

Talley L.D., P.Ya. Tishchenko, G. Mitchell, D.-J. Kang, D.-H. Min, A. Nedashkovskii, D. Masten, and P. Robbins, 2001. Nitrite in a deep, oxygenated environment the Japan/East Sea and Ulleung Basin. CREAMS 2001, Honolulu.

Talley, L.D., D.-H. Min, V.B. Lobanov, V.A. Luchin, V.I. Ponomarev, A.N. Salyuk, A.Y. Shcherbina, P.Y. Tishchenko, and I. Zhabin, 2006. Japan/East Sea water masses and their relation to the sea's circulation, Oceanography, 19(3), 32-49.

Talley, L.D., P.Ya. Tischenko, V. Luchin, A. Nedashkovskiy, S. Sagalaev, D.-J. Kang, M. Warner, and D.-H. Min, 2004. Atlas of Japan (East) Sea hydrographic properties in summer, 1999. Progress in Oceanography, 61, 277-348.

Tishchenko, P.Ya., L.D. Talley, V.B. Labanov, A.P. Nedashkovskii, G.Yu. Pavlova, and S.G. Sagalaev, 2007. The influence of geochemical processes in the near-bottom layer on the hydrochemical characteristics of the waters of the Sea of Japan. Oceanology, 47(3), 350-359.

Tomczak, M., and D.G.B. Large, 1989. Optimum Multiparameter analysis of mixing in the thermocline of the Eastern Indian Ocean. Journal of Geophysical Research, 94, 16141-16149.

Van Heuven, S., D. Pierrot, E. Lewis, and D.W.R. Wallace, D.W.R. 2009. MATLAB program developed for CO2 system calculations. ORNL/CDIAC-105b, Carbon Dioxide

Information Analysis Center, Oak Ridge National Laboratory, US Department of Energy, Oak Ridge, Tennessee.

Wolgast, D.M., A.F. Carlucci, and J.E. Bauer, 1998. Nitrate respiration associated with detrital aggregates in aerobic bottom waters of the abyssal NE Pacific. Deep-Sea Research II 45, 881-892.

Yanagi, T., 2002. Water, salt, phosphorus and nitrogen budgets of the Japan Sea. Journal of Oceanography, 58, 797-804.

Yang, H.S., S.S. Kim, C.G. Kang, and K.D. Cho, 1991. A study on sea water and ocean current in the sea adjacent to Korea Peninsula. Ⅲ. Chemical characteristics of water masses in the polar front area of the central Korean East Sea. Journal of the Korean Fisheries Society, 24(3), 185-192.

Zeebe, R.E., and D. Wolf-Gladrow, 2001. CO_2 in seawater: Equilibrium, kinetics, isotopes. Elsevier Oceanography Series, 65, 83.

Zehr, J.P., and R.M. Kudela, 2011. Nitrogen cycle of the open ocean: From genes to ecosystems. Annual Review of Marine Science, 3, 197-225.

Table 3.1: Summary of the N/P ratios estimated in the East/Japan Sea.

N/P ratio			
Ref.	Whole (W/EJB + UB + YB)	UB	season
Kido and Nishimura (1973)	13.6 (≥0m)		summer
Shim et al. (1989)		12.5 (≤100m)	spring
Chung et al. (1989)		13.4 (≤150m)	fall
Yang et al. (1991)		12.1 (≤500m)	fall
		9.8 (≤500m)	winter
Moon et al. (1996)		14.4 (≤1000m)	fall
Chen et al. (1996)	14.7 (300-600m)		summer
	13.0 (≥2000m)		
Yanagi (2002)	11.4 (≥0m)		annual
***This study**	**12.4 (≥300dbar)**		**summer**
range	**9.8 - 14.7**		

*1999 observation data

W(E)JB: Western (Eastern) Japan Basin, UB: Ulleung Basin, YB: Yamato Basin

Table 3.2: Estimated denitrification rates in the Ulleung Basin (Stas. 10 and 121) and Eastern Japan Basin (Sta. 129) of the EJS. Both observed (N/O_2=12.4/118 and N/P=12.4/1) and traditional (16/138 and 16/1) Redfield ratios are used for computation of expected nitrate concentrations.

St. (Basin)	[+]Obs. NO3 (μmol kg^{-1})	Exp. NO3 (μmol kg^{-1})	ΔN (μmol m^{-3})	ΔH (m)	Δage (yr)	Deni. rates (μmol N $m^{-2}\cdot d^{-1}$)	Cont. Slope
129 (EJB)	25.0	26.6 ($R_{N/O2=16/138}$)	1660	100	7	33.2	Upper
		26.4 ($R_{N/O2=12.4/118}$)	1470			29.9	
		26.1 ($R_{N/P=16/1}$)	1100			22.4	
		25.8 ($R_{N/P=12.4/1}$)	859			17.5	
10 (UB)	25.2	25.7 ($R_{N/O2=16/138}$)	483	65	9	4.7	Middle
		25.6 ($R_{N/O2=12.4/118}$)	438			4.2	
		26.1 ($R_{N/P=16/1}$)	944			9.1	
		25.9 ($R_{N/P=12.4/1}$)	742			7.2	
121 (UB)	25.5	26.3 ($R_{N/O2=16/138}$)	760	108	26	4.4	Lower
		26.2 ($R_{N/O2=12.4/118}$)	690			4.0	
		26.1 ($R_{N/P=16/1}$)	606			3.5	
		26.0 ($R_{N/P=12.4/1}$)	485			2.8	

[+]Obs. NO3 is the observed NO3 linearly extrapolated to the bottom sediment-water interface depth.

ΔN = (Exp. NO3 – Obs. NO3) (μmol kg^{-1}) x ρ (kg m^{-3}).

ΔH is the height between the upper and lower boundary of the triangular area shown in Fig. 3.6.

Δage is the estimated age difference between the upper and lower boundary of the triangular area shown in Fig. 3.6.

Table 3.3: physicochemical characteristics of source water types used for the extended OMP analysis in the East/Japan Sea (adopted from Table 2 of Kim and Lee, 2004).

SWT	*PT (℃)	S (psu)	DO (μmol kg^{-1})	Si (μmol kg^{-1})	NO_3 (μmol kg^{-1})	PO_4 (μmol kg^{-1})	TALK. (μmol kg^{-1})	DIC (μmol kg^{-1})
TMW	19.5	34.5	219	2.9	0.9	0.2	2282	2004
LCW	1.7	33.8	351	6.2	3.6	0.5	2263	2092
ESIW	1.4	34.0	319	16.8	11.4	0.9	2265	2143
ESPW	0.1	34.1	198	89.4	25.9	2.1	2285	2258

*PT: potential temperature

TMW: Tsushima Middle Water, LCW: Liman Cold Water, ESIW: East Sea Intermediate Water, ESPW: East Sea Proper Water

Table 3.4: Four different cases of Redfield ratios applied to the extended OMP analysis.

Case	$r_{-O2/P}$	$r_{P/P}$	$r_{N/P}$	$r_{Si/P}$	$r_{C/P}$	Ref.
1	138	1	16	28	106	Redfield et al. (1963)
2	170	1	16	28	117	Anderson and Sarmiento (1994)
3	150	1	16	28	106	Anderson (1995)
4	118	1	12.4	28	103	This study (2011)

Table 3.5: Weight values assigned to each parameter in the extended OMP analysis.

Parameter	PT (℃)	S (psu)	DO (μmol kg^{-1})	Si (μmol kg^{-1})	NO_3 (μmol kg^{-1})	PO_4 (μmol kg^{-1})	TALK. (μmol kg^{-1})	DIC (μmol kg^{-1})
Weight	142	142	45	43	31	30	3	3

Table 3.6: Magnitude and rates of denitrification estimated at eight stations as the potential denitrification locations expected from the extended OMP analysis.

Case	Basin	UB						EJB	
	St.	10	16	17	19	118	120	126	129
	ΔT (yr)	9.2	4.5	37.8	16.3	22.3	52.9	5.7	6.7
	ΔH (m)	64.9	43.8	197.3	57.3	82.0	231.9	69.7	99.7
1	ΔN_{deni} (μmol N m^{-3})	236	269	333	116	50.8	68.3	454	939
	ΔN_{deni} rate (μmol N m^{-2} d^{-1})	2.3	3.6	2.4	0.6	0.3	0.4	7.7	19.1
2	ΔN_{deni} (μmol N m^{-3})	192	193	333	116	50.9	68.1	12.2	267
	ΔN_{deni} rate (μmol N m^{-2} d^{-1})	1.9	2.6	2.4	0.6	0.3	0.4	0.2	5.4
3	ΔN_{deni} (μmol N m^{-3})	217	236	333	116	50.8	68.3	263	652
	ΔN_{deni} rate (μmol N m^{-2} d^{-1})	2.1	3.1	2.4	0.6	0.3	0.4	4.4	13.2
4	ΔN_{deni} (μmol N m^{-3})	196	188	333	116	50.8	68.3	14.5	258
	ΔN_{deni} rate (μmol N m^{-2} d^{-1})	1.9	2.5	2.4	0.6	0.3	0.4	0.2	5.2
Mean range		51±0.1–529±330 μmol N m^{-3} (0.3±0–11±7 μmol N m^{-2} d^{-1})							

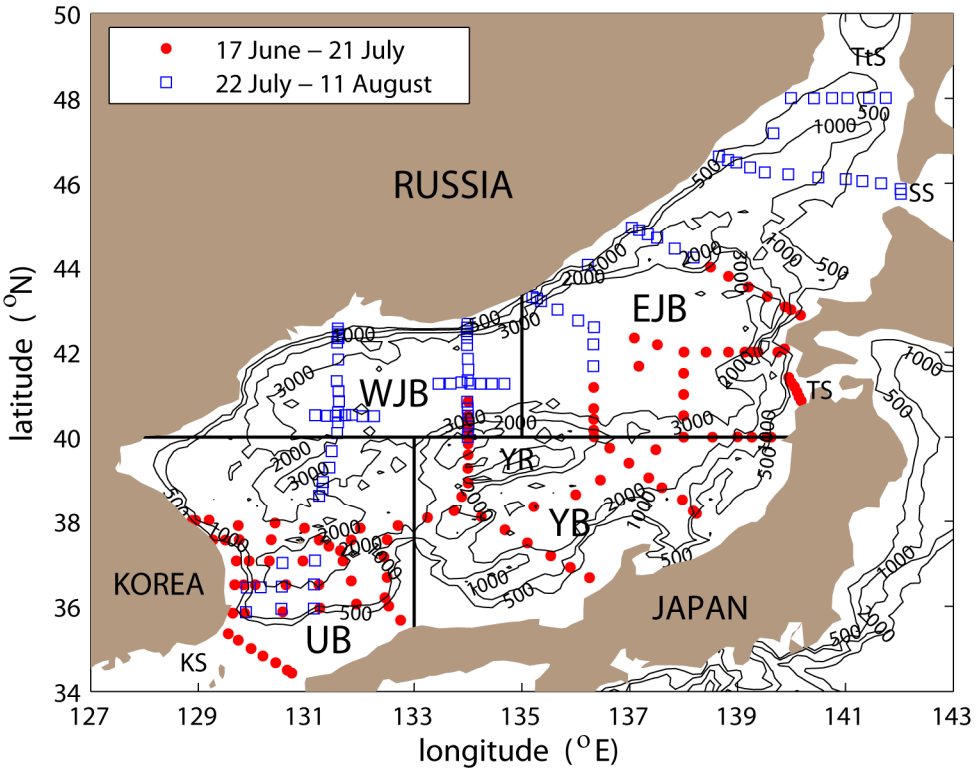

Figure 3.1: The hydrographic station map of CREAMS II observation (summer 1999) with topography of the East/Japan Sea (EJS). The EJS has three main basins: JB (Japan basin), YB (Yamato Basin), and UB (Ulleung Basin). It has one rise: YR (Yamato Rise), and four straits: KR (Korea Strait), TS (Tsugaru Strait), ST (Soya Strait), and TtS (Tatar Strait). The JB is distinguished to the Western Japan Basin (WJB) and the Eastern Japan Basin (EJB) at 135°E for data analysis.

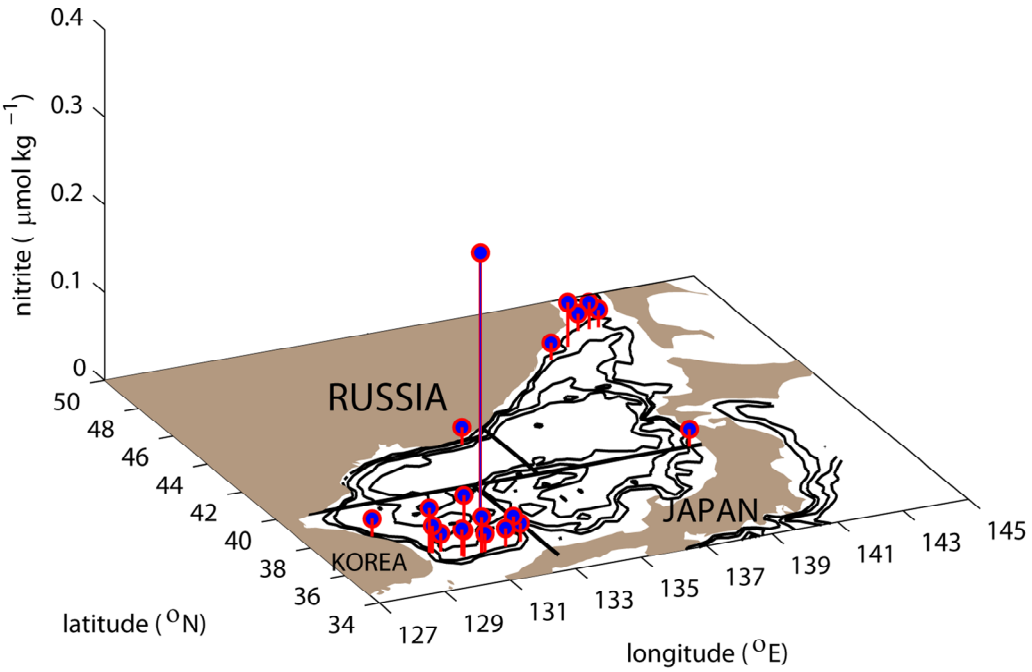

Figure 3.2: The distribution of stations with deep nitrite signals (>0.01 μmol kg^{-1}) found below 300dbar depths from the CREAMS II observation in the EJS (summer 1999).

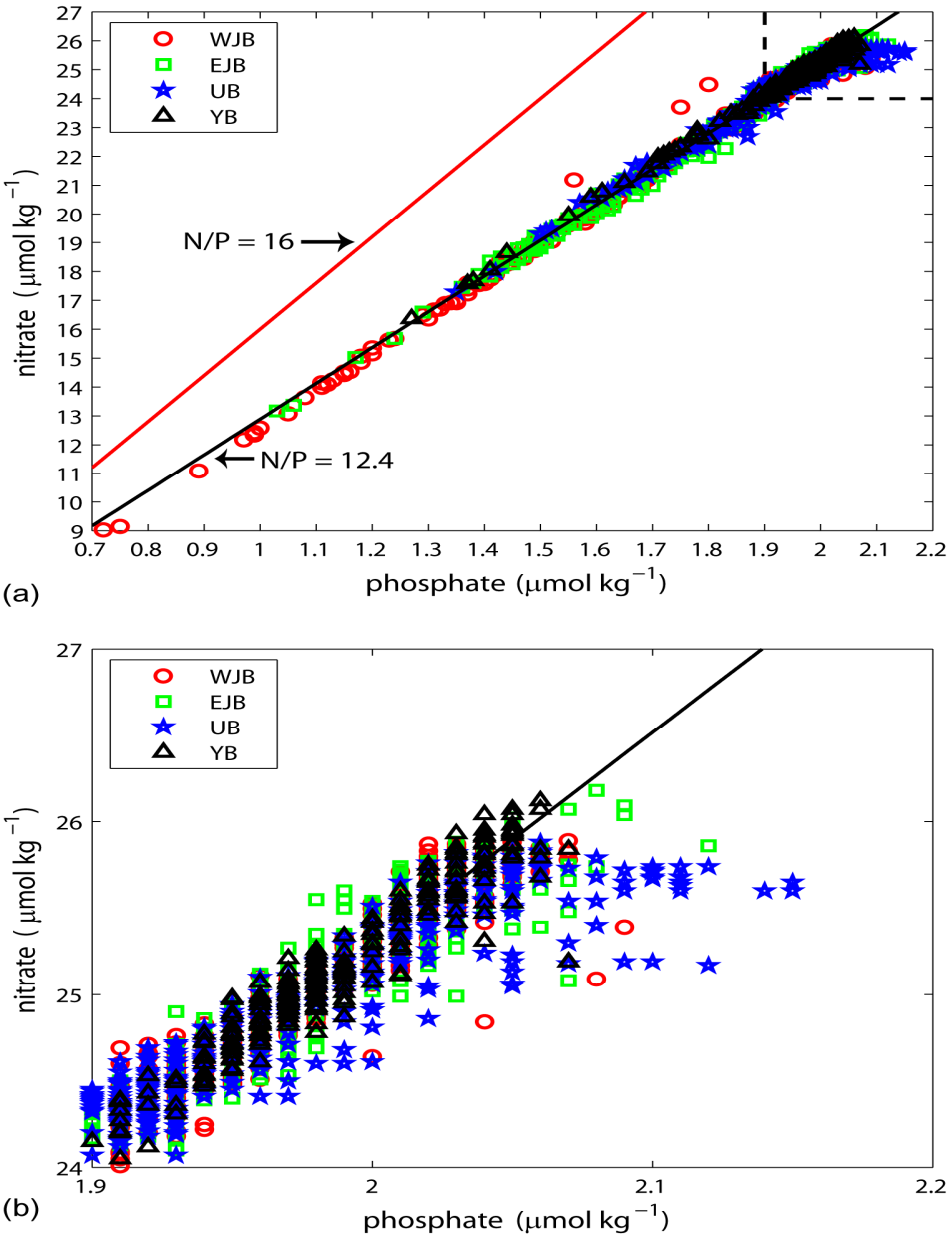

Figure 3.3: The N/P ratio of the East/Japan Sea below 300dbar depths observed during the CREAMS II (summer 1999) in EJS below 300dbar. (a) The N/P slope estimated by a least square method for the observed data (black solid line) vs. the traditional Redfield ratio line with a slope of 16 (red solid line), (b) A magnified view of Figure 2a for the dotted line area for higher nutrient concentration ranges. Different symbols are for different basins and sub-basins of EJS.

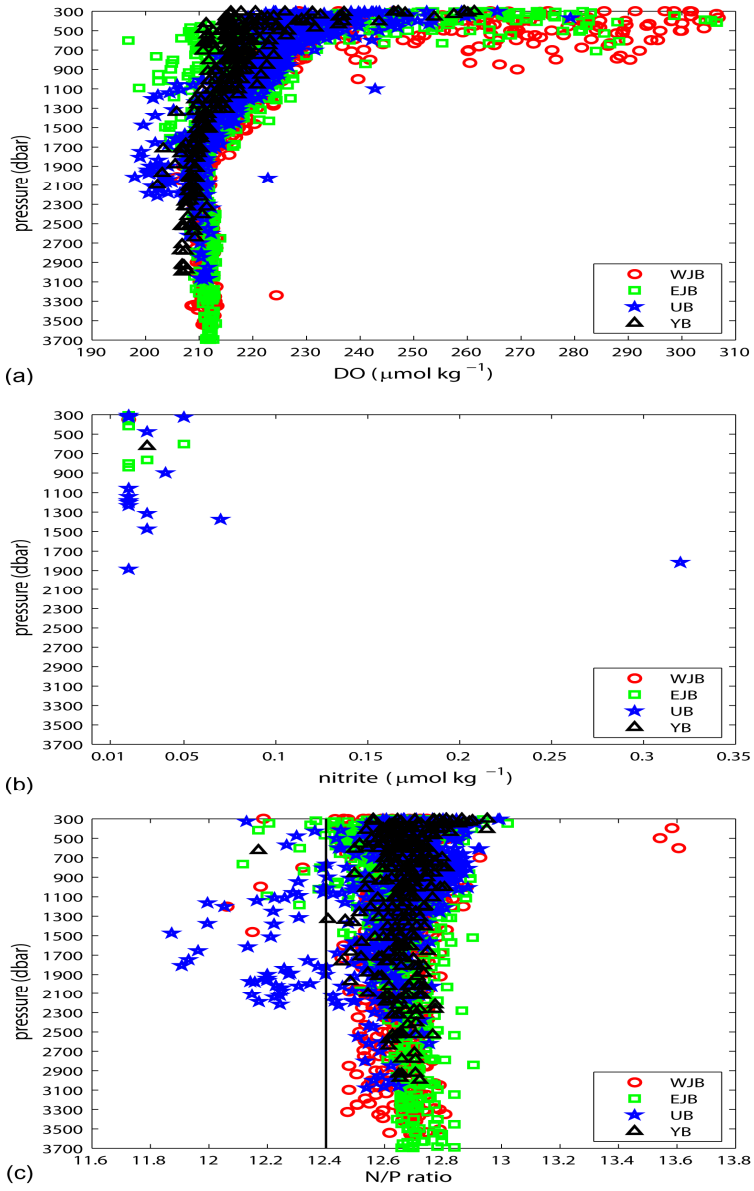

Figure 3.4: The vertical distributions of dissolved oxygen, nitrite, and N/P ratio in the EJS observed from the CREAMS II (summer 1999). (a) Dissolved oxygen (μmol kg^{-1}), (b) nitrite (μmol kg^{-1}), and (c) individual N/P ratio $\left(\left[NO_3^-\right]_i / \left[PO_4^{3-}\right]_i\right)$. Individual N/P ratio is computed by nitrate concentration, $[NO_3^-]$, divided by phosphate concentration, $[PO_4^{3-}]$, at each data point (*i*). Different symbols represent individual basins: WJB (red circle), EJB (green square), UB (blue star), and YB (black triangle). The vertical line in (c) indicates the observed mean N/P ratio (=12.4).

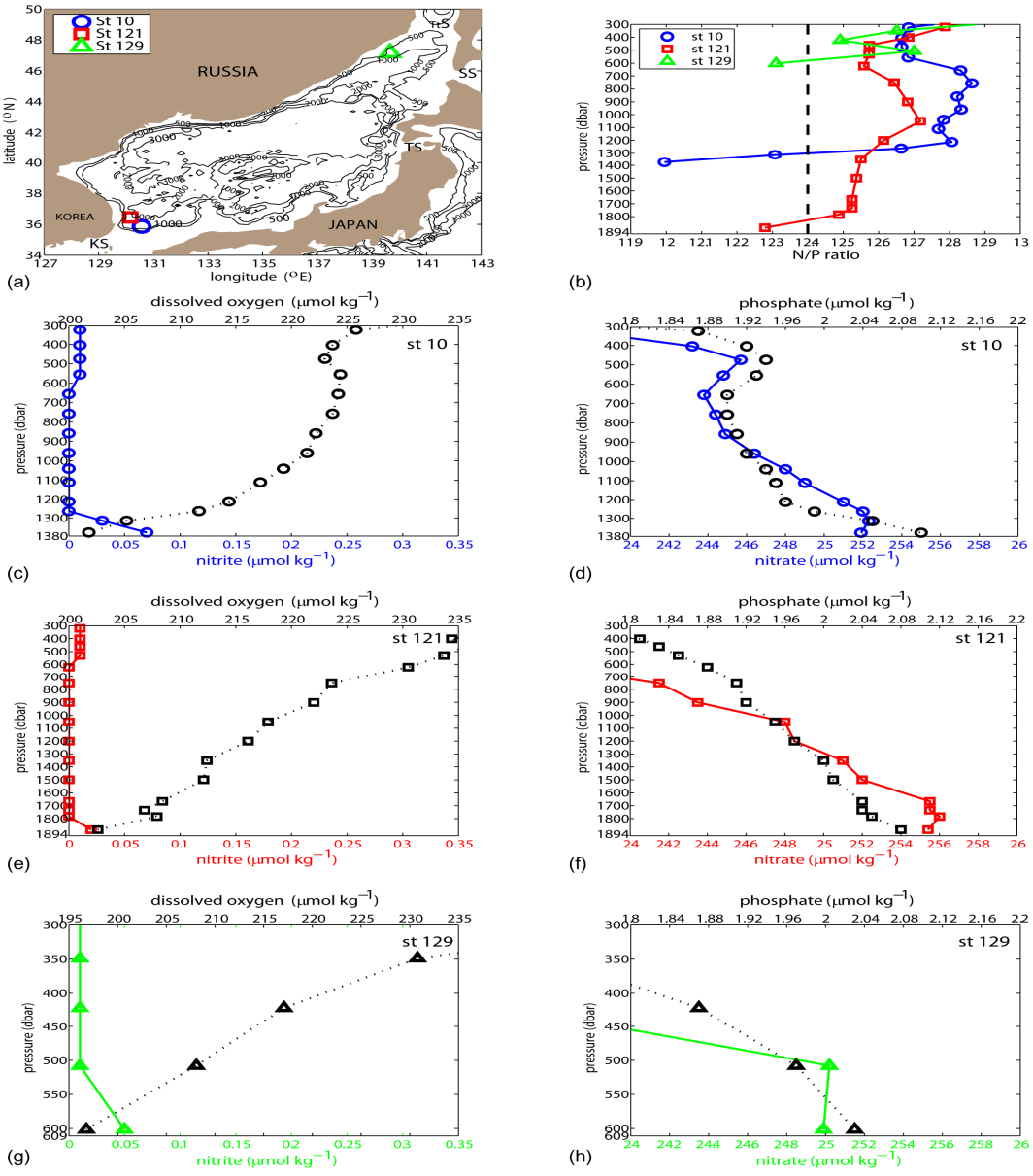

Figure 3.5: Vertical profiles of nitrate, phosphate, dissolved oxygen, nitrite, and N/P ratio at two stations (10 and 121) in UB and one station (Sta. 129) in EJB near TtS. (a) Locations of the three stations in the study area map, (b) vertical profiles of N/P ratio at Stas. 10, 121, and 129 (the dotted line represents the mean N/P ratio of 12.4 of the East/Japan Sea), (c)-(d) vertical profiles of nitrate (μmol kg^{-1}), phosphate (μmol kg^{-1}), nitrite (μmol kg^{-1}), and dissolved oxygen (μmol kg^{-1}) at Sta. 10, (e)-(f) same property profiles at Sta. 121 as (c)-(d), and (g)-(h) same property profiles at Sta. 129 as (c)-(d).

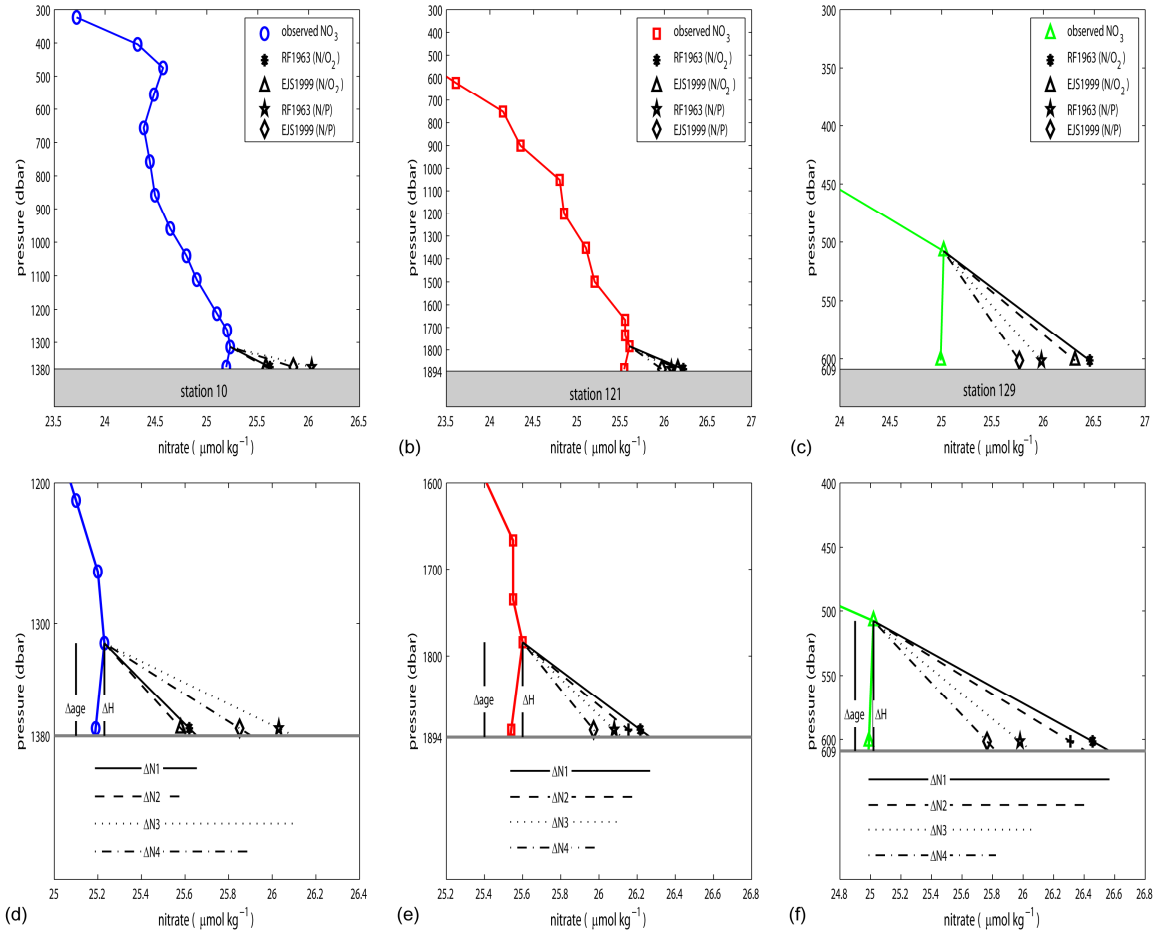

Figure 3.6: Vertical profiles of the observed and estimated nitrate for the bottom boundary layer at the study sites. (a) below 1314dbar at Sta. 10, (b) below 1784dbar at Sta. 121, (c) below 508dbar at Sta. 129. (d)-(f) are magnified versions of the (a)-(c), respectively. Blue circle, red square, and green triangle symbols represent observed nitrate at Stas. 10, 121, and 129, respectively. Black asterisk, triangle, star, and diamond symbols represent estimated nitrate from $\Delta N/-\Delta O_2$=16/138 and $\Delta N/-\Delta O_2$=12.4/118, and estimated nitrate from $\Delta N/\Delta P$=16/1 and $\Delta N/\Delta P$=12.4/1, respectively. ΔN is the different between the expected and observed nitrate concentrations at the sediment surface, ΔH is the height between the upper and lower boundary of the triangular area, and Δage is the estimated relative age difference between the upper and lower boundary of the triangular area.

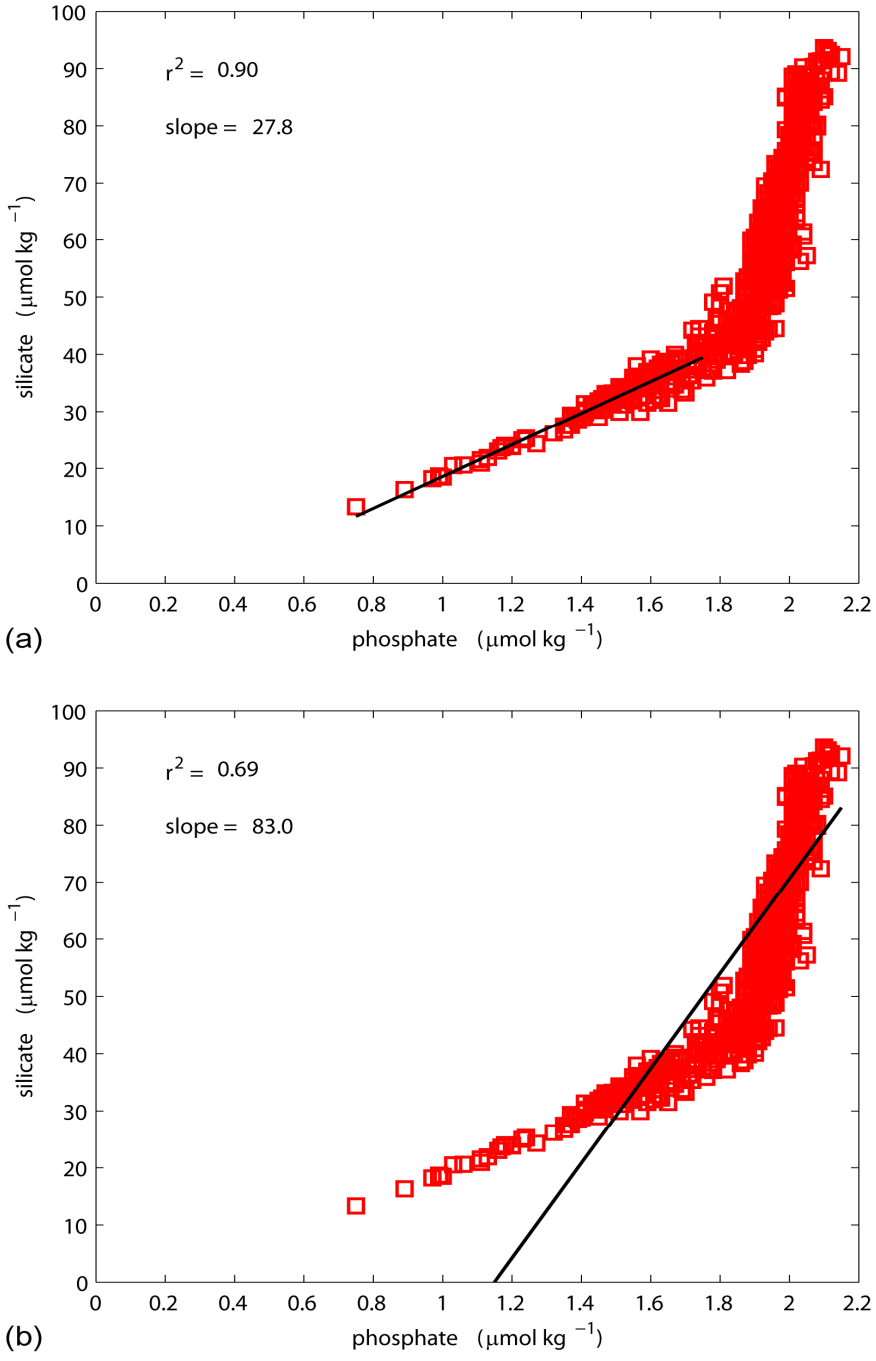

Figure 3.7: Si/P ratio of the EJS below 300dbar. (a) The fitted regression line of silicate vs. phosphate including the processes of silicate remineralization and dissolution, and (b) within the silicate remineralization.

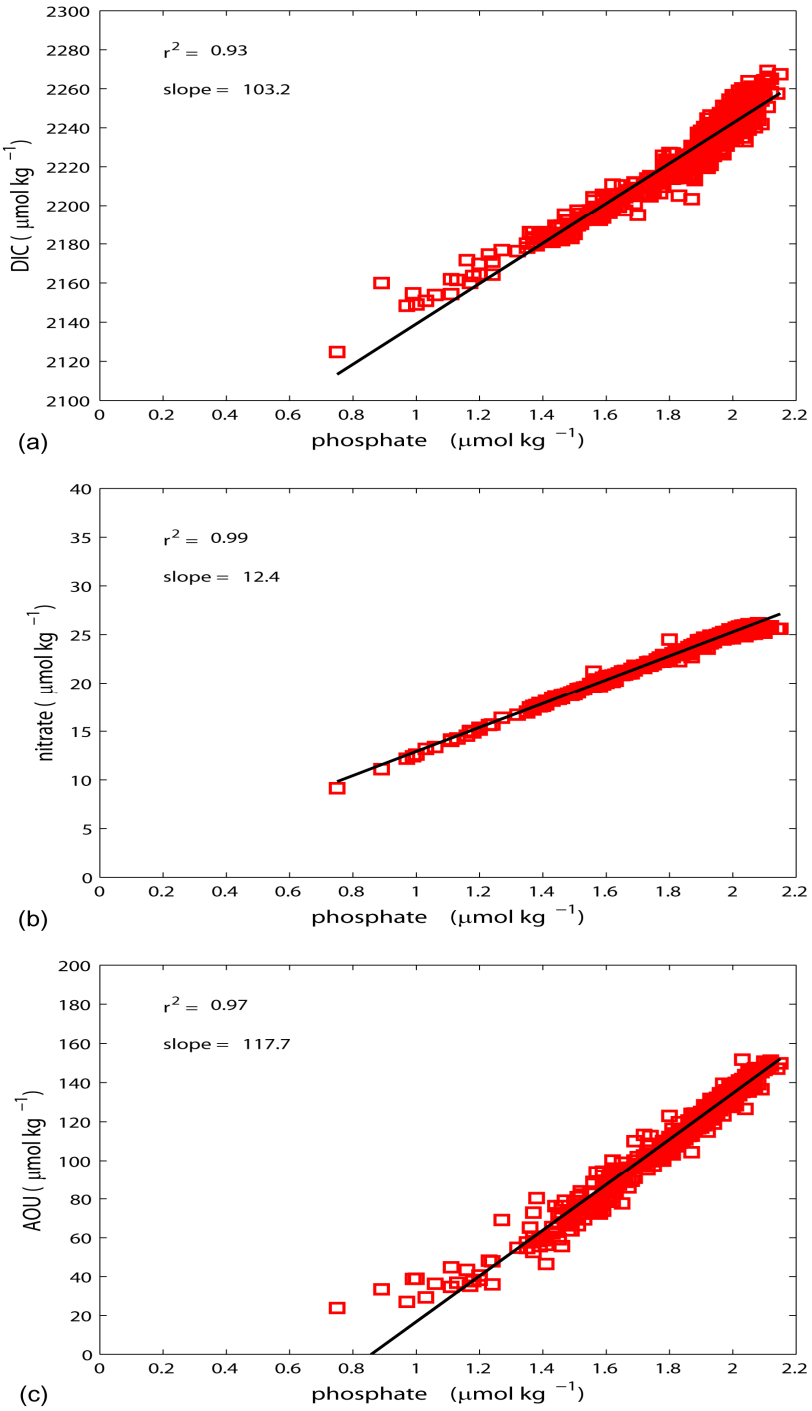

Figure 3.8: The EJS's Redfield ratios ($r_{C:N:P:-O2}$) below 300dbar. (a) Dissolved inorganic carbon (DIC) vs. phosphate ($r_{C:P}$), (b) Nitrate vs. phosphate ($r_{N:P}$), and (c) Apparent oxygen utilization (AOU) vs. phosphate ($r_{-O2:P}$).

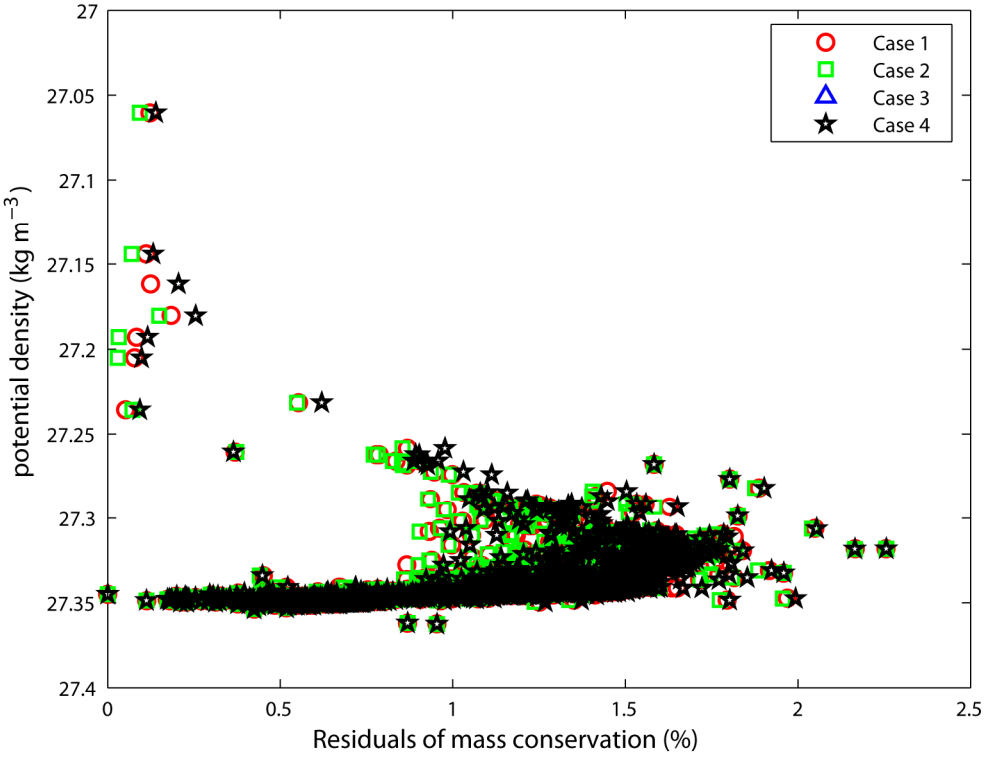

Figure 3.9: Plot of potential density (kg m^{-3}) vs. residuals of mass conservation (%). The residuals of mass conservation are calculated by ($\sum x_i - 1$) x 100 (%).

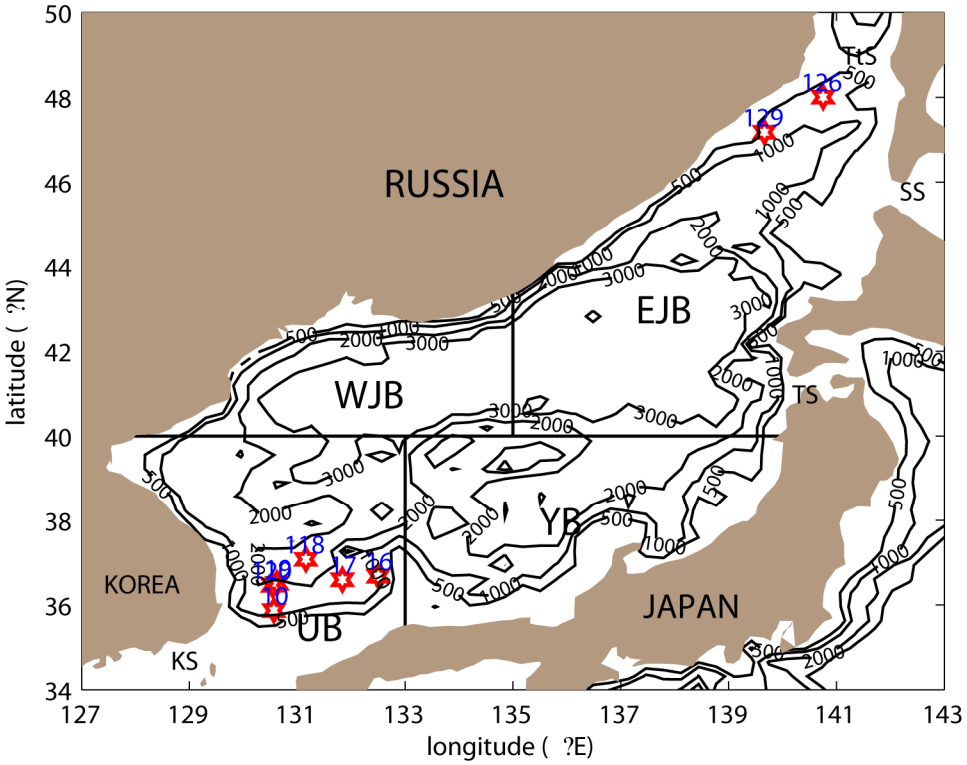

Figure 3.10: The potential denitrification locations expected from the extended OMP analysis. Those of stations were intersected collectively from the cases 1-4.

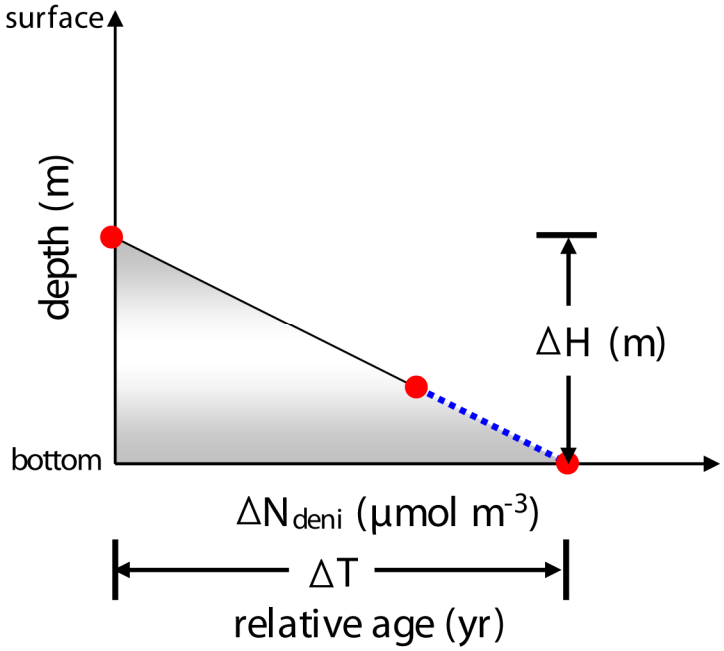

Figure 3.11: An illustration to estimate denitrification rate. It is assumed that denitrification is occurring within the triangular area (=1/2·ΔN_{deni}·ΔH), and the time information (ΔT) between the upper and the lower boundary is estimated from the concept of relative age (see details at Section 3.2.1).

Chapter 4: Estimation of water column denitrification rates in the oxygen minimum layer of open Pacific Ocean along 32°S and their significance to the Pacific nitrogen budget

1. INTRODUCTION

The marine nitrogen cycle exhibits a variety of complicated pathways (e.g. nitrogen fixation, denitrification, dissimilatory nitrate reduction to ammonium, anaerobic ammonia oxidation, and etc.) in ocean biogeochemical processes (Brandes et al., 2007). Among the sink processes in marine nitrogen cycle, denitrification ($NO_3^- \rightarrow NO_2^- \rightarrow N_2O/N_2$) generally plays a dominant role in removing nitrogen in the ocean environment. Owing to widely nitrogen-limited conditions of the oceans, it has a direct influence on biological productivity (Falkowski, 1997). Study of the global nitrogen balance between sources (i.e. nitrogen fixation) and sinks (i.e. denitrification) provides important insights into both glacial-interglacial climate change and the global carbon cycle by which the availability of nitrogen controls the efficiency of biological pump absorbing atmospheric CO_2 (Gruber and Sarmiento, 1997; Karl et al., 2002; Gruber, 2008; Gruber and Galloway, 2008).

At large scales in the open ocean, the N^* (=N - 16P + 2.9 μmol kg^{-1}; $N^*>0$: nitrogen fixation, $N^*<0$: denitrification) has been a convenient method for estimating global water column denitrification (Gruber and Sarmiento, 1997; Deutsch et al., 2001), because direct measurements have been substantially limited in space and time. Generally, the measurements of ocean parameters are determined by physical mixing combined with biogeochemical processes (Anderson and Sarmiento, 1994). The extended optimum multi-parameter analysis (OMP) analysis provides a way to quantify the contributions from physical mixing and biogeochemical changes together. Hupe and Karstensen (2000) applied the extended optimum multi-parameter (OMP) analysis to estimate physical mixing ratios and biogeochemical changes in the Arabian Sea, and demonstrated this technique to be a viable alternative to estimate denitrification using hydrographic data on smaller basin scales.

At present, estimates of water column denitrification rates in global- and basin-scale nitrogen budgets do not include any open ocean values for the full water-column. This is partly because denitrification rates are expected to be significantly lower or non-existent in the open ocean compared to that in the oxygen minimum zones (OMZs), and also because high-quality hydrographic data and time dependent tracers (e.g. Chlorofluorocarbons and SF_6) are required. Macroscopic aggregates of detritus (i.e. 'marine snow') are ubiquitous in the pelagic water column in the world oceans (Alldredge and Silver, 1988), although their density is low, providing 'reducing microenvironments' within detrital aggregates (Alldredge and Cohen, 1987; Shanks and Reeder, 1993; Ploug et al., 1997; Wolgast et al., 1998), so denitrification may occur in the microzones despite aerobic condition in ambient waters. Yamagishi et al., (2005) recently reported that denitrification at Station KNOT (44°N, 155°W) in the OMZ might be driven by the microzones of aggregates despite aerobic conditions. Active microbial respiration in water column occurs in the oxygen minimum layer (OML) of the open ocean and favorable space for microzones of aggregates may be formed in this layer. Although the magnitude of denitrification in OML might be very low, the area involved is substantially larger than that associated with OMZs, suggesting that the magnitude of the integrated effect may be substantial. Readily available high-quality long-line transect observations across open oceans make this analysis feasible.

Gruber and Sarmiento (1997) described N^* minima in the Eastern Tropical North and South Pacific (ETNP and ETSP) where there are oxygen minimum zones (OMZs). They showed that variation of N^* in the Pacific Ocean outside of OMZs was small, and suggested that either N_2 fixation is small or denitrification in anoxic microzones is large to maintain the balance between them. More recently, Deutsch et al., (2001) recently estimated water column denitrification rates in the ETNP (110°W-coast and 10°S-20°N, 22 Tg N yr^{-1}) and the ETSP (110°W-coast and 10°S-25°S, 26 Tg N yr^{-1}), using the N^* method with CFC12 tracer ages. Furthermore, Deutsch et al., (2007) estimated nitrogen fixation rates with an ocean general circulation model applied at global and basin scales, and suggested that nitrogen fixation rates are higher in the nutrient depleted subtropical

Pacific Ocean than elsewhere except for the regions of ETNP and ETSP. To improve the accuracy of the mass balance of the oceanic nitrogen inventory, it is crucial to estimate denitrification rates in unexplored regions. At present, the estimate of nitrogen fixation rate (93-108=100±8 Tg N yr^{-1}; 40°S-65°N; Deutsch et al., 2007) is much larger than those of denitrification rates (water denitrification rate in OMZs + benthic denitrification rate=48±5 + 15±5=63±10 Tg N yr^{-1}; 30°S-60°N; Deutsch et al., 2001) in the Pacific Ocean. This condition conflicts with the current issue of global oceanic nitrogen mass balance that nitrogen sinks are greater than nitrogen sources. Here, I investigate water column denitrification rates in OML outside of OMZs to determine whether the estimated denitrification rates at OML can represent a significant portion in the Pacific nitrogen budget.

Shipboard measurement of nitrogen fixation is difficult. Historically it has been estimated from the difference between sources and sinks in nitrogen budget or using modeling tools. The technique of CFC12 tracer ages that Deutsch et al., (2001) used for their analysis is based on the assumption that a water parcel moves from the surface mixed layer into the interior through advection alone, with no significant bias from mixing with surrounding waters. However, in reality, physical mixing is ubiquitous in the ocean, even though the shallow depth thermocline ventilation might experience minimum bias for tracer age from mixing. The effect of mixing on the estimation of water parcel age is just as important (Karstensen and Tomczak, 1998; Hall et al., 2004) as the magnitude of denitrification itself to the calculation of water column denitrification rates. Thus, I use an advanced technique, transit time distribution (TTD) technique for our analysis (see Section 4.4.1).

The South Pacific Ocean hydrographic survey at ~32°S, known as the P06 line, was occupied approximately decadally (1992, 2003, and 2010) as part of the U.S. World Ocean Circulation Experiment (WOCE), the Blue Earth Global Expedition (BEAGLE), and CO_2/Climate Variability and Predictability Research (CLIVAR) Repeat Hydrography programs. These high-quality observations give us an opportunity to estimate open-ocean denitrification rates away from OMZ.

As in the N^* technique, estimation of denitrification by extended OMP analysis is based on the difference between expected and observed nitrate concentrations, assuming all the nitrate deficit is from denitrification. Neither method can distinguish between denitrification signals derived from the water column along and those derived from sedimentary interaction especially near the bottom layer, without using additional tracers such as nitrite, nitrogen and oxygen isotopes. In addition, the part of P06 (~32°S) line is close to the OMZs distributed along the coast of South America. The methods used here N^* and extended OMP analysis cannot distinguish denitrification signals produced through local diffusive processes from those advected in from the coastal OMZs (ca. <500dbar). In order to minimize the limitations above, I estimate denitrification rates only in the OML (1100-2000dbar) away from sediment-water interface, and assume that the estimated rates are from water column denitrification process in the P06 line. The denitrification may occur at reducing microzones of marine snow.

To investigate the hypothesis that the integrated effect of open-ocean water column denitrification in the OML may be a significant component of the basin-scale nitrogen budget, this study (1) estimates water column denitrification in the South Pacific with the P06 (~32°S) hydrographic dataset using the N^* method as well as the extended OMP analysis, (2) compares the magnitude of the differences between the two methods, (3) estimates mean water column denitrification rates in OML of P06 (~32°S) using the TTD method, and (4) discusses the resulting implications for the nitrogen budget of Pacific Ocean.

2. DATA

The P06 (~32°S) repeat hydrographic transects in 1992, 2003, and 2010 (Fig. 4.1). These data as well as the other datasets described below and Fig. 4.1 are available from the Climate Variability and Predictability (CLIVAR) and Carbon Hydrographic Data Office (CCHDO: http://cchdo.ucsd.edu/).

The parameters used for the extended OMP analysis are latitude, longitude, pressure, potential temperature (PT), salinity (S), dissolved oxygen (DO), nitrate (N),

phosphate (P), silicate (Si), total alkalinity (Talk), and dissolved inorganic carbon (DIC). Missing Talk and DIC values were estimated from paired DIC - total pH data and paired Talk - total pH data, respectively, through the CO2SYS program (Van Heuven et al., 2009). Note that only the data with 'acceptable' quality flag were used. To reduce bias from seasonal variation at the surface layer, only the data deeper than 600dbar were included in the extended OMP analysis.

3. THE EXTENDED OMP ANALYSIS

Extended OMP analysis is an inverse method based on an over-determined system (Hupe and Karstensen, 2000). Such systems have multiple solutions; that is, the number of equations is greater than number of unknown variables. Solutions are found using non-negative least squares method (NNLS) with the constraint of mass conservation $\left(\sum_{i=1}^{n} x_i = 1\right)$ (Tomczak and Large, 1989). Here, modified silicate and total alkalinity equations were included (see Chapter 3 at Section 3.2.2), and the matrix form for the extended OMP analysis is given as:

$$\begin{bmatrix} PT_1 & + \cdots + & PT_4 & + & 0 & + & 0 & + & 0 & + & 0 \\ S_1 & + \cdots + & S_4 & + & 0 & + & 0 & + & 0 & + & 0 \\ DO_1 & + \cdots + & DO_4 & - & r_{O2/P} & + & 0 & + & 0 & + & 0 \\ P_1 & + \cdots + & P_4 & + & 1 & + & r_D & + & 0 & + & 0 \\ N_1 & + \cdots + & N_4 & + & r_{N/P} & - & 1 & + & 0 & + & 0 \\ Si_1 & + \cdots + & Si_4 & + & r_{Si/P} & + & 0 & + & 0 & + & 1 \\ TALK_1 & + \cdots + & TALK_4 & - & (r_{N/P}+1) & + & (1-r_D) & + & 2 & + & 0 \\ DIC_1 & + \cdots + & DIC_4 & + & r_{Corg/P} & + & r_D r_{Corg/P} & + & 1 & + & 0 \\ 1 & + \cdots + & 1 & + & 0 & + & 0 & + & 0 & + & 0 \end{bmatrix} \times \begin{bmatrix} x_1 \\ x_2 \\ x_3 \\ x_4 \\ \Delta P_{remi} \\ \Delta N_{deni} \\ \Delta C_{inorg} \\ \Delta Si_{inorg} \end{bmatrix} - \begin{bmatrix} PT_{obs} \\ S_{obs} \\ DO_{obs} \\ P_{obs} \\ N_{obs} \\ Si_{obs} \\ TALK_{obs} \\ DIC_{obs} \\ 1 \end{bmatrix} = \begin{bmatrix} R_{PT} \\ R_S \\ R_{DO} \\ R_P \\ R_N \\ R_{Si} \\ R_{TALK} \\ R_{DIC} \\ R_{MC} \end{bmatrix}$$

$$\boldsymbol{A} \cdot \boldsymbol{X} - \boldsymbol{b} = \boldsymbol{R} \quad (1)$$

where, the matrix **A** is defined as the physicochemical characteristics of the source water types, the vector **X** is composed of mixing ratios (x_i) for the source water types, the amount of remineralized phosphate (ΔP_{remi}), the amount of denitrification (ΔN_{deni}), the amount of inorganic carbonate dissolution (ΔC_{inorg}), and the amount of inorganic silicate dissolution (ΔSi_{inorg}). The vector **b** represents observed concentrations, and the vector **R**,

constraint residuals. The ratios of $r_{C:Si:N:P:-O2}$ indicate the Redfield ratios (Redfield et al., 1963), and r_D is a ratio to express the amount of phosphate produced by denitrification and is given as 1/104 (Gruber and Sarmiento, 1997; Hupe and Karstensen, 2000). The detailed information on the extended OMP analysis is described in Chapter 3.

3.1 Physicochemical characteristics of source water types for the 32°S line

The South Pacific Ocean is biogeochemically important as it acts as a sole source of dissolved oxygen to the deep North Pacific basin through the deep western boundary current (DWBC) system (Tomczak and Godfrey, 1994). Major water masses present at the 32°S line below 600dbar include Antarctic Intermediate Water (AAIW), Pacific Deep Water (PDW), Upper/Lower Circumpolar Deep Water (U/LCDW), and Antarctic Bottom Water (AABW) (Tomczak and Godfrey, 1994; Wijffels et al., 2001; Murata et al., 2007; Talley et al., 2011). All these waters include admixtures of waters ventilated in the Southern Ocean. As extended OMP analysis requires the physicochemical characteristics of source water types to be defined at their source regions, these characteristics are defined far away from the 32°S in the following manner.

Pacific Antarctic Intermediate Water (AAIW) is formed through strong convective overturning of Subantarctic Mode Waters off southern Chile, and is identified typically by salinity minimum characteristics (θ: 4-6°C and S: 34.1-34.5) (England et al., 1993; Tsuchiya and Talley, 1996; Stanton, 2002; Bostock et al., 2010; Hartin et al., 2011; Talley et al., 2011). Here, the source water characteristics for Pacific AAIW were defined using the WOCE-era P19C line (88°W to the coast of South America and south of 50°S) near the AAIW formation region and the salinity minimum (Fig. 4.1).

Pacific Deep Water (PDW) is the oldest water in global oceans formed as the result of mixing amongst AABW, CDW, and AAIW in the deep Pacific farther away from both the surface and the formation regions for the individual components (Tomczak and Godfrey, 1994). PDW is therefore characterized by silicate maximum (Mantyla and Reid, 1983; Talley and Joyce, 1992; Johnson and Toole, 1993; Tsuchiya and Talley, 1996). In addition, since PDW is more corrosive than other waters with higher CO_2

concentrations (Bostock et al., 2011), it could be also characterized by a total alkalinity maximum (Fiadeiro, 1980). Because PDW is formed within the deep interior through mixing throughout the North Pacific Ocean, the source water characteristics of PDW are defined at three different sites along the P16N/17N line (at 152°W and 135°W, north of 40°N), P03 (~24°N), and P21 (~18°S) transects, with the criteria of silicate and alkalinity maximum for comparison (Fig. 4.1 and Table 4.3). The effect of spatially varying PDW's definitions on the results of extended OMP analysis is discussed in Section 4.1. The nominal results based on the extended OMP analysis using PDW defined at 24°N are used elsewhere.

CDW is distinguished to Upper and Lower varieties based on different characteristics: UCDW and LCDW. UCDW is generally characterized as low oxygen and high nutrient water (Tomczak and Liefrink, 2005). However, these features (i.e. low oxygen and high nutrients) are quite similar to those of PDW. CDW and AABW cross 32°S within the DWBC system (Reid, 1986; Reid, 1997; Kawabe et al., 2009). UCDW source water characteristics were therefore defined at the P15S line (170°W and south of 50°S) (Fig. 4.1), where there is the indication of a nutrient maximum (Tomczak and Liefrink, 2005) south of where the DWBC begins its journey into the South Pacific, and where there is little expected PDW influence.

LCDW and AABW are identified typically by a salinity maximum and a potential temperature minimum, respectively (Mantyla and Reid, 1983; Johnson and Toole, 1993; Tomczak and Godfrey, 1994; Johnson and Orsi, 1997; Orsi et al., 1999; Orsi et al., 2002; Tomczak and Liefrink, 2005; McCave et al., 2008; Talley et al., 2011). In addition, dissolved oxygen and nutrient concentrations of the more recently ventilated AABW are higher than those of LCDW, which is greatly influenced by North Atlantic Deep Water which has traveled the length of the Atlantic and nearly circumnavigated the globe on its journey to the South Pacific. The physicochemical source water characteristics of LCDW and AABW were defined at the P15S line (170°W and south of 50°S) according to the observed salinity maximum and potential temperature minimum (Fig. 4.1).

The physicochemical characteristics of source water types defined for the extended OMP analysis are summarized in Table 4.1, and a temperature-salinity diagram is shown in Fig. 4.2. Recently, Kawano et al., (2006) reported warming of LCDW by ~0.005-0.01°C in recent decades in the Pacific Ocean. The magnitude of this physical change is not discernable in the extended OMP analysis, and here it is assumed that the biogeochemical changes at 32°S during the study period (1992, 2003, and 2010) are represented reasonably with the physicochemical characteristics of source water types as defined through the extended OMP analysis.

Five different source water types were defined to explain the physical mixing in the 32°S line below 600dbar. Due to the limitation of number of source water types that can be simultaneously analyzed in the extended OMP analysis (i.e. x_1-x_4 in the **X** vector of eqn. 1), the five different source water types have been divided into two groups. Group 1 consists of AAIW, UCDW, PDW, and LCDW, and the Group 2 with UCDW, PDW, LCDW, and AABW, with substantial amount of overlap between the two groups. Later, the depth ranges for the Group 1 and Group 2 are determined (see Section 3.4).

3.2 Assignment of Redfield ratios

The extended OMP analysis calculates amounts of biogeochemical changes based on prescribed stoichiometric ratios ($r_{C:Si:N:P:-O2}$) (see matrix A in equation 1) (Redfield et al., 1963). The traditional Redfield ratios ($r_{C:N:P:-O2}$=106:16:1:138) have been widely used to account for the biogeochemical changes in a variety of ways. However, more recent studies have used the revised Redfield ratios e.g., $r_{C:N:P:-O2}$=117±14:16±1:1:170 (Anderson and Sarmiento, 1994) and $r_{C:N:P:-O2}$=106:16:1:150±10 (Anderson, 1995). To estimate the regionally representative Redfield ratios for the Pacific 32°S line below 600dbar, the P06 hydrographic data, and the GLODAP (Global Ocean Data Analysis Project database) and the CARINA (CARbon in the North Atlantic database) data (≥600dbar) between 40°S and 20°S (available at http://cdiac3.ornl.gov/waves/discrete/) were used (Fig. 4.1). Assuming $r_{C:P}$=106, the regional Redfield ratios for the P06 line were estimated as $r_{C:Si:N:P:-O2}$=106:18.5:13.6:1:126. Human-induced anthropogenic

perturbations are altering the global carbon and nitrogen cycles (Gruber and Galloway, 2008; Deutsch and Weber, 2011). This ongoing spatiotemporal changes imply that it might be difficult to determine a representative Redfield ratio. Therefore, the 4 different cases of Redfield ratios mentioned above were considered (Table 4.2): case 1 $r_{C:Si:N:P:-O2}$=106:18.5:16:1:138; case 2 $r_{C:Si:N:P:-O2}$=117:18.5:16:1:170; case 3 $r_{C:Si:N:P:-O2}$=117:18.5:16:1:170;, and case 4 of $r_{C:Si:N:P:-O2}$=106:18.5:13.6:1:126. The Si:P ratio ($r_{Si:P}$=18.5) derived from the regionally observed Redfield ratios for the P06 line was collectively assigned to the cases of 1-3.

3.3 Weights for each parameter

The extended OMP analysis uses conservative parameters (i.e. temperature and salinity) as well as non-conservative parameters (i.e. dissolved oxygen, nutrients, and carbonate systems) together. The conservative parameters have high accuracy, whereas the non-con-conservative parameters show relatively lower accuracy and are influenced by biological activities. To resolve this systematic problem, Tomczak and Large (1989) assigned weights to each parameter:

$$W_j = \frac{\sigma_j^2}{\delta_{j\max}} \tag{2}$$

where, σ_j^2 is the variance of parameter j calculated from the physicochemical characteristics of source water types, and δ_{jmax} is the largest observed variance in parameter j in the source region. Equation (2) requires the information of δ_{jmax} obtained at the time water formation was just occurred. Due to the difficulty to determine δ_{jmax}, a different weight equation modified by Kim and Lee (2004) was used, that is:

$$W_j = \frac{\sigma_j}{accuracy_j} \tag{3}$$

where, σ_j is the standard deviation of parameter j calculated from the physicochemical characteristics of source water types, and $accuracy_j$ is the measurement error of parameter j. The weights of each parameter are summarized in Table 4.1.

3.4 Determination of depth range validated by Group 1 (AAIW, UCDW, PDW, and LCDW) and Group 2 (UCDW, PDW, LCDW, and AABW)

Five different source water types are assumed to be involved in the physical mixing in the 32°S line below 600dbar. Due to the limitation of the extended OMP analysis at once (i.e. x_1-x_4 in the **X** vector of eqn. 1), the data are calculated for the two groups: AAIW, UCDW, PDW, and LCDW (Group 1) and UCDW, PDW, LCDW, and AABW (Group 2).

Examination of mass conservation residuals (R_{MC}) was used to validate solutions (Tomczak and Large, 1989; Kim and Lee, 2004).

$$R_{MC}(\%) = \left(\sum_{i=1}^{4} x_i - 1 \right) \times 100 \quad (4)$$

The R_{MC} (%) of Group 1 is well confined within 5% between 1100dbar and 2800dbar, whereas the R_{MC} (%) of Group 1 becomes larger in 600-1100dbar and below 2800dbar (Fig. 4.3a). The higher R_{MC} (%) of Group 1 in 600-1100dbar is derived from the influence of South Pacific Central Water (SPCW) and Subantarctic Mode Water (SAMW) (see Table S10.4 of Talley et al., 2011), and below 2800dbar is from influence of AABW, that is not included in the Group 1. The R_{MC} (%) of Group 2 is confined within 5% the depth layer below 2400dbar (Fig. 4.3b). In summary, seawater properties between 1100dbar and 2800dbar are well described by the Group 1, and those below 2400dbar by the Group 2. With the cut off at the mid-depth of 2600dbar (i.e. between lower limit of 2800dbar for Group 1 and upper limit of 2400dbar for Group 2 based on a threshold within 5% residuals), the results of extended OMP analysis by the Group 1 cover the depths from 1100-2600dbar, and those by the Group 2 represent below 2600dbar (Fig. 4.3c). Note that the mean ΔN_{deni} and x_i averaged from the cases 1-4 are described in the Results below.

4. RESULTS AND DISCUSSIONS

4.1 The effect of PDW definition on extended OMP results

The extended OMP analysis requires the physicochemical characteristics of source water types defined at their source regions (Tomczak and Large, 1989). However, PDW is formed internally by the mixing among intermediate-deep-bottom waters in the North Pacific (Tomczak and Godfrey, 1994). PDW source water characteristics were defined at three different sections of P16N-17N (>40°N), P03 (~24°N), and P21 (~18°S) (Fig. 4.1 and Table 4.3), and the 2010 ΔN_{deni} results for these differing PDW definitions were compared (Fig. 4.4). The differences in mean ΔN_{deni} are small (less than ~0.1 μmol kg^{-1}) between 27.2-27.7 σ_θ. Although the ΔN_{deni} estimates based on different PDW definitions are not significantly different from one another (1100-~6100dbar), their variation becomes apparent below 27.7 σ_θ, and they converge at the range of 27.82-27.84 σ_θ (~3400-6100dbar). The largest difference in mean ΔN_{deni} is ~0.4 μmol kg^{-1} within the 27.74-27.76 σ_θ (~2200-4400dbar) layer, and overall the averaged difference based on the various PDW definitions is 0.1±0.2 μmol kg^{-1}. Thus, the effect of spatially varying PDW's definitions on the results of extended OMP analysis is small.

4.2 Vertical distribution of potential density vs. physical mixing ratios

Mixing ratios describe how much the observed data are influenced by each of the defined source water types. For example, if the mixing ratios at an observed point are composed of AAIW (50%), PDW (40%), and UCDW (10%), it means that the observed properties are determined by 50% of AAIW's characteristics, 40% of PDW's characteristics, and 10% of UCDW characteristics.

Profiles of mixing ratios in the study area (Fig. 4.5) indicate that AAIW (≥50% mixing ratio) is dominant in the range of 27.2-27.4 σ_θ, which is reasonable as the core potential density of AAIW in its formation region is identified typically as ~27.1 σ_θ (England et al., 1993; Bostock et al., 2010), and here results are confined to depths greater than 1100dbar. It is also expected that the mixing ratios would indicate a

somewhat denser AAIW as a consequence of mixing with other higher salinity waters above and below along its path (Stanton, 2002). The potential density layer between 27.5 and 27.8 is mainly composed by UCDW (~20%), PDW (~30%), and LCDW (~50%). The effect of LCDW dominates in this density range at 32°S. This feature is likely related to a large amount of northward transport of LCDW (~13.6 Sv at 28°S) crossing the 32°S line (Talley, 2008). Not surprisingly, AABW is the dominant source water below 27.8 σ_θ (=32.47 σ_1=32.92 σ_2=41.51 σ_3=45.87 σ_4).

4.3 Vertical distribution of denitrification: extended OMP analysis vs. N^*

The mean ΔN_{deni} estimated by the extended OMP analysis gradually increases from close to zero at 27.2-27.3 σ_θ (1100-~1200dbar) to ~0.6-1.0 μmol N kg^{-1} at 27.6-27.7 σ_θ (~1600-2900dbar), and it remains constant within ~0.5-0.9 μmol N kg^{-1} below 27.7 σ_θ (Fig. 4.6a). On the other hand, the mean ΔN_{deni} estimated by the N^* method rapidly increases from -0.8-0 μmol N kg^{-1} at 27.2 σ_θ to -1.9--1.5 μmol N kg^{-1} at 27.5-27.6 σ_θ (~1250-1750dbar) layer. Then it gradually decreases with an increase of potential density (Fig. 4.6a). The mean ΔN_{deni} estimated by the N^* is higher by ~0.6 μmol N kg^{-1} on average than that computed with the extended OMP analysis, but overall the patterns of two methods are similar.

Although the estimated denitrification for the different years (1992, 2003, and 2010) do not differ significantly from one another, the temporal pattern of N^*-based estimates shows that the mean ΔN_{deni} of 2010 (-1.4±0.4 μmol kg^{-1}) was overall slightly larger than those of 2003 (-1.0±0.4 μmol N kg^{-1}) and 1992 (-1.3±0.3 μmol N kg^{-1}) (Fig. 4.6a). The extended OMP analysis-based mean ΔN_{deni} of 2010 (0.7±0.2 μmol N kg^{-1}) was slightly higher than those of 2003 (0.6±0.1 μmol N kg^{-1}) and 1992 (0.6±0.3 μmol N kg^{-1}) (Fig. 4.6a). Although it is difficult to determine whether the estimated denitrification in 2010 different from previous years is within natural variation or is an example demonstrating that denitrification has increased over the last few decades (Gruber, 2008; Deutsch and Weber, 2012), we need to pay attention on such a biogeochemical change.

4.4 Estimating water column denitrification rates using transit time distribution (TTD)

4.4.1 Transit time distribution (TTD) method

TTD is mathematically based on the Green's function (G), translating the surface concentration of transient tracers into the ocean interior by advective and diffusive processes (Holzer and Hall, 2000; Waugh et al., 2003; Waugh et al., 2006). The general form of the TTD method is expressed as:

$$C(x_{\text{interior}},t)=\int_0^{\infty}C_0(x_{surface},t-t')\cdot G(x,t')dt' \tag{5}$$

where, $C(x_{interior},t)$ is the concentration of a passive tracer at time (t) and interior position ($x_{interior}$), $C_0(x_{surface},t)$ is the surface boundary condition representing the history of surface concentration, t-t' is the elapsed time since the water parcel was last in contact with the atmosphere, and G(x,t') is the Green's function (i.e. TTD) that propagates the surface concentration of transient tracer into the ocean interior. It is assumed that a TTD at its interior position is determined by the inverse Gaussian function as follows (Waugh et al., 2003):

$$G(t,\Gamma,\Delta)=\sqrt{\frac{\Gamma^3}{4\pi\Delta^2t^3}}\exp\left(\frac{-\Gamma(t-\Gamma)^2}{4\Delta^2t}\right) \tag{6}$$

Although Waugh et al., (2004) reported that TTDs calculated such that the mean age (Γ) equals the width of TTD (Δ) does well reproduce the transient tracers (e.g. CFCs, tritium, and helium) features in the sub-polar North Atlantic Ocean. To reduce the uncertainty of TTD method (Tanhua et al., 2008), however, it is important to find an appropriate Δ/Γ ratio for a specific study area. Higher Δ/Γ ratio means that the effect of physical mixing is large and water parcel ages are older, whereas lower Δ/Γ ratio indicates that advection process is dominant and water parcel ages are younger. Here, the combination of three transit tracers, such as CFC11, CFC12, and SF_6, was used to find an appropriate Δ/Γ ratio for the 32°S line with the data observed in 2010. Ideally, the TTDs from different tracers should be identical. However, since there are some potential errors

such as measurement error, different nonlinear input history of tracers into the interior of the ocean, and uncertainty in initial surface water saturation conditions (Tanhua et al., 2008), some data deviate from the 1:1 regression line (Fig. 4.7), Here, the best Δ/Γ ratio for the 32°S line was defined as the one with the highest correlation coefficient (r) between tracer TTDs and was determined to range between 0.4-0.8 depending on the tracer pair combination used. The mean Δ/Γ=0.6 (the best estimate for P06) were used along with available CFC12 measurements (2003 and 2010) to estimate TTD ages (Fig. 4.8). The estimated TTD_{CFC12} ages were distributed between ~100 and ~350 years, indicating mean ages when water parcels were transferred from surface to their interior locations by advection-diffusion processes. Using the TTD_{CFC12} age information, mean water denitrification rates were estimated. Not many CFC12 measurements were made in 1992 observation, so 1992 data were not included in the estimation of water column denitrification rates.

4.4.2 Water column denitrification rates in 2003 and 2010 at the P06 (~32°S)

One of the main goals of this research is to estimate water column denitrification rates on open ocean scales, in order to test whether open-ocean water column denitrification rates are significant in Pacific nitrogen budget. The water column denitrification rates (μmol N m^{-3} yr^{-1}) are estimated from the slope of the regression line (i.e. mean ΔN_{deni} vs. TTD_{CFC12} ages). Since it is expected to be lower water column denitrification rates in open ocean, I primarily focus on open ocean oxygen minimum layer (OML) between 1100 and 2000dbar along the transect (Fig. 4.9a) and investigate spatial variation of water column denitrification rates between the western part (ca. 150°E-140°W) and the eastern part (140°W-ca.70°W) based on vertical distribution of dissolved oxygen (Fig. 4.9b).

The extended OMP-based water column denitrification rates within the open ocean OML for the whole transect of the P06 in 2010 are estimated at 3.1±0.4 μmol N m^{-3} yr^{-1} (Fig. 4.10a), and those estimated by the N^* are 7.5±0.7 μmol N m^{-3} yr^{-1} ($7.5x10^{-3}$ μmol N kg^{-1} yr^{-1}) (Fig. 4.10b). Note that the negative N^* values have been multiplied by -

1 to facilitate comparison between the two methods (Fig. 4.10). The estimated denitrification rates by the N^* were about 2-3 times higher than those by the extended OMP (Figs. 4.10a and b). The N^* was based on only the N/P ratio of 16, while the extended OMP analysis considered regional observed N/P ratio (13.6) as well as the traditional N/P ratio (16) (Table 4.2), and also included the effect of physical mixing. Although we don't know at present which of methods is more accurate without direct measurements, I suppose that such slightly different conditions for estimating denitrification result in somewhat different denitrification rates between the two methods.

Deutsch et al., (2001) estimated the water column denitrification rates using N^* in the OMZs of ETNP and ETSP at 0.4±0.1 μmol N kg^{-1} yr^{-1} (25.08-26.75 σ_θ) and 1.2±0.7 μmol N kg^{-1} yr^{-1} (25.8-26.6 σ_θ), respectively. Although the water column denitrification rates estimated in the OML of 32°S line (27.2-27.84 σ_θ) are 2-3 orders of magnitudes lower than those estimated in the ETP, their significant to Pacific nitrogen budget is explored below.

The extended OMP-based water column denitrification rates estimated in OML of P06 in 2010 according to the western and eastern parts are 3.2±0.6 μmol N m^{-3} yr^{-1} (Fig. 4.10c) and 4.9±0.6 μmol N m^{-3} yr^{-1} (Fig. 4.10d), respectively, and those estimated by the N^* are 4.8±0.6 μmol N m^{-3} yr^{-1} (Fig. 4.10e) and 8.8±1.2 μmol N m^{-3} yr^{-1} (Fig. 4.10f), respectively. The water column denitrification rates in the OML of eastern P06 by the extended OMP analysis and the N^* in 2003 are estimated at 3.8±0.8 μmol N m^{-3} yr^{-1} (Fig. 4.10g) and 6.6±1.7 μmol N m^{-3} yr^{-1} (Fig. 4.10h), respectively. The data for the western P06 in 2003 were few, so the western P06 was excluded. These indicate that overall the water column denitrification rates in the eastern P06 (140°W-ca. 70°W) are about two times higher than those in the western P06 (140°W-ca. 70°W). This spatial variation of water column denitrification rates in the study area is consistent with spatial gradients of dissolved oxygen and nitrate concentrations during the WOCE period (http://www.ewoce.org/gallery/Map_Pacific.html).

With thickness of OML ($\Delta H \approx 900$m in Fig. 4.9), the water column denitrification rates in the P06 line are calculated to 2.8-6.8 mmol N m^{-2} yr^{-1} (western: 2.9-4.3 mmol N

m^{-2} yr^{-1}, eastern: 4.4-7.9 mmol N m^{-2} yr^{-1}) by multiplying ΔH (m) to the denitrification rate (μmol N m^{-3} yr^{-1}) (Table 4.4). The variation of PDW definitions on the estimation of denitrification rates were investigated (Table 4.5). The estimated denitrification rates based on PDW defined at the P16N-17N (>40°N) and the P21 (~18°S) were 3.0±0.4 μmol N m^{-3} yr^{-1} and 2.9±0.4 μmol N m^{-3} yr^{-1}, respectively, and the corresponding denitrification rates with ΔH≈900m were calculated at 2.7±0.4 mmol N m^{-2} yr^{-1} and 2.6±0.4 mmol N m^{-2} yr^{-1}, respectively (Table 4.5). These indicated that the effect of spatially varying PDW definitions on the results of extended OMP analysis is small (Tables 4.4 and 5).

Considering the effect of all potential uncertainties on the results, such as the variation of PDW definitions and the different methodology (extended OMP vs. the N^*), this analysis suggests the ranges of denitrification rates estimated along 32°S in the Pacific Ocean by the extended OMP analysis and N^* using the TTD method to be 3.1-7.5 μmol N m^{-3} yr^{-1} (2.6-6.8 mmol N m^{-2} yr^{-1} with ΔH=900m) (Tables 4.4 and 5).

4.5 Implication of open-ocean water column denitrification rates to the Pacific Ocean nitrogen budget

Nitrogen fixation rates have been estimated at station ALOHA (22.48°N, 158°W) in the subtropical North Pacific Ocean during 1988-1995 ranges from 31-51 (=41±10) mmol N m^{-2} yr^{-1} (Karl et al., 1997). The estimated open-ocean water column denitrification rates (2.6-6.8 mmol N m^{-2} yr^{-1}) in OML of 32°S is an order of magnitude lower than the long-term nitrogen fixation rates. The oceanic nitrogen mass balance between sources (e.g. nitrogen fixation) and sinks (e.g. denitrification) in the Pacific Ocean can be approximately investigated by a simple calculation. The OML water column denitrification and nitrogen fixation rates are extrapolated to the entire Pacific basin (40°S-65°N; area=$130x10^{12}m^2$, Deutsch et al., 2007), and combined the water column denitrification (48±5 Tg N yr^{-1}) at OMZs of ETP and benthic denitrification (15±5 Tg N yr^{-1}) for total denitrification rates in the Pacific Ocean (Deutsch et al., 2001).

The integrated nitrogen fixation rates are 56-93 (=75±18) Tg N yr^{-1}, and the integrated denitrification rates are 58-86 (=72±14) Tg N yr^{-1} in this calculation. This result suggests a possibility that a balance between total denitrification rates and total nitrogen fixation rates might be reached in the Pacific Ocean. However, the suggested balance assumes that the North Pacific ALOHA nitrogen fixation rates and our South Pacific denitrification rates are each representative for the entire Pacific basin. Recent studies have reported somewhat lower nitrogen fixation rates in the South Pacific Ocean (~20 mmol m^{-2} yr^{-1}) compared to the North Pacific Ocean (ALOHA: ~40 mmol m^{-2} yr^{-1}) (Karl et al., 1997; Sohm et al., 2011), and no estimate of open-ocean water column denitrification rates is presently available for the North Pacific. To verify the possibility of a mass balance between nitrogen fixation and denitrification in the Pacific Ocean will require measurement of nitrogen fixation rates and estimates denitrification rates across broader regions of the full Pacific.

In the mean time, Deutsch et al., (2007) recently estimated the nitrogen fixation rates from the observed nutrient data using an ocean circulation model as 93-108, 13-25, and 130-158 Tg N yr^{-1} in the Pacific Ocean, the Atlantic Ocean, and the global ocean, respectively (see their Table 1). They reported that the Pacific Ocean is a major source of oceanic nitrogen, and that the nitrogen fixation is highest in ETP. The nitrogen fixation rates, modeled by Deutsch et al., (2007), were ~100±8 Tg N yr^{-1} for the whole Pacific Ocean (0-120m, 40°S-65°N; area=130x$10^{12}$$m^2$). These rates ($100 \pm 8\ Tg\ N\ yr^{-1} \times area^{-1} \times \frac{1 mol\ N}{14 g} \approx 55 \pm 4\ mmol\ N\ m^{-2}\ yr^{-1}$) are somewhat higher than the integrated nitrogen fixation rates (~75±18 Tg N yr^{-1}≈41±10 mmol N m^{-2} yr^{-1}) based on Karl et al., (1997). Although we don't know at present if the modeled nitrogen fixation rates were overestimated, this discrepancy must be examined in the future.

Nevertheless, in order to make a balance between Pacific nitrogen fixation rates (~100±8 Tg N yr^{-1}) modeled by Deutsch et al., (2007) and Pacific denitrification rates (~72±14 Tg N yr^{-1}), it requires more nitrogen removal via denitrification (~28 Tg N yr^{-1}). If we extend the estimation of open-ocean water column denitrification rates to water

column below OML (i.e. ≥1100dbar), although the ΔN_{deni}, denitrified nitrate, is fairly small in deep waters, the water column denitrification rates are estimated at 2.6-3.9 μmol N m^{-3} yr^{-1} (=11.7-17.6 mmol N m^{-2} yr^{-1} with ΔH=4500m) (Fig. 4.11). However, the correlations of regression analysis are somewhat poor. Nevertheless, if we assume that these water column denitrification rates estimated at 32°S are mean values for the whole water column and representative throughout the Pacific Ocean outside OMZs, the open-ocean water column denitrification rates are estimated at 21-32 (=27±5) Tg N yr^{-1}. Total Pacific denitrification rate (i.e. open-ocean water column denitrification outside the OMZs + water column denitrification within OMZs + benthic denitrification) becomes ~90±15 Tg N yr^{-1}. Although very roughly estimated, this total Pacific denitrification rate (~90±15 Tg N yr^{-1}) is comparable to the total nitrogen fixation rate (~100±8 Tg N yr^{-1}) modeled by Deutsch et al., (2007). Otherwise, water column denitrification within OMZs and/or benthic denitrification rates, estimated by Deutsch et al., (2001), might be underestimated. Thus, we need to examine whether modeled nitrogen fixation rates were overestimated or water column denitrification within OMZs and/or benthic denitrification rates were underestimated in future study. In addition, we will need to investigate open ocean thermocline layer to get more accurate open ocean water column denitrification rates as well.

As shown in the examples above, it implies that open-ocean water column denitrification outside OMZs must be considered as an important component of the Pacific nitrogen budget.

5. CONCLUSIONS

The amount of denitrification in the water column below 1100dbar (27.2-27.84 σ_θ) was estimated along the P06 (32°S) line of South Pacific Ocean with the hydrographic data observed in 1992, 2003, and 2010 by the extended OMP analysis and the N^*. The water column denitrification rates in OML of P06 line were estimated for 2003 and 2010 using the relationship between the amount of denitrification (ΔN_{deni}) and TTD_{CFC12} ages through the linear regression analysis. The mean water column

denitrification rate estimated by the extended OMP analysis was estimated at 3.1±0.4 μmol N m^{-3} yr^{-1}, and that estimated by the N^* was 7.5±0.4 μmol N m^{-3} yr^{-1}. Spatial variation of the water column denitrification rates showed that the water column denitrification rates in the eastern P06 (140°W-~70°W) were about two times higher than those in the western P06 (~150°E-140°W). The mean water column denitrification rates estimated in OML of P06 line (1100-2000dbar) were 2-3 orders of magnitudes lower than those estimated in OMZs of ETP. The water column denitrification rates in the OML were estimated as 3.1-7.5 μmol N m^{-3} $yr^{-}1$ (=2.6-6.8 mmol N m^{-2} yr^{-1} with ΔH=900m), and whole water column below 1100dbar were estimated as 2.6-3.9 μmol N m^{-3} yr^{-1} (=11.7-17.6 mmol N m^{-2} yr^{-1} with ΔH=4500m). Although roughly estimated, the results suggested that the water column denitrification of the open Pacific Ocean outside OMZs may also be a key component of the present nitrogen budget in Pacific Ocean and possibly in the global ocean as well.

REFERENCES

Alldredge, A.L., and M.W. Silver, 1988. Characteristics, dynamics and significance of marine snow. Progress in Oceanography, 20, 41-82.

Alldredge, A.L., and Y. Cohen, 1987. Can microscale chemical patches persist in the sea? Microelectrode study of marine snow, fecal pellets. Science, 235, 689-691.

Anderson, L.A., 1995. On the hydrogen and oxygen content of marine phytoplankton. Deep-Sea Research I, 42, 1675-1680.

Anderson, L.A., and J.L. Sarmiento, 1994. Redfield ratios of remineralization determined by nutrient data analysis. Global Biogeochemical Cycles, 8(1), 65-80.

Bostock, H.C., B.N. Opdyke, and M.J.M. Williams, 2010. Characterizing the intermediate depth waters of the Pacific Ocean using $\delta^{13}C$ and other geochemical tracers. Deep-Sea Research I, 57, 847-859.

Bostock, H.C., B.W. Hayward, H.L. Neil, K.I. Currie, and G.B. Dunbar, 2011. Deep-water carbonate concentrations in the southwest Pacific. Deep-Sea Research I, 58, 72-85.

Brandes, J.A., A.H. Devol, and C. Deutsch, 2007. New developments in the marine nitrogen cycle. Chemical Reviews, 107, 577-589.

Deutsch C., N. Gruber, R.M. Key, and J. Sarmiento, 2001. Denitrification and N_2 fixation in the Pacific Ocean. Global Biogeochemical Cycles, 15, 483-506.

Deutsch, C., and T. Weber, 2012. Nutrient ratios as a tracer and driver of ocean biogeochemistry. The Annual Review of Marine Science, 4, 113-141.

Deutsch, C., J.L. Sarmiento, D.M. Sigman, N. Gruber, and J.P. Dunne, 2007. Spatial coupling of nitrogen inputs and losses in the ocean. Nature, 445, 163-167.

England, M.H., J.S. Godfrey, A.C. Hirst, and M. Tomczak, 1993. The mechanism for Antarctic Intermediate Water renewal in a world ocean model. Journal of Physical Oceanography, 23, 1553-1560.

Falkowski, P.G., 1997. Evolution of the nitrogen cycle and its influence on the biological sequestration of CO_2 in the ocean, Nature, 272-275.

Fiadeiro, M., 1980. The alkalinity of the deep Pacific. Earth and Planetary Science Letters, 49, 499-505.

Gruber, N., 2008. The marine nitrogen cycle: Overview of distributions and processes, In: Nitrogen in the marine environment, 2nd edition, edited by D.G. Capone, D.A. Bronk, M.R. Mulholland, and E.J. Carpenter, Elsevier, Amsterdam, 1-50.

Gruber, N., and J.L. Sarmiento, 1997. Global patterns of marine nitrogen fixation and denitrification, Global Biogeochemical Cycles, 11(2), 235-266.

Gruber, N., and J.L. Sarmiento, 2002. Biogeochemical/physical interactions in elemental cycles; in The Sea, edited by A.R. Robinson, J.J. McCarthy, and B.J. Rothschild, 12, 337-339.

Gruber, N., and J.N. Galloway, 2008. An Earth-system perspective of the global nitrogen cycle. Nature, 451, 293-296.

Hall, T.M., D.W. Waugh, T.W.N. Haine, P.E. Robbins, and S. Khatiwala, 2004. Estimates of anthropogenic carbon in the Indian Ocean with allowance for mixing and time-varying air-sea CO_2 disequilibrium. Global Biogeochemical Cycles, 18, GB1031, doi:10.1029/2003GB002120.

Hartin, C.A., R.A. Fine, B.M. Sloyan, L.D. Talley, T.K. Chereskin, and J. Happell, 2011. Formation rates of Subantarctic mode water and Antarctic intermediate water within the South Pacific. Deep-Sea Research I, 58, 524-534.

Holzer, M., and T.M. Hall, 2000. Transit-time and tracer-age distributions in geophysical flows. Journal of the Atmospheric Sciences, 57, 3539-3558.

Hupe, A., and J. Karstensen, 2000. Redfield stoichiometry in Arabian Sea subsurface waters, Global Biogeochemical Cycles, 14(1) 357-372.

Johnson, G.C., and A.H. Orsi, 1997. Southwest Pacific Ocean water-mass changes between 1968/69 and 1990/91. Journal of Climate, 10, 306-316.

Johnson, G.C., and J.M. Toole, 1993. Flow of deep and bottom waters in the Pacific at 10°N. Deep-Sea Research I, 40, 371-394.

Karl, D., A. Michaels, B. Bergman, D. Capone, E. Carpenter, R. Letelier, F. Lipschultz, H. Paerl, D. Sigman, and L. Stal, 2002. Dinitrogen fixation in the world's oceans. Biogeochemistry, 57, 47-98.

Karl, D., R. Letelier, L. Tupas, J. Dore, J. Christian, and D. Hebel, 1997. The role of nitrogen fixation in biogeochemical cycling in the subtropical North Pacific Ocean. Nature, 388, 533-538.

Karstensen, J., and M. Tomczak, 1998. Age determination of mixed water masses using CFC and oxygen data. Journal of Geophysical Research, 103(C9), 18599-18609.

Kawabe, M., S. Fujio, D. Yanagimoto, and K. Tanaka, 2009. Water masses and currents of deep circulation southwest of the Shatsky Rise in the western North Pacific. Deep-Sea Research I, 56, 1675-1687.

Kawano, T., M. Fukasawa, S. Kouketsu, and H. Uchida, 2006. Bottom water warming along the pathway of lower circumpolar deep water in the Pacific Ocean. Geophysical Research Letters, 33, L23613, doi:10.1029/2006GL027933.

Kim, I.-N., and T. Lee, 2004. Summer hydrographic features of the East Sea analyzed by the Optimum Multiparameter method, Ocean and Polar Research, 26(4), 581-594.

Mantyla, A.W., and J.L. Reid, 1983. Abyssal characteristics of the World Ocean waters. Deep-Sea Research, 30, 805-833.

McCave, I.N., L. Carter, and I.R. Hall, 2008. Glacial-interglacial changes in water mass structure and flow in the SW Pacific Ocean. Quaternary Science Reviews, 27, 1886-1908.

Murata, A., Y. Kumamoto, S. Watanabe, and M. Fukasawa, 2007. Decadal increase of anthropogenic CO_2 in the South Pacific subtropical ocean along 32S. Journal of Geophysical Research, 112, C05033, doi:10.1029/2005JC003405.

Orsi, A.H., G.C. Johnson, and J.L. Bullister, 1999. Circulation, mixing, and production of Antarctic Bottom Water. Progress in Oceanography, 43, 55-109.

Orsi, A.H., W.M. Smethie Jr., and J.L. Bullister, 2002. On the total input of Antarctic waters to the deep ocean: A preliminary estimate from chlorofluorocarbon measurements. Journal of Geophysical Research, 107 (C8), 3122, 10.1029/2001JC000976.

Ploug, H., M. Kühl, B. Buchholz-Cleven, B.B. Jørgensen, 1997. Anoxic aggregates-an ephemeral phenomenon in the pelagic environment?. Aquatic Microbial Ecology, 13, 285-294.

Redfield, A.C., B.H. Ketchum, and F.A. Richards, 1963. The influence of organism on the composition of sea water; in The Sea, edited by M.N. Hill, 2, 26-77.

Reid, J.L., 1986. On the total geostrophic circulation of the South Pacific Ocean: Flow patterns, Tracers and Transports. Progress in Oceanography, 16, 1-61.

Reid, J.L., 1997. On the total geostrophic circulation of the South Pacific Ocean: Flow patterns, Tracers and Transports. Progress in Oceanography, 39, 263-352.

Shanks, A.L., and M.L. Reeder, 1993. Reducing microzones and sulfide production in marine snow. Marine Ecology Progress Series, 96, 43-47.

Sohm, J.A., E.A. Webb, and D.G. Capone, 2011. Emerging patterns of marine nitrogen fixation. Nature Reviews Microbiology, 9, 499-508.

Stanton, B.R., 2002. Antarctic Intermediate Water variability in the northern New Zealand region. New Zealand Journal of Marine and Freshwater Research, 36, 645-654.

Talley, L.D., 2008. Freshwater transport estimates and the global overturning circulation: Shallow, deep and throughflow components. Progress in Oceanography, 78, 257-303.

Talley, L.D., and T.M. Joyce, 1992. The double silica maximum in the North Pacific. Journal of Geophysical Research, 97, 5465-5480.

Talley, L.D., G.L. Pickard, W.J. Emery, and J.H. Swift, 2011. Descriptive Physical Oceanography: An Introduction (Sixth edition), Elsevier, Boston, 1-560.

Tanhua, T., D.W. Waugh, and D.W.R. Wallace, 2008. Use of SF_6 to estimate anthropogenic CO_2 in the upper ocean. Journal of Geophysical Research, 113, C04037, doi:10.1029/2007JC004416.

Tomczak, M. and D.G.B. Large. 1989. Optimum Multiparameter analysis of mixing in the thermocline of the Eastern Indian Ocean. Journal of Geophysical Research, 94, 16141-16149.

Tomczak, M., and J.S. Godfrey, 1994. Regional Oceanography: An Introduction. Pergamon Press, Oxford, UK, 1-422.

Tomczak, M., and S. Liefrink, 2005. Interannual variations of water mass volumes in the Southern Ocean. Journal of Atmospheric and Ocean Science, 10, 31-42.

Tsuchiya, M., and L.D. Talley, 1996. Water-property distributions along an eastern Pacific hydrographic section at 135W. Journal of Marine Research, 54, 541-564.

Van Heuven, S., D., Pierrot, E. Lewis, and D.W.R. Wallace, 2009. MATLAB program developed for CO2 system calculations. ORNL/CDIAC-105b, Carbon Dioxide Information Analysis Center, Oak Ridge National Laboratory, US Department of Energy, Oak Ridge, Tennessee.

Waugh, D.W., T.M. Hall, and T.W.N. Haine, 2003. Relationship among tracer ages. Journal of Geophysical Research, 108 (C5), 3138, doi:10.1029/2002JC001325.

Waugh, D.W., T.M. Hall, B.I. McNeil, R. key, and R.J. Matear, 2006. Anthropogenic CO_2 in the oceans estimated using transit time distributions. Tellus, 58B, 376-389.

Waugh, D.W., T.W.N. Haine, and T.M. Hall, 2004. Transport times and anthropogenic carbon in the subpolar North Atlantic Ocean. Deep-Sea Research I, 51, 1475-1491.

Wijffels, S.E., J.M. Toole, and R. Davis, 2001. Revisiting the South Pacific subtropical circulation: A synthesis of World Ocean Circulation Experiment observations along 32°S. Journal of Geophysical Research, 106, 19481-19513.

Wolgast, D.M., A.F. Carlucci, and J.E. Bauer, 1998. Nitrate respiration associated with detrital aggregates in aerobic bottom waters of the abyssal NE Pacific. Deep-Sea Research II 45, 881-892.

Yamagishi, H., N. Yoshida, S. Toyoda, B.N. Popp, M.B. Westley, and S. Watanabe, 2005. Contributions of denitrification and mixing on the distribution of nitrous oxide in the North Pacific. Geophysical Research Letters, 32, L04603, doi:10.1029/2004GL021458.

Table 4.1: The physicochemical characteristics of source water types and weights for each parameter used in the extended OMP analysis at the P06 line (~32°S) of South Pacific Ocean.

Group 1								
SWT	*PT (℃)	S (psu)	DO (μmol kg^{-1})	Si (μmol kg^{-1})	NO_3 (μmol kg^{-1})	PO_4 (μmol kg^{-1})	TALK. (μmol kg^{-1})	DIC (μmol kg^{-1})
AAIW	5.0	34.2	270	12.3	24.0	1.7	2277	2137
UCDW	2.5	34.5	179	65.7	34.5	2.4	2328	2238
+PDW	1.3	34.7	128	170	37.9	2.7	2436	2353
LCDW	1.6	34.7	194	94.6	31.2	2.1	2359	2249
weight	340	117	29	63	21	21	37	59

Group 2								
SWT	*PT (℃)	S (psu)	DO (μmol kg^{-1})	Si (μmol kg^{-1})	NO_3 (μmol kg^{-1})	PO_4 (μmol kg^{-1})	TALK. (μmol kg^{-1})	DIC (μmol kg^{-1})
UCDW	2.5	34.5	179	65.7	34.5	2.4	2328	2238
+PDW	1.3	34.7	128	170	37.8	2.7	2436	2353
LCDW	1.6	34.7	194	94.6	31.2	2.1	2359	2249
AABW	0.5	34.7	211	126	32.4	2.2	2369	2259
weight	167	57	18	43	10	12	25	35

*PT: potential temperature

+PDW was defined at the P03 line in the North Pacific Ocean (Fig. 4.1).

AAIW: Antarctic Intermediate Water, U(L)CDW: Upper (Lower) Circumpolar Deep Water, PDW: Pacific Deep Water, AABW: Antarctic Bottom Water

Table 4.2: Four different cases of Redfield ratios applied to the extended OMP analysis.

Case	$r_{-O2/P}$	$r_{P/P}$	$r_{N/P}$	$r_{Si/P}$	$r_{C/P}$	Ref.
1	138	1	16	18.5	106	Redfield et al. (1963)
2	170	1	16	18.5	117	Anderson and Sarmiento (1994)
3	150	1	16	18.5	106	Anderson (1995)
4	126	1	13.6	18.5	106	This study (2012)

Table 4.3: Physicochemical characteristics of Pacific Deep Water (PDW) defined at the P16N-17N (>40°N), P03 (~24°N), and P21 (~18°S) lines of Pacific Ocean (Fig. 4.1).

PDW	PT (℃)	S (psu)	DO (μmol kg^{-1})	Si (μmol kg^{-1})	NO_3 (μmol kg^{-1})	PO_4 (μmol kg^{-1})	TALK. (μmol kg^{-1})	DIC (μmol kg^{-1})
P16N-17N	1.4	34.7	106	183	38.8	2.8	2449	2359
P03	1.3	34.7	128	170	37.9	2.7	2436	2353
P21	1.6	34.7	134	143	37.0	2.6	2429	2342

Table 4.4: Estimated mean water column denitrification rates in the oxygen minimum layer (1100-2000dbar, ΔH≈900m) of the P06 line in the South Pacific Ocean. Note that the negative numbers of N^* slopes are converted to positive numbers. Uncertainty of 1 standard deviation is represented.

Year	method	Data (#)	Mean ΔN_{deni} rate (μmol N m^{-3} yr^{-1})	ΔH (m)	Mean ΔN_{deni} rate (mmol N m^{-2} yr^{-1})	remark
2003	eOMP	63	3.8±0.8	900	3.4±0.7	*eastern
2003	N^*	63	6.6±1.7		5.9±1.5	eastern
2010	eOMP	388	3.2±0.6		2.9±0.5	*western
2010	N^*	347	4.9±0.6		4.4±0.5	eastern
2010	eOMP	388	4.8±0.6		4.3±0.5	western
2010	N^*	347	8.8±1.2		7.9±1.0	eastern
2010	eOMP	735	3.1±0.4		2.8±0.4	P06
2010	N^*	735	7.5±0.7		6.8±0.6	P06

*western is 150°E-140°W, and *eastern is 140°W-70°W (Fig. 4.9b).

Table 4.5: Extended OMP analysis estimates of mean water column denitrification rates at 32°S in the Pacific according to PDW definitions at the P16N-17N (>40°N) and P21 (~18°S) lines in the OML of P06 (~32°S) line (Fig. 4.1). Uncertainty of 1 standard deviation is represented. To estimate mean water column denitrification rates, a ΔH= 900m is used.

Year	PDW defined at	Mean ΔN_{deni} rate ($\mu mol\ N\ m^{-3}\ yr^{-1}$)	Mean ΔN_{deni} rate ($mmol\ N\ m^{-2}\ yr^{-1}$)
2010	P16N-17N	3.0±0.4	2.7±0.4
2010	P21	2.9±0.4	2.6±0.4

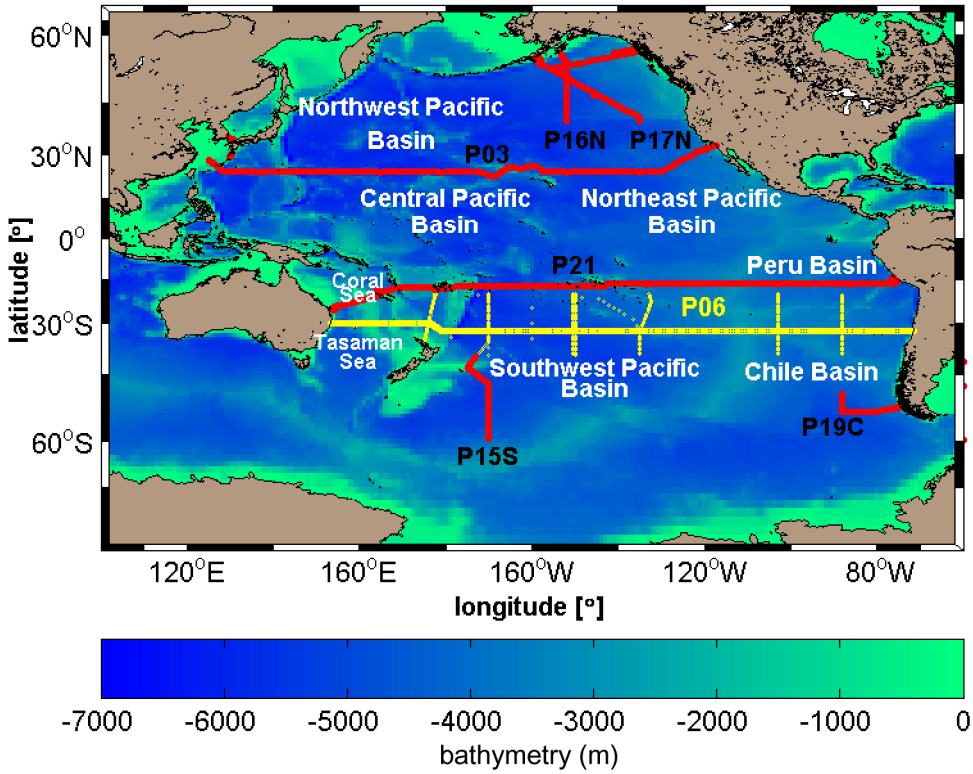

Figure 4.1: Map showing the hydrographic section of P06 (~32°S) and bottom topography of the Pacific Ocean. The hydrographic data of P16N-17N, P03, P21, P15S, and P19C (CCHDO: http://cchdo.ucsd.edu/) were used to define the physicochemical characteristics of source water types (i.e. AAIW, PDW, U/LCDW, and AABW). The GLODAP (Global Ocean Data Analysis Project database) and the CARINA (CARbon in the North Atlantic database) data extracted between 40°S and 20°S (http://cdiac3.ornl.gov/waves/discrete/) (≥600dbar) were used to estimate the regional Redfield ratios for the P06 line with the observed P06 data together.

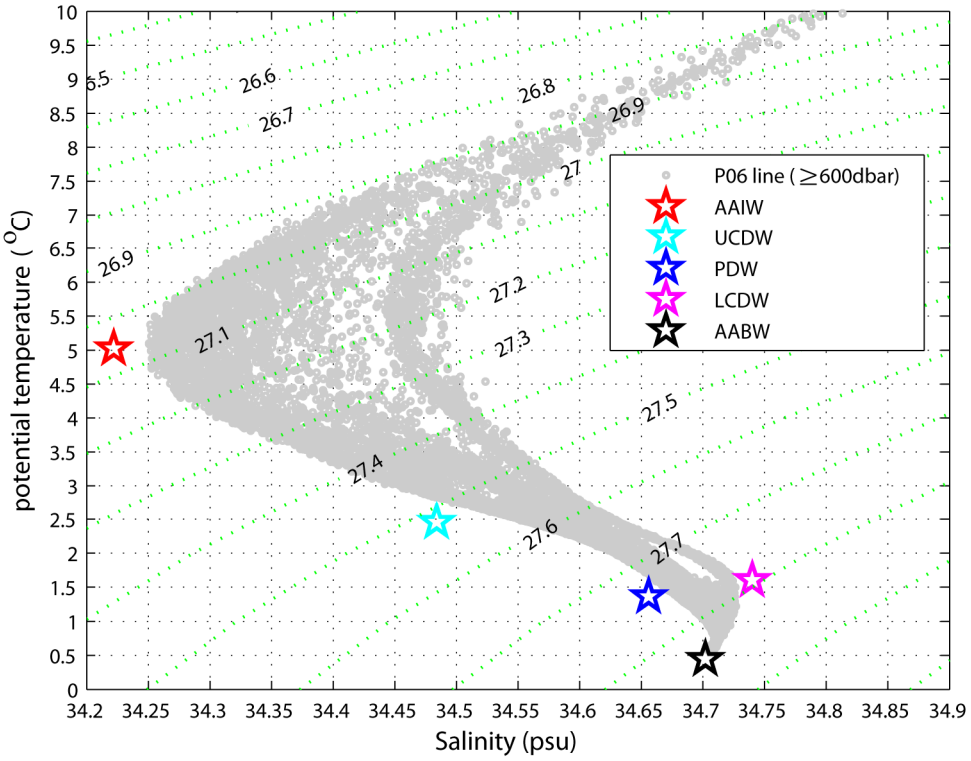

Figure 4.2: Temperature-salinity diagram for P06 (~32°S) based the 1992, 2003, and 2010 datasets. The physical characteristics of source water types (stars) defined are also shown.

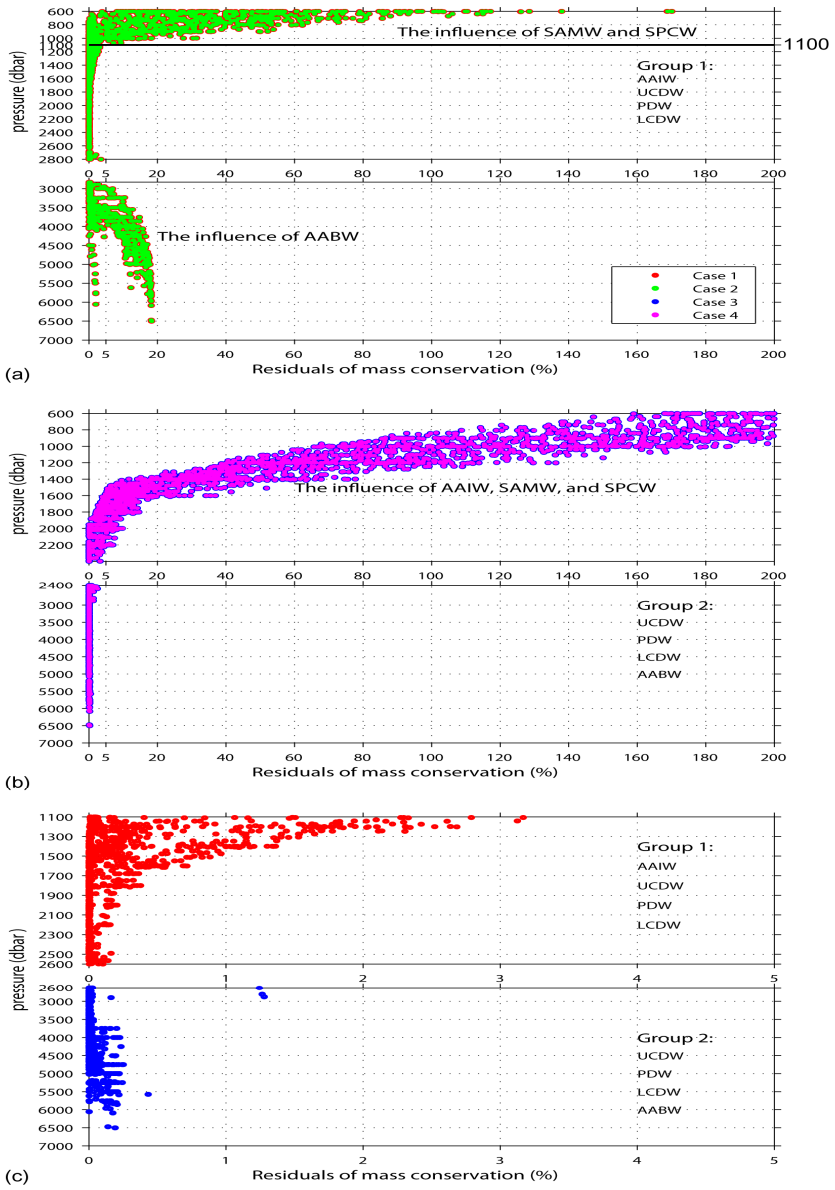

Figure 4.3: (a) Pressure (≥600dbar) vs. residuals of mass conservation for 4 different Redfield ratios cases and the Group 1 (i.e. AAIW, UCDW, PDW, and LCDW). The higher residuals in 600-1100dbar are caused by the influence of South Pacific Central Water (SPCW) and Subantarctic Mode Water (SAMW) (Talley et al., 2011), (b) Pressure (≥600dbar) vs. residuals of mass conservation for 4 different Redfield cases and the Group 2 (i.e. UCDW, PDW, LCDW, and AABW), and (c) Pressure vs. residual of mass conservation defined by the Group 1 (1100-2600dbar) and Group 2 (>2600dbar), respectively, with the criterion of residuals (<5%).

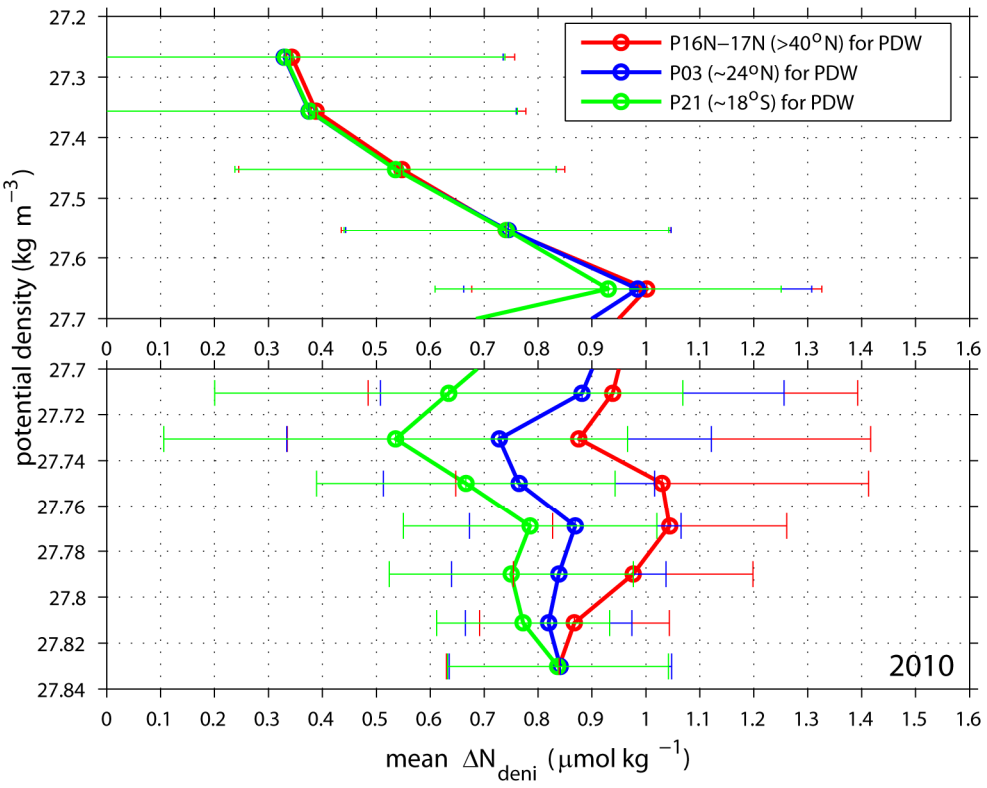

Figure 4.4: Vertical profiles of denitrification (μmol kg^{-1}) estimated by extended OMP analysis vs. potential density (kg m^{-3}) according to the PDW definitions defined at the P16N-17N (red), P03 (blue), and P21 (green), respectively. Note that the values (ΔN_{deni} and x_i) averaged from the cases 1-4 are used. Error bars represent standard deviation.

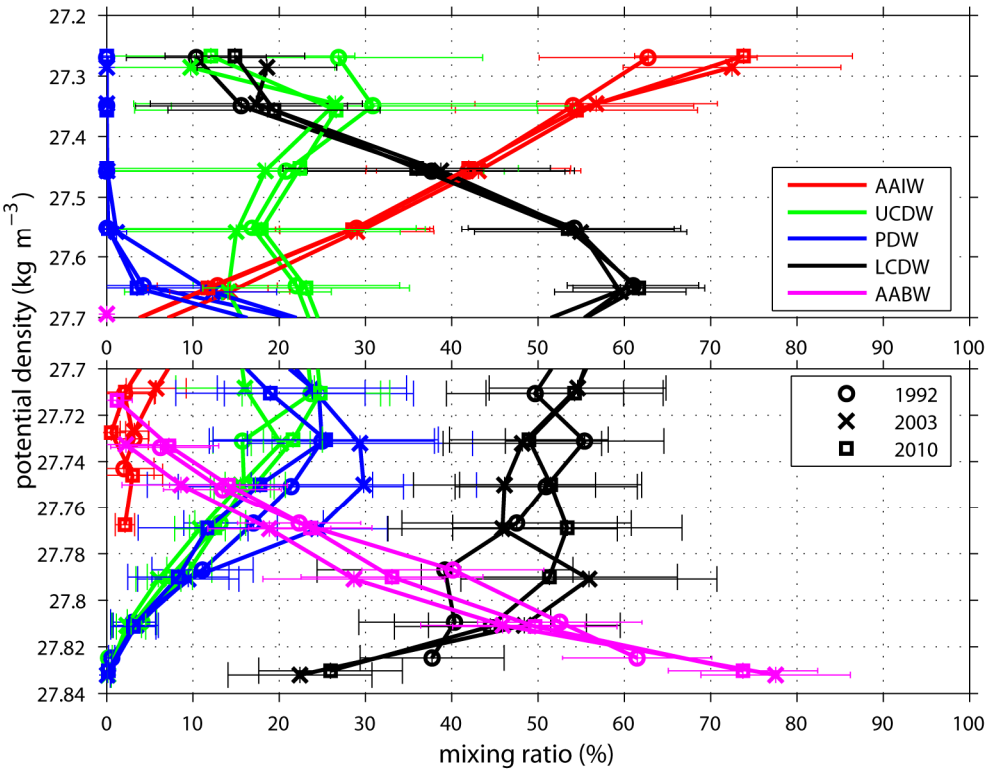

Figure 4.5: Vertical profile of the physical mixing ratios (%) of source water types (AAIW-red, UCDW-green, PDW-blue, LCDW-black, and AABW-magenta) estimated by the extended OMP analysis at the P06 (1992-circles, 2003-crosses, and 2010-squares) vs. potential density (kg m^{-3}). Error bars represent standard deviation.

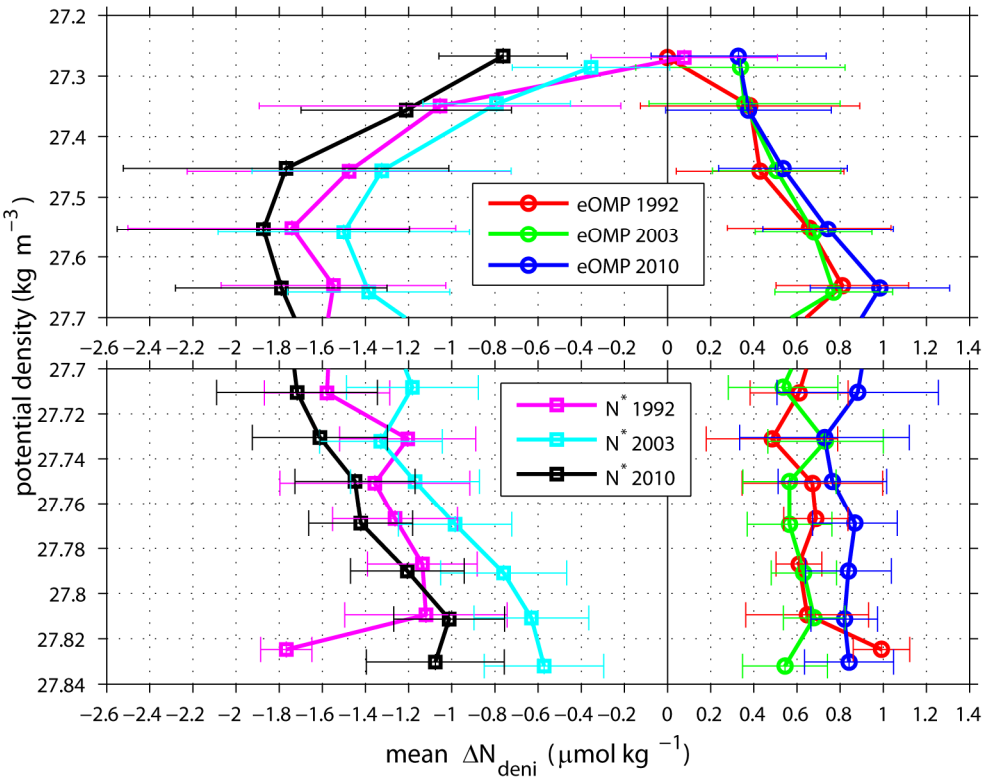

Figure 4.6: Vertical profile of the potential density (kg m^{-3}) vs. the denitrification (μmol kg^{-1}) estimated at the P06 (1992, 2003, and 2010) by the extended OMP analysis (red, green, and blue circles, respectively) and the N* method (magenta, cyan, and black squares, respectively). Error bars represent standard deviation.

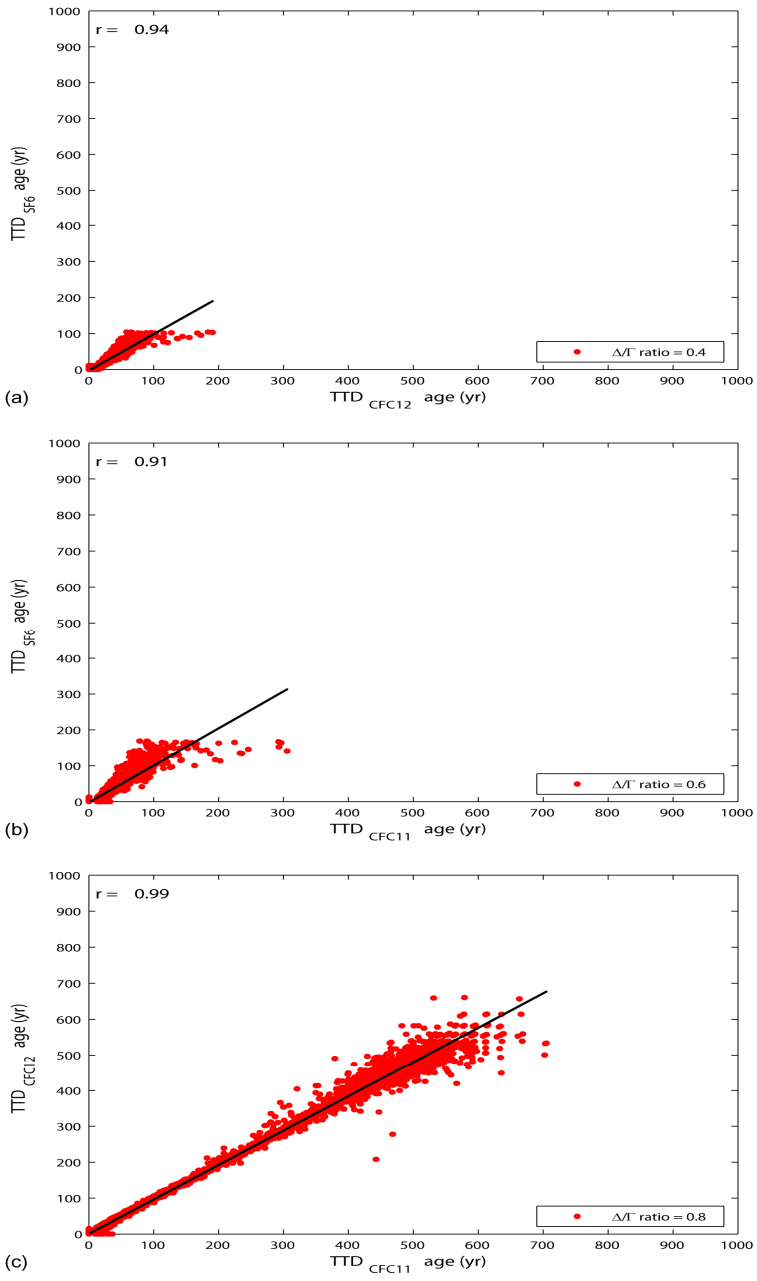

Figure 4.7: Determination of an appropriate ratio of TTD width (Δ)/the mean age (Γ) ratio for the study area. The combination of three transient tracers, such as CFC11, CFC12, and SF_6, is used to find an appropriate Δ/Γ ratio for the P06 line with the data observed in 2010. (a) TTD_{SF6} vs. TTD_{CFC12} (r=0.94 with Δ/Γ ratio=0.4), (b) TTD_{SF6} vs. TTD_{CFC11} (r=0.91 with Δ/Γ ratio=0.6), and (c) TTD_{CFC12} vs. TTD_{CFC11} (r=0.99 with Δ/Γ ratio=0.8).

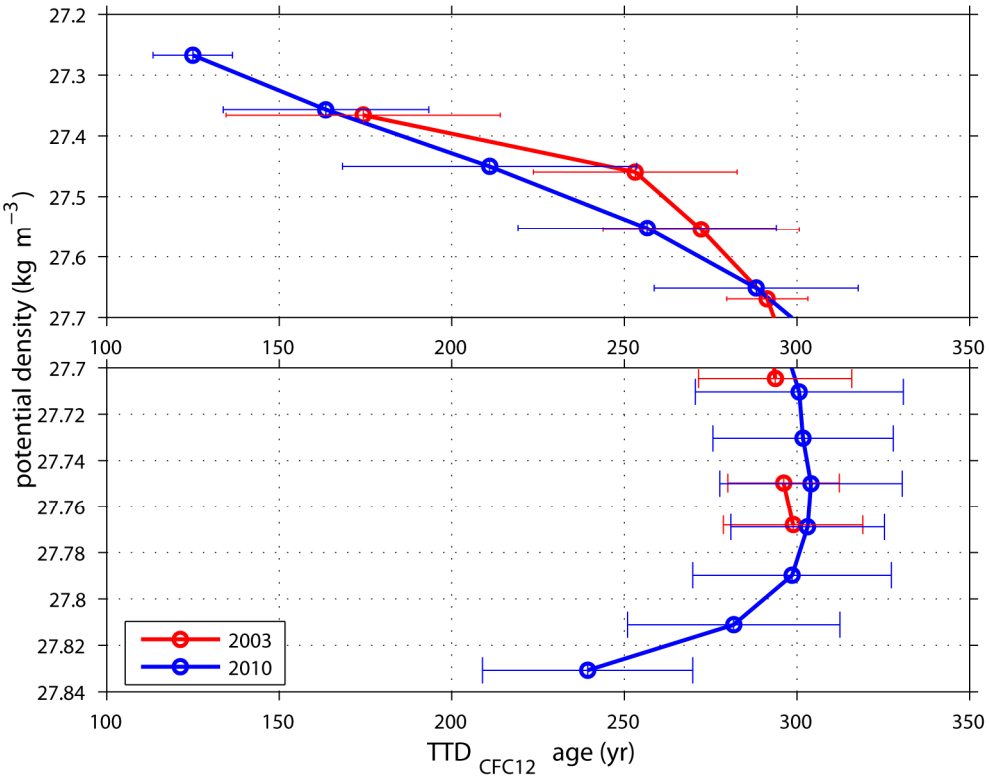

Figure 4.8: Vertical profile of potential density (kg m^{-3}) vs. TTD_{CFC12} age (yr) estimated at the P06 line (2003-red and 2010-blue). Error bars represent standard deviation.

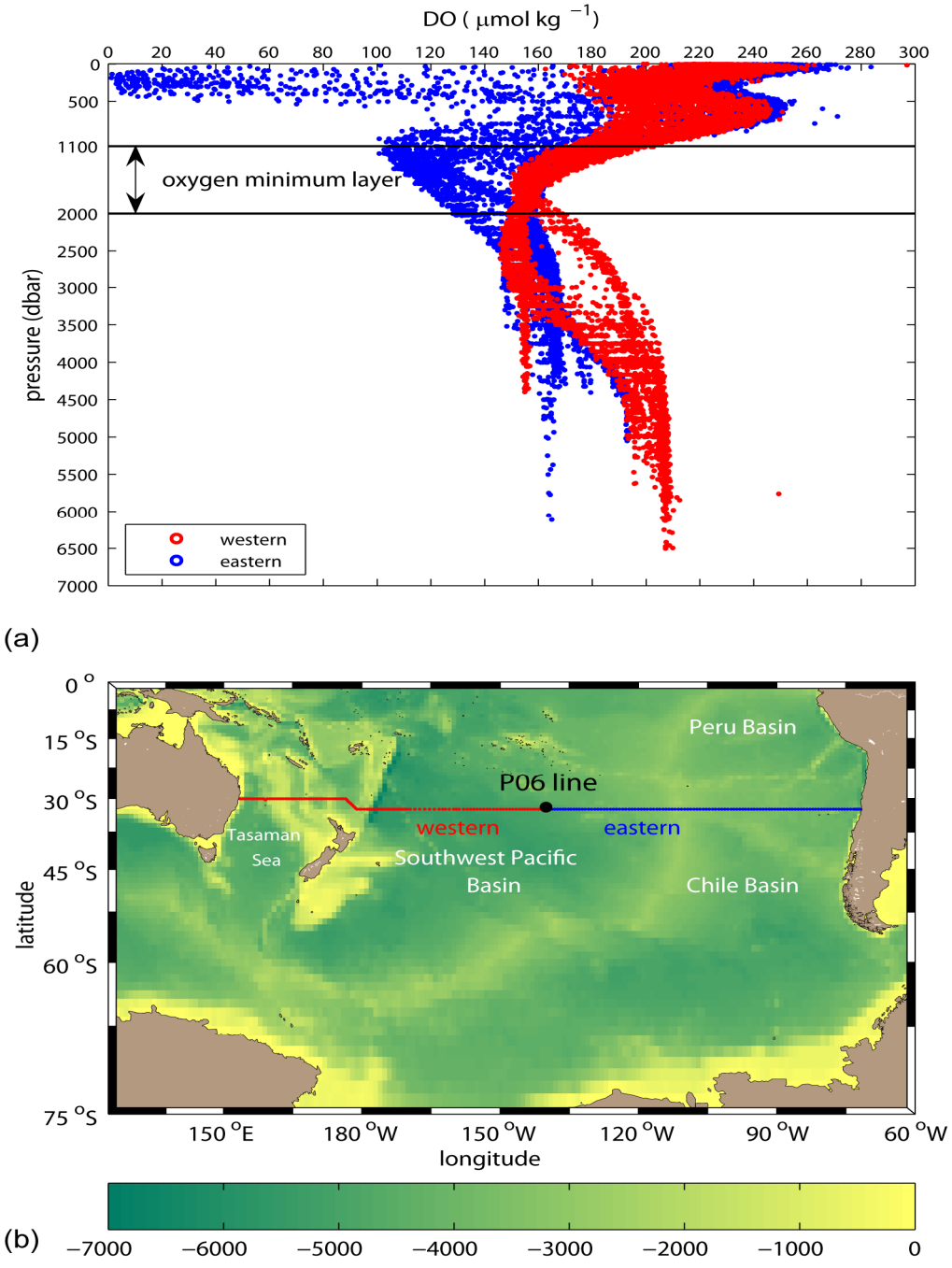

Figure 4.9: (a) Vertical profile of dissolved oxygen (µmol kg^{-1}), and (b) A study area map. The P06 line is divided into two regions at 140°W based on the distribution of oxygen minimum layer (Western: 150 ° E-140 ° W red, Eastern: 140°W-70°W blue).

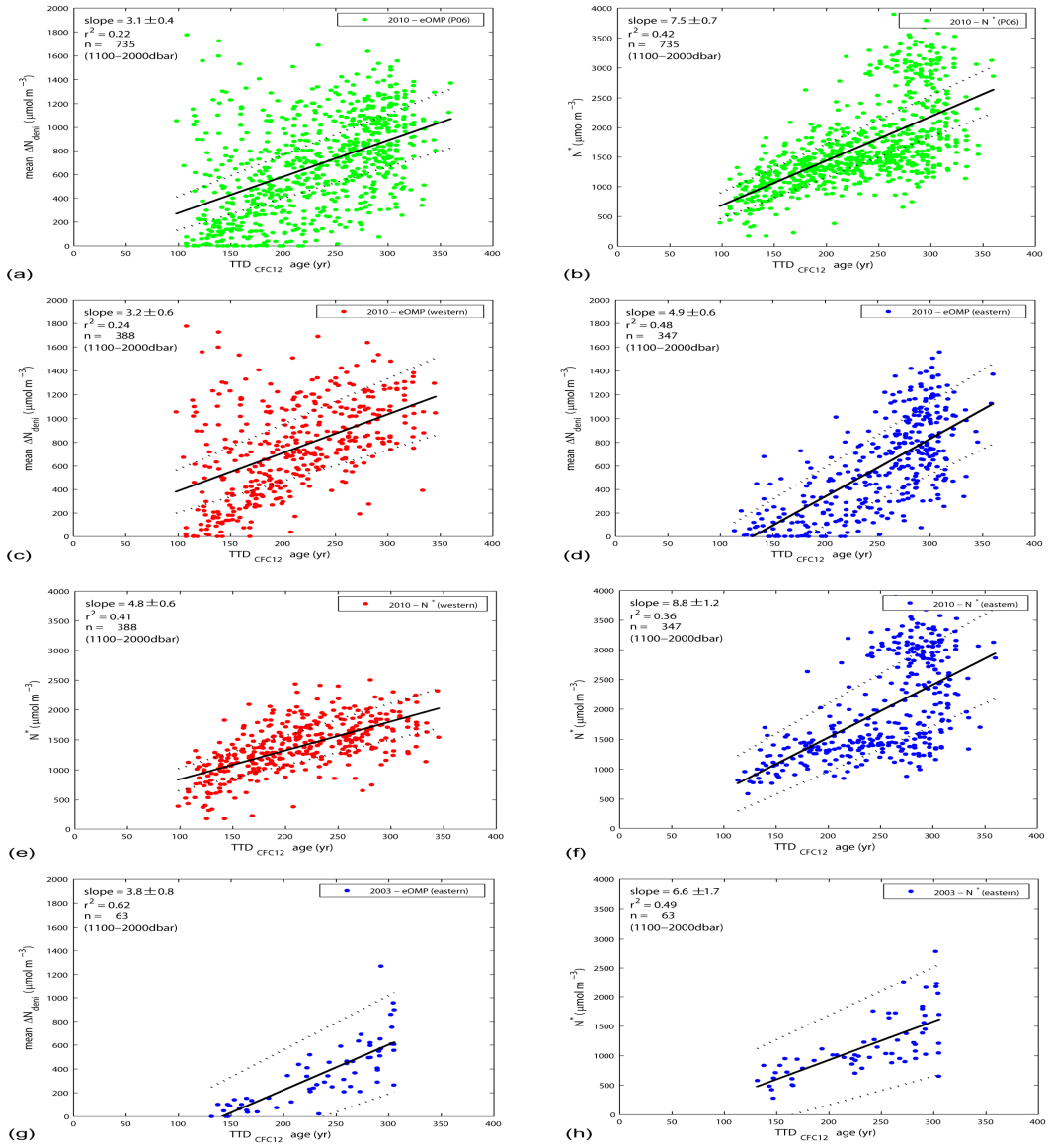

Figure 4.10: (a)-(b) Mean water column denitrification rates in the oxygen minimum layer (1100-2000dbar) of P06 line for 2010 (green) estimated by regression analysis between the extend OMP-based and N^*-based denitrification (μmol kg^{-1}) vs. TTD_{CFC12} age (yr), (c)-(d) Mean water column denitrification rates in the western (red) and eastern (blue) P06 for 2010 by the extended OMP analysis, (e)-(f) Mean water column denitrification rates in the western (red) and eastern (blue) P06 for 2010 by the N^*, and (g)-(h) Mean water column denitrification rates in the eastern (blue) P06 for 2003 by the extended OMP analysis and the N^*. Dotted lines represent standard deviation.

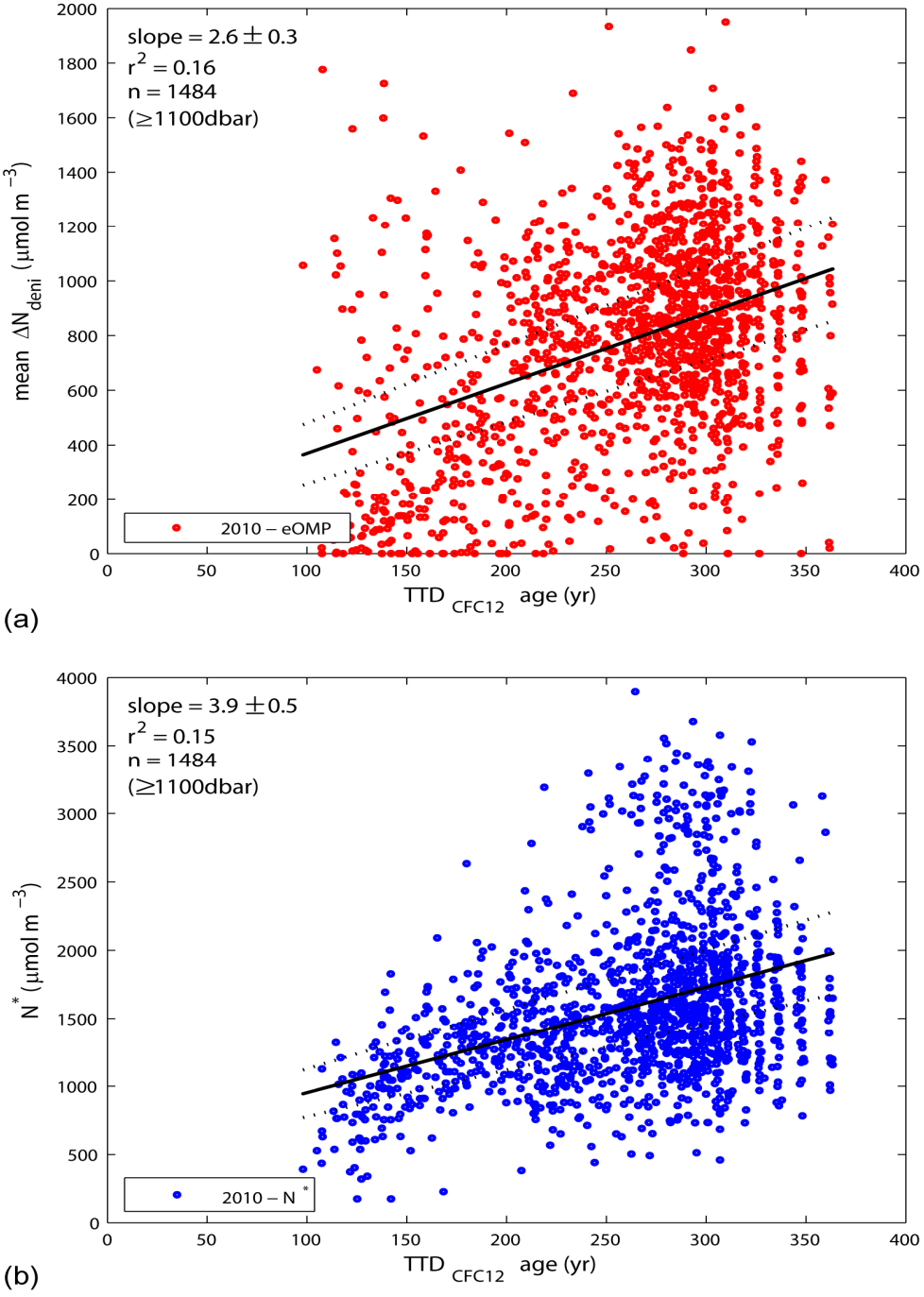

Figure 4.11: (a) Mean water column denitrification rates in the P06 (below 1100dbar) for 2010 by the extended OMP analysis (red), and (b) Mean water column denitrification rates in the P06 (below 1100dbar) for 2010 by the N^* (blue).

Chapter 5: Summary

While the understanding of the nitrogen balance is key to predictions of future climate change, including atmospheric CO_2 variation, the imbalance of oceanic nitrogen sources and sinks remains controversial (Gruber and Sarmiento, 1997; Codispoti et al., 2001; Deutsch et al., 2001; Gruber and Sarmiento, 2002; Codispoti, 2007; Deutsch et al., 2007; Gruber, 2008), because precise quantitative information on the oceanic nitrogen inventory is lacking. Denitrification is especially important because it relates directly to modern climate change through the production of N_2O as a strong greenhouse gas (Nevison and Holland, 1997; Nevison et al., 2003; Naqvi et al., 2010). It relates indirectly to glacial-interglacial climate change by controlling bio-available nitrogen in the ocean (McElroy, 1983; Altabet et al., 1995; Ganeshram et al., 1995; Falkowski, 1997; Ganeshram et al., 2000; Brandes and Devol, 2002; Ganeshram et al., 2002).

Recent studies have reported increased denitrification over the last few decades (Gruber, 2008; Deutsch and Weber, 2012), while other have suggested that global ocean nitrogen fixation rates had been underestimated in previous studies in earlier investigations (Karl et al., 2002; Deutsch et al., 2007). Furthermore, anthropogenic perturbations have altered the global nitrogen cycle (Falkowski et al., 2000; Gruber and Galloway, 2008). Taken together, the suggestions above imply that research focused on accurate estimations of the oceanic nitrogen inventory is currently lacking and needs further attention. In addition, the current estimates of the $N_{sources}$ and N_{sinks} terms should be reexamined due to large uncertainties.

With this background in mind, I estimated denitrification rates in three different locations: the northern Gulf of Mexico, the East/Japan Sea, and the South Pacific Ocean, representing coastal, marginal, and open ocean scales with different oceanographic characteristics, respectively.

The northern GOM on the shallow continental shelf is recognized for hypoxic water conditions ($O_2 \leq 2$ mg L^{-1}), which is often referred to as the "Dead Zone". The size of the "Dead Zone" area has grown larger during recent decades (~1000 km^2 during 1985-1992 to ~15000 km^2 during 1993-2000) due to increased coastal eutrophication

(Rabalais et al., 2002). Under such conditions, denitrification, the main process removing "available nitrogen" from a system, is likely to become more active. Denitrification rates should be quantified better to understand the nitrogen cycle in the northern GOM. Despite its significance, however, only a few denitrification studies have been reported for this region (Gardner et al., 1993; Childs et al., 2003; Gardner et al., 2010). Here, temporal variation of denitrification rates in the bottom layer at the northern GOM, encompassing the "Dead Zone", is estimated using extended Optimum Multi-Parameter (OMP) analysis with historical hydrographic data during the July months of the period 1985-2007 (excluding 1988-1990). Denitrification rates in the region gradually decreased from 1985 to 1997, and then increased to 2007. The water mass mixing composition of bottom waters on the Texas-Louisiana inner shelf has changed since ~1997. The Texas-Louisiana Coastal Water has increased, whereas the Subtropical Underwater has decreased during this time period. This change appears to have influenced the denitrification rates in the study area. The denitrification rates in the northern GOM are controlled not only by biogeochemical factors such as organic matter supply and remineralization, but also by physical factors such as stratification and the relative contributions from different water masses.

I focused on denitrification in the East/Japan Sea (EJS) in Chapter 3. The EJS is a well-oxygenated marginal sea (deep water O_2>190 μmol kg^{-1}) due to its own deep-water formation system (Talley et al., 2006). For this reason, denitrification has not been considered as a significant biogeochemical process in the EJS's nitrogen cycle. However, indirect and direct evidence suggest that denitrification does actually play an important role (Talley et al., 2001; Yanagi, 2002; Lee et al., 2007; Tischenko et al., 2007; Kim et al., 2010). I presented evidence of denitrification on the continental slopes of the Ulleung Basin and the Eastern Japan Basin near the Tatar Strait in EJS, despite high dissolved oxygen concentrations. The N/P ratio is lower (12.4 below 300dbar) in EJS than the traditional Redfield ratio (16). Low nitrate concentrations smaller than the expected nitrate level, low N/P ratio (<12.4), and secondary nitrite peaks occurred near the bottom of these two regions collectively indicate the losses of nitrate and presence of

denitrification. Active remineralization and denitrification may occur simultaneously at the organic matter-rich bottom layer on the slope environment. The denitrification rates near the bottom of the continental slope of these two regions were estimated as a range 0.3–33.2 μmol N m^{-2} d^{-1} using the two approaches (i.e. the simple relationship of the Redfield ratio from nitrate profiles and the extended OMP analysis). Although the N/P ratio is low like other hypoxic/anoxic marginal seas, the current denitrification rates do not support active basin-wide denitrification. Considering the decadal-scale physical and biogeochemical changes in EJS, further investigation of EJS denitrification processes is needed to predict future changes of the nitrogen cycle in this well-oxygenated marginal sea.

I studied the basin-scale denitrification in the South Pacific Ocean along ~32°S in Chapter 4. Prior to this work, quantitative estimates of water column denitrification rates in global/basin nitrogen budgets did not include any open ocean values outside the OMZs. The high quality data from the repeat hydrographic surveys along ~32°S in the South Pacific conducted in 1992, 2003, and 2010 offer an opportunity to estimate denitrification rates in the open ocean scale. The water column denitrification rates in the OML were estimated at 3.1-7.5 μmol N m^{-3} yr-1 (=2.6-6.8 mmol N m^{-2} yr^{-1} with ΔH=900m). The extended OMP analysis and N^* methods were compared. The estimated mean denitrification (ΔN_{deni}) is larger in 2010 by an average 0.1-0.4 μmol N kg^{-1}, compared to 2003 and 1992. Water column denitrification rates of 2003 and 2010 were estimated from the regression analysis between the amount of ΔN_{deni} and TTD_{CFC12} ages. If we extend water column denitrification rates to deeper layers below 1100dbar, despite somewhat poor correlation in regression, the estimated rates become 2.6-3.9 μmol N m^{-3} yr^{-1} (=11.7-17.6 mmol N m^{-2} yr^{-1} with ΔH=4500m). It is substantially small compared to the denitrification rates estimated in the OMZs, but the magnitude integrated amount over the entire basin becomes substantial. This result implies that the water column denitrification at the open ocean scale outside the OMZs should be considered as a significant component in the Pacific Ocean nitrogen budget.

To conclude, I demonstrated that denitrification rates are variable with time in the northern GOM, and I suppose that similar patterns likely present in other productive coastal oceans. We should consider temporal variability of denitrification rates when estimating total nitrogen loss by denitrification in the coastal oceans instead of using a single representative value. I illustrated in the EJS study how some parts of nitrogen in a marginal sea can be removed via denitrification, despite the high oxygen environment. Although little net denitrification occurs in EJS at present, considering increasing anthropogenic perturbations in the global nitrogen cycle (Falkowski et al., 2000; Gruber and Galloway, 2008), and rapid environmental changes in EJS, it would behoove us to pay more attention so we can better predict how rapidly and significantly such biogeochemical changes may proceed in the future. I suggested in the South Pacific Ocean study that the water column denitrification rates estimated in the open ocean, outside of the oxygen minimum zones, should be considered in the nitrogen budget of Pacific Ocean. The information on open-ocean denitrification rates along with improved nitrogen fixation rates will contribute significantly to our current knowledge of the global nitrogen budget. Denitrification is subject to seasonal, decadal and possibly climate scale variations. While it is most often associated with oxygen minimum zones, it is not confined to such regions only, and small amounts integrated over broader areas indicate its quantitative significance through the world's oceans. From coastal ocean to marginal sea to broad basin scales, denitrification is playing a significant role in local, regional, and global nitrogen budgets.

In the future, we need to estimate coastal denitrification rates using the coupling of direct measurements and modeling to reconcile the overestimation issue, resulting from high variability of coastal regions. I suppose that 'marine snow' provides reducing microzones within detrital aggregates despite highly oxygenated water column, and the estimated denitrification rates in the EJS and the South Pacific Ocean seem to be related to this. To verify the estimates, we need to measure multi-tracers such as nitrate, nitrite, $\delta^{15}N$ and $\delta^{18}O$ isotopes, and nitrous oxide simultaneously in the whole water column of open oceans. Finally, in order to improve our knowledge on global oceanic nitrogen mass

balance, we need to extend the approach applied for the South Pacific Ocean to the rest of the Pacific Ocean, and the Indian and Atlantic Oceans.

REFERENCES

Altabet, M.A., R. Francols, D.W. Murray, and W.L. Prell, 1995. Climate-related variations in denitrification in the Arabian Sea from sediment 15N/14N ratios, Nature, 506-508.

Brandes, J.A., and A.H. Devol, 2002. A global marine-fixed nitrogen isotopic budget: Implication for Holocene nitrogen cycling. Global Biogeochemical Cycles, 16(4), 1120, doi:10.1029/2001GB001856.

Childs, C.R., N.N. Rabalais, R.E. Turner, and L.M. Proctor, 2003. Sediment denitrification in the Gulf of Mexico zone of hypoxia (Erratum), Marine Ecology Progress Series, 274, 310.

Codispoti, L.A., 2007. An oceanic fixed nitrogen sink exceeding 400 Tg N a^{-1} vs the concept of homeostasis in the fixed-nitrogen inventory. Biogeosciences, 4, 233-253.

Codispoti, L.A., J.A. Brandes, J.P. Christensen, A.H. Devol, S.W.A. Naqvi, H.W. Paerl, and T. Yoshinari, 2001. The oceanic fixed nitrogen and nitrous oxide budgets: Moving targets as we enter the anthropocene?. Scientia Marina, 65, 85-105.

Deutsch C., N. Gruber, R.M. Key, and J. Sarmiento, 2001. Denitrification and N_2 fixation in the Pacific Ocean. Global Biogeochemical Cycles, 15, 483-506.

Deutsch, C., and T. Weber, 2012. Nutrient ratios as a tracer and driver of ocean biogeochemistry. The Annual Review of Marine Science, 4, 113-141.

Deutsch, C., J.L. Sarmiento, D.M. Sigman, N. Gruber, and J.P. Dunne, 2007. Spatial coupling of nitrogen inputs and losses in the ocean. Nature, 445, 163-167.

Falkowski, P., R.J. Scholes, E. Boyle, J. Canadell, D. Canfield, J. Elser, N. Gruber, H. Hibbard, P. Högberg, S. Linder, F.T. Mackenzie, B. Moore III, T. Pedersen, Y. Rosenthal, S. Seitzinger, V. Smetacek, W. Steffen, 2000. The global carbon cycle: A test of our knowledge of Earth as a system. Science, 290, 291-296.

Falkowski, P.G., 1997. Evolution of the nitrogen cycle and its influence on the biological sequestration of CO_2 in the ocean, Nature, 272-275.

Ganeshram, R.S., T.F. Pedersen, S.E. Calvert, and J.W. Murray, 1995. Large changes in oceanic nutrient inventories from glacier to interglacial periods, Nature, 755-758.

Ganeshram, R.S., T.F. Pedersen, S.E. Calvert, G.W. McNeill, and M.R. Fontugne, 2000. Glacial-interglacial variability in denitrification in the world's oceans: Causes and consequences, Paleoceanography, 15(4), 361-376.

Ganeshram, R.S., T.F. Pedersen, S.E. Calvert, S.E. Calvert, and R. Francois, 2002. Reduced nitrogen fixation in the glacial ocean inferred from changes in marine nitrogen and phosphorus inventories, Nature, 415, 156-159.

Gardner, W.S., E.E. Briones, and E.C. Kaegi, 1993. Ammonium excretion by benthic invertebrates and sediment-water nitrogen flux in the Gulf of Mexico near the Mississippi River outflow, Estuaries, 16(4), 799-808.

Gardner, W.S., M.J. McCarthy, and L. Xiao, 2010. Denitrification as a mechanism causing nitrogen limitation of microbial activities at the sediment water interface in the

hypoxic region of the eutrophic northern Gulf of Mexico. 2010 Gulf Estuarine Research Society (GERS) Meeting, Port Aransas, TX.

Gruber, N., 2008. The marine nitrogen cycle: Overview of distributions and processes, In: Nitrogen in the marine environment, 2nd edition, edited by D.G. Capone, D.A. Bronk, M.R. Mulholland, and E.J. Carpenter, Elsevier, Amsterdam, 1-50.

Gruber, N., and J.L. Sarmiento, 1997. Global patterns of marine nitrogen fixation and denitrification, Global Biogeochemical Cycles, 11(2), 235-266.

Gruber, N., and J.L. Sarmiento, 2002. Biogeochemical/physical interactions in elemental cycles; in The Sea, edited by A.R. Robinson, J.J. McCarthy, and B.J. Rothschild, 12, 337-339.

Gruber, N., and J.N. Galloway, 2008. An Earth-system perspective of the global nitrogen cycle. Nature, 451, 293-296.

Karl, D., A. Michaels, B. Bergman, D. Capone, E. Carpenter, R. Letelier, F. Lipschultz, H. Paerl, D. Sigman, and L. Stal, 2002. Dinitrogen fixation in the world's oceans. Biogeochemistry, 57, 47-98.

Kim, T.-H. Y.-W. Lee, and G. Kim, 2010. Hydrographically mediated patterns of photosynthetic pigments in the East/Japan Sea: Low N:P ratios and cyanobacterial dominance. Journal of Marine Systems, 82, 72-79.

Lee, T., I.-N. Kim, D.-J. Kang and D. Kim, 2007. Implications of deep nitrite in the Ulleung Basin. The Sea, 12(3), 239-243.

McElroy, M.B., 1983. Marine biological controls on atmospheric CO_2 and climate, Nature, 302, 328-329.

Naqvi, S.W.A., H.W. Bange, L. Farias, P.M.S. Monteiro, M.I. Scranton, and J. Zhang, 2010. Marine hypoxia/anoxia as a source of CH_4 and N_2O, Biogeosciences, 7, 2159-2190.

Nevison, C., and E. Holland, 1997. A reexamination of the impact of anthropogenically fixed nitrogen on atmospheric N_2O and the stratospheric O_3 layer, Journal of Geophysical Research, 102, 25519-25536.

Nevison, C., J.H. Butler, and J.W. Elkins, 2003. Global distribution of N2O and the ΔN_2O-AOU yield in the subsurface ocean, Global Biogeochemical Cycles, 17(4), 1119, doi:10.1029/2003GB002068.

Rabalais, N.N., R.E. Turner, and D. Scavia, 2002. Beyond science into policy: Gulf of Mexico hypoxia and the Mississippi River, BioScience, 52(2), 129-142.

Talley, L.D., D.-H. Min, V.B. Lobanov, V.A. Luchin, V.I. Ponomarev, A.N. Salyuk, A.Y. Shcherbina, P.Y. Tishchenko, and I. Zhabin, 2006. Japan/East Sea water masses and their relation to the sea's circulation, Oceanography, 19(3), 32-49.

Talley L.D., P.Ya. Tishchenko, G. Mitchell, D.-J. Kang, D.-H. Min, A. Nedashkovskii, D. Masten, and P. Robbins, 2001. Nitrite in a deep, oxygenated environment the Japan/East Sea and Ulleung Basin. CREAMS 2001, Honolulu.

Tishchenko, P.Ya., L.D. Talley, V.B. Labanov, A.P. Nedashkovskii, G.Yu. Pavlova, and S.G. Sagalaev, 2007. The influence of geochemical processes in the near-bottom layer on the hydrochemical characteristics of the waters of the Sea of Japan. Oceanology, 47(3), 350-359.

Yanagi, T., 2002. Water, salt, phosphorus and nitrogen budgets of the Japan Sea. Journal of Oceanography, 58, 797-804.

REFERENCES

Alldredge, A.L., and M.W. Silver, 1988. Characteristics, dynamics and significance of marine snow. Progress in Oceanography, 20, 41-82.

Alldredge, A.L., and Y. Cohen, 1987. Can microscale chemical patches persist in the sea? Microelectrode study of marine snow, fecal pellets. Science, 235, 689-691.

Altabet, M.A., R. Francols, D.W. Murray, and W.L. Prell, 1995. Climate-related variations in denitrification in the Arabian Sea from sediment 15N/14N ratios. Nature, 506-508.

Anderson, L.A., 1995. On the hydrogen and oxygen content of marine phytoplankton. Deep-Sea Research I, 42, 1675-1680.

Binnerup, S.J. K. Jensen, N.P. Revsbech, M.H. Jensen, and J. Sørensen, 1992. Denitrification, dissimilatory reduction of nitrate to ammonium, and nitrification in a bioturbated estuarine sediments as measured with ^{15}N and microsensor techniques. Applied and Environmental Microbiology, 58(1), 303-313.

Bostock, H.C., B.N. Opdyke, and M.J.M. Williams, 2010. Characterizing the intermediate depth waters of the Pacific Ocean using $\delta^{13}C$ and other geochemical tracers. Deep-Sea Research I, 57, 847-859.

Brandes, J.A., A.H. Devol, and C. Deutsch, 2007. New developments in the marine nitrogen cycle. Chemical Reviews, 107, 577-589.

Burgin, A.J., and S.K. Hamilton, 2007. Have we overemphasized the role of denitrification in aquatic ecosystems? A review of nitrate removal pathways. Frontiers in Ecology and the Environment, 5(2), 89-96.

Cha, H.-J., M.S. Choi, C.-B. Lee, and D.-H. Shin, 2007. Geochemistry of surface sediments in the southwestern East/Japan Sea. Journal of Asian Earth Sciences, 29, 685-697.

Chae, Y.K., Y.H. Seung, and S.K. Kang, 2005. Mode change of deep water formation deduced from slow variation of thermal structure: one-dimensional model study. Ocean and Polar Research, 27(2), 115-123.

Chang, K.-I., W.J. Teague, S.J. Lyu, H.T. Perkins, D.-K. Lee, D.R. Watts, Y.-B. Kim, D.A. Mitchell, C.M. Lee, and K. Kim, 2004. Circulation and currents in the southwestern East/Japan Sea: Overview and review. Progress in Oceanography, 61, 105-156.

Chen, C.-T.A., A.S. Bychkov, S.L. Wang, and G.Yu. Pavlova, 1999. An anoxic Sea of Japan by the year 2200?. Marine Chemistry, 67, 249-265.

Chen, C.-T.A., G..-C. Gong, S.-L. Wang, and A.S. Bychkov, 1996. Redfield ratios and regeneration rates of particulate matter in the Sea of Japan as a model of closed system. Geophysical Research Letters, 23(14), 1785-1788.

Childs, C.R., N.N. Rabalais, R.E. Turner, and L.M. Proctor, 2002, Sediment denitrification in the Gulf of Mexico zone of hypoxia. Marine Ecology Progress Series, 240, 285-290.

Childs, C.R., N.N. Rabalais, R.E. Turner, and L.M. Proctor, 2003. Sediment denitrification in the Gulf of Mexico zone of hypoxia (Erratum). Marine Ecology Progress Series, 274, 310.

Chung, C.S., J.H. Shim, Y.C. Park, and S.G. Park, 1989. Primary productivity and nitrogenous nutrient dynamics in the East Sea of Korea. The Sea, 24, 52-61.

Codispoti, L.A., 2007. An oceanic fixed nitrogen sink exceeding 400 Tg N a-1 vs the concept of homeostasis in the fixed-nitrogen inventory. Biogeosciences, 4, 233-253.

Codispoti, L.A., J.A. Brandes, J.P. Christensen, A.H. Devol, S.W.A. Naqvi, H.W. Paerl, and T. Yoshinari, 2001. The oceanic fixed nitrogen and nitrous oxide budgets: Moving targets as we enter the anthropocene?. Scientia Marina, 65, 85-105.

Dagg, M.J., and G.A. Breed, 2003. Biological effects of Mississippi River nitrogen on the northern Gulf of Mexico-a review and synthesis. Journal of Marine Systems, 43, 133-152.

Deutsch C., N. Gruber, R.M. Key, and J. Sarmiento, 2001. Denitrification and N_2 fixation in the Pacific Ocean. Global Biogeochemical Cycles, 15, 483-506.

Deutsch, C., J.L. Sarmiento, D.M. Sigman, N. Gruber, and J.P. Dunne, 2007. Spatial coupling of nitrogen inputs and losses in the ocean. Nature, 445, 163-167.

Deutsch, C, and T. Weber, 2012. Nutrient ratios as a tracer and driver of ocean biogeochemistry. Annual Review of Marine Science, 4, 113-141.

Deutsch, C., D.M. Sigman, R.C. Thunell, A.N. Meckler, and G.H. Haug, 2004. Isotopic constraints on glacial/interglacial changes in the oceanic nitrogen budget. Global Biogeochemical Cycles, 18, GB4012, doi:10.1029/2003GB002189.

Deutsch, C., J.L. Sarmiento, D.M. Sigman, N. Gruber, and J.P. Dunne, 2007. Spatial coupling of nitrogen inputs and losses in the ocean. Nature, 445, 163-167.

Diaz, R.J., and R. Rosenberg, 2008. Spreading dead zones and consequences for marine ecosystems. Science, 321, 926-929.

England, M.H., J.S. Godfrey, A.C. Hirst, and M. Tomczak, 1993. The mechanism for Antarctic Intermediate Water renewal in a world ocean model. Journal of Physical Oceanography, 23, 1553-1560.

Falkowski, P.G., 1997. Evolution of the nitrogen cycle and its influence on the biological sequestration of CO_2 in the ocean, Nature, 272-275.

Falkowski, P., R.J. Scholes, E. Boyle, J. Canadell, D. Canfield, J. Elser, N. Gruber, H. Hibbard, P. Högberg, S. Linder, F.T. Mackenzie, B. Moore III, T. Pedersen, Y. Rosenthal, S. Seitzinger, V. Smetacek, W. Steffen, 2000. The global carbon cycle: A test of our knowledge of Earth as a system. Science, 290, 291-296.

Fiadeiro, M., 1980. The alkalinity of the deep Pacific. Earth and Planetary Science Letters, 49, 499-505.

Gamo, T., 1999. Global warming may have slowed down the deep conveyor belt of a marginal sea of the northwestern Pacific: Japan Sea. Geophysical Research Letters, 26, 3137-3140.

Gamo, T., N. Momoshima, and S. Tolmacheyov, 2001. Recent upward shift of the deep convection system in the Japan Sea, as inferred from the geochemical tracers tritium, oxygen, and nutrients. Geophysical Research Letters, 28(21), 4143-4146.

Ganeshram, R.S., T.F. Pedersen, S.E. Calvert, and J.W. Murray, 1995. Large changes in oceanic nutrient inventories from glacier to interglacial periods. Nature, 755-758.

Ganeshram, R.S., T.F. Pedersen, S.E. Calvert, G.W. McNeill, and M.R. Fontugne, 2000. Glacial-interglacial variability in denitrification in the world's oceans: Causes and consequences. Paleoceanography, 15(4), 361-376.

Ganeshram, R.S., T.F. Pedersen, S.E. Calvert, S.E. Calvert, and R. Francois, 2002. Reduced nitrogen fixation in the glacial ocean inferred from changes in marine nitrogen and phosphorus inventories. Nature, 415, 156-159.

Gao, H., F. Schreiber, G. Collins, M.M. Jensen, J.E. Kostka, G. Lavik, D.d. Beer, Zhou, H.-Y., M.M.M. Kuypers, 2010. Aerobic denitrification in permeable Wadden Sea sediments. The ISME Journal, 4, 417-426.

Gardner, W.S., E.E. Briones, and E.C. Kaegi, 1993. Ammonium excretion by benthic invertebrates and sediment-water nitrogen flux in the Gulf of Mexico near the Mississippi River outflow. Estuaries, 16(4), 799-808.

Gardner, W.S., M.J. McCarthy, and L. Xiao, 2010. Denitrification as a mechanism causing nitrogen limitation of microbial activities at the sediment water interface in the hypoxic region of the eutrophic northern Gulf of Mexico. 2010 Gulf Estuarine Research Society (GERS) Meeting, Port Aransas, TX.

Gruber, N., 2008. The marine nitrogen cycle: Overview of distributions and processes, In: Nitrogen in the marine environment, 2nd edition, edited by D.G. Capone, D.A. Bronk, M.R. Mulholland, and E.J. Carpenter, Elsevier, Amsterdam, 1-50.

Gruber, N., and J.L. Sarmiento, 1997. Global patterns of marine nitrogen fixation and denitrification, Global Biogeochemical Cycles, 11(2), 235-266.

Gruber, N., and J.L. Sarmiento, 2002. Biogeochemical/physical interactions in elemental cycles; in The Sea, edited by A.R. Robinson, J.J. McCarthy, and B.J. Rothschild, 12, 337-339.

Gruber, N., and J.N. Galloway, 2008. An Earth-system perspective of the global nitrogen cycle. Nature, 451, 293-296.

Hall, T.M., D.W. Waugh, T.W.N. Haine, P.E. Robbins, and S. Khatiwala, 2004. Estimates of anthropogenic carbon in the Indian Ocean with allowance for mixing and time-varying air-sea CO_2 disequilibrium. Global Biogeochemical Cycles, 18, GB1031, doi:10.1029/2003GB002120.

Hartin, C.A., R.A. Fine, B.M. Sloyan, L.D. Talley, T.K. Chereskin, and J. Happell, 2011. Formation rates of Subantarctic mode water and Antarctic intermediate water within the South Pacific. Deep-Sea Research I, 58, 524-534.

Holzer, M., and T.M. Hall, 2000. Transit-time and tracer-age distributions in geophysical flows. Journal of the Atmospheric Sciences, 57, 3539-3558.

Hulth, S., R.C. Aller, D.E. Canfield, T. Dalsgaard, P. Engström, F. Gilbert, K. Sundbäck, and B. Thamdrup, 2005. Nitrogen removal in marine environments: recent findings and future research challenges. Marine Chemistry, 94, 125-145.

Hupe, A., and J. Karstensen, 2000. Redfield stoichiometry in Arabian Sea subsurface waters. Global Biogeochemical Cycles, 14(1), 357-372.

Hyun, J.-H., D. Kim, C.-W. Shin, J.-H. Noh, E.-J. Yang, J.-S. Mok, S.-H. Kim, H.-C. Kim, and S. Yoo, 2009. Enhanced phytoplankton and bacterioplankton production

coupled to coastal upwelling and an anticyclonic eddy in the Ulleung Basin, East Sea. Aquatic Microbial Ecology, 54, 45-54.

Hyun, J.-H., J.-S. Mok, O.-R. You, D. Kim, and D.-L. Choi, 2010. Variations and controls of sulfate reduction in the continental slope and rise of the Ulleung Basin off the southeast Korean upwelling system in the East Sea. Geomicrobiology Journal, 27, 212-222.

Jarosz, E., and S.P. Murray, 2005. Velocity and transport characteristics of the Louisiana-Texas Coastal Current; Circulation in the Gulf of Mexico: Observations and Models. Geophysical Monograph Series 161, 143-156.

Jeong, J.H., D.S. Kim, T.H. Lee, and S. An, 2009. High remineralization and denitrification activity in the shelf sediments of Dok Island, East Sea. The Sea, 14(2), 80-89.

Jochens, A.E., S.F. DiMarco, 2008. Physical oceanographic conditions in the deepwater Gulf of Mexico in summer 2000-2002. Deep-Sea Research II, 55, 2541-2554.

Johnson, G.C., and A.H. Orsi, 1997. Southwest Pacific Ocean water-mass changes between 1968/69 and 1990/91. Journal of Climate, 10, 306-316.

Johnson, G.C., and J.M. Toole, 1993. Flow of deep and bottom waters in the Pacific at 10°N. Deep-Sea Research I, 40, 371-394.

Justic, D., N.N. Rabalais, and R.E. Turner, 1995. Stoichiometric nutrient balance and origin of coastal eutrophication. Marine Pollution Bulletin, 30(1), 41-46.

Kang, D.-J., J.-Y. Kim, T. Lee, and K.-R. Kim, 2004. Will the East/Japan Sea become an anoxic sea in the next century?. Marine Chemistry, 91, 77-84.

Kang, D.-J., S. Park, Y.-G. Kim, K. Kim, and K.-R. Kim, 2003. A moving-boundary box model (MBBM) for oceans in change: An application to the East/Japan Sea. Geophysical Research Letters, 30(6), 1299, doi:10.1029/2002GL016486.

Kang, D.-J., Y.-B. Kim, and K.-R. Kim, 2011. Dissolved oxygen at the bottom boundary layer of the Ulleung Basin, East Sea. Ocean and Polar Research, 32(4). 439-448.

Karl, D., A. Michaels, B. Bergman, D. Capone, E. Carpenter, R. Letelier, F. Lipschultz, H. Paerl, D. Sigman, and L. Stal, 2002. Dinitrogen fixation in the world's oceans. Biogeochemistry, 57, 47-98.

Karl, D., R. Letelier, L. Tupas, J. Dore, J. Christian, and D. Hebel, 1997. The role of nitrogen fixation in biogeochemical cycling in the subtropical North Pacific Ocean. Nature, 388, 533-538.

Karstensen, J., and M. Tomczak, 1998. Age determination of mixed water masses using CFC and oxygen data. Journal of Geophysical Research, 103(C9), 18599-18609.

Karstensen, J., L. Stramma, and M. Visbeck, 2008. Oxygen minimum zones in the eastern tropical Atlantic and Pacific oceans. Progress in Oceanography, 77, 331-350.

Kaspar, H.F., 1983. Denitrification, nitrate reduction to ammonium, and inorganic nitrogen pools in intertidal sediments. Marine Biology, 74, 133-139.

Kawabe, M., S. Fujio, D. Yanagimoto, and K. Tanaka, 2009. Water masses and currents of deep circulation southwest of the Shatsky Rise in the western North Pacific. Deep-Sea Research I, 56, 1675-1687.

Kawano, T., M. Fukasawa, S. Kouketsu, and H. Uchida, 2006. Bottom water warming along the pathway of lower circumpolar deep water in the Pacific Ocean. Geophysical Research Letters, 33, L23613, doi:10.1029/2006GL027933.

Kelso, B.H.L., R.V. Smith, R.J. Laughlin, and S.D. Lennox, 1997. Dissimilatory nitrate reduction in anaerobic sediments leading to river nitrite accumulation. Applied and Environmental Microbiology, 63(12), 4679-4685.

Kido K. and M. Nishimura. 1973. Regeneration of silicate in the ocean. Journal of the Oceanographical Society of Japan. **29**, 185-192.

Kim, I.-N., and T. Lee, 2004. Summer hydrographic features of the East Sea analyzed by the Optimum Multiparameter method. Ocean and Polar Research, 26(4), 581-594.

Kim, I.-N., D.-H. Min, D.H. Kim, and T. Lee, 2010a. Investigation of the physicochemical features and mixing of East/Japan Sea Intermediate Water: An isopycnic analysis approach. Journal of Marine Research, 68, 799-818.

Kim, I.-N., D.-H. Min, and T. Lee, 2010b. Estimates of basin-specific oxygen utilization rates (OURs) in the East Sea (Sea of Japan). The Sea, 15(2), 86-96.

Kim, J.-Y., D.-J. Kang, E, Kim, J.H. Cho, C.R. Lee, K.-R. Kim, and T. Lee, 2003. Biological pump in the East Sea estimated by a box model. The Sea, 8(3), 295-306.

Kim, K.-R., and K. Kim, 1996. What is happening in the East Sea (Japan Sea)?; Recent chemical observations during CREAMS 93-96. Journal of the Korean Society of Oceanography, 31(4), 164-172.

Kim, K.-R., T.S. Rhee, and K. Kim, 1992. A note on initial nitrate and initial phosphate as tracers for the origin of East Sea (Japan Sea) Proper Water, La mer, 30, 149-155.

Kim, K., K.-R. Kim, D. Min, Y. Volkov, J.-H. Yoon, and M. Takematsu, 2001. Warming and Structural Changes in the East Sea (Japan Sea): A clue to future changes in Global Oceans?. Geophysical Research Letters, 28, 3293-3296.

Kim, K., K.-R. Kim, D. Min, Y. Volkov, J.-H. Yoon, and M. Takematsu, 2001. Warming and Structural Changes in the East Sea(Japan Sea): A clue to future changes in Global Oceans?. Geophysical Research Letters, 28, 3293-3296.

Kim, K., K.-R. Kim, Y.-G. Kim, Y.-K. Cho, D.-J. Kang, M. Takematsu, and Y. Volkov, 2004. Water masses and decadal variability in the East Sea (Sea of Japan). Progress in Oceanography, 61, 157-174.

Kim, T.-H. Y.-W. Lee, and G. Kim, 2010c. Hydrographically mediated patterns of photosynthetic pigments in the East/Japan Sea: Low N:P ratios and cyanobacterial dominance. Journal of Marine Systems, 82, 72-79.

Kim, T.-W., K. Lee, R.G. Najjar, H.-D. Jeong, and H.J. Jeong, 2011. Increasing N abundance in the marginal seas of the Northwestern Pacific Ocean due to atmospheric nitrogen deposition. Science, 334, 505-509.

Lee T, D. Kim, B.-K. Khim, and D.-L. Choi, 2010. Organic carbon cycling in Ulleung Basin sediments, East Sea. Ocean and Polar Research, 32(2), 145-156.

Lee, T. J.-H. Hyun, J.S. Mok, and D. Kim, 2008. Organic carbon accumulation and sulfate reduction rates in slope and basin sediments of the Ulleung Basin East/Japan Sea, Geo-Marine Letters, 28, 153-159.

Lee, T., and I.-N. Kim, 2003. Chemical imprints of the upwelled waters off the coast of the southern East Sea of Korea. Journal of the Korean Society of Oceanography, 38, 101-110.

Lee, T., I.-N. Kim, D.-J. Kang, and D. Kim, 2007. Implications of deep nitrite in the Ulleung Basin. The Sea, 12(3), 239-243.

Leffanue, H., and M. Tomczak, 2004. Using OMP analysis to observe temporal variability in water mass distribution. Journal of Marine Systems, 48, 3-14.

Lomas, M.W., and F. Lipschultz, 2006. Forming the primary nitrite maximum: Nitrifiers or phytoplankton?, Limnology and Oceanography, 51(5), 2453-2467.

Mantyla, A.W., and J.L. Reid, 1983. Abyssal characteristics of the World Ocean waters. Deep-Sea Research, 30, 805-833.

McCarthy, J.J. A. Yilmaz, Y. Coban-Yildiz, and J.L. Nevins, 2007. Nitrogen cycling in the offshore waters of the Black Sea. Estuarine, Coastal and Shelf Science. 74, 493-514.

McCave, I.N., L. Carter, and I.R. Hall, 2008. Glacial-interglacial changes in water mass structure and flow in the SW Pacific Ocean. Quaternary Science Reviews, 27, 1886-1908.

McElroy, M.B., 1983. Marine biological controls on atmospheric CO_2 and climate. Nature, 302, 328-329.

Min, H.S., and C.-H. Kim, 2006. Water mass formation variability in the intermediate layer of the East Sea. Ocean Science Journal, 41(4), 255-260.

Moon, C.H., H.S. Yang, and K.W. Lee, 1996. Regeneration Processes of nutrients in the Polar Front Area of the East Sea I. Relationship between Water Mass and nutrient Distribution Pattern in Autumn. Journal of the Korean Fisheries Society, 29(4): 503-526.

Morrison, J.M., and W.D. Nowlin, Jr., 1977. Repeated nutrient oxygen and density sections through the Loop Current. Journal of Marine Research, 35, 105-128.

Morrison, J.M., W.J. Merrell, R.M. Key, and T.C. Key, 1983. Property distributions and deep chemical measurements within the Western Gulf of Mexico. Journal of Geophysical Research, 88, 2601-2608.

Murata, A., Y. Kumamoto, S. Watanabe, and M. Fukasawa, 2007. Decadal increase of anthropogenic CO2 in the South Pacific subtropical ocean along 32S. Journal of Geophysical Research, 112, C05033, doi:10.1029/2005JC003405.

Naqvi, S.W.A., H.W. Bange, L. Farias, P.M.S. Monteiro, M.I. Scranton, and J. Zhang, 2010. Marine hypoxia/anoxia as a source of CH_4 and N_2O. Biogeosciences, 7, 2159-2190.

Nevison, C., and E. Holland, 1997. A reexamination of the impact of anthropogenically fixed nitrogen on atmospheric N_2O and the stratospheric O_3 layer. Journal of Geophysical Research, 102, 25519-25536.

Nevison, C., J.H. Butler, and J.W. Elkins, 2003. Global distribution of N2O and the ΔN_2O-AOU yield in the subsurface ocean. Global Biogeochemical Cycles, 17(4), 1119, doi:10.1029/2003GB002068.

O'Connor, B.M., R.A. Fine, and D.B. Olson, 2005. A global comparison of subtropical underwater formation rates. Deep Sea Research I, 52, 1569-1590.

Orsi, A.H., G.C. Johnson, and J.L. Bullister, 1999. Circulation, mixing, and production of Antarctic Bottom Water. Progress in Oceanography, 43, 55-109.

Orsi, A.H., W.M. Smethie Jr., and J.L. Bullister, 2002. On the total input of Antarctic waters to the deep ocean: A preliminary estimate from chlorofluorocarbon measurements. Journal of Geophysical Research, 107 (C8), 3122, 10.1029/2001JC000976.

Pakulski, J.D., R. Benner, T. Whitledge, R. Amon, B. Eadie, L. Cifuentes, J. Ammerman, and D. Stockwell, 2000. Microbial metabolism and nutrient cycling in the Mississippi and Atchafalaya River plumes. Estuarine, Coastal and Shelf Science, 50, 173-184.

Park, K., 1967. Nutrient regeneration and preformed nutrients off Oregon. Limnology and Oceanography, 12, 353-357.

Ploug, H., M. Kühl, B. Buchholz-Cleven, B.B. Jørgensen, 1997. Anoxic aggregates-an ephemeral phenomenon in the pelagic environment?. Aquatic Microbial Ecology, 13, 285-294.

Poole, R., and M. Tomczak, 1999. Optimum multiparameter analysis of the water mass structure in the Atlantic Ocean thermocline. Deep-Sea Research I, 46, 1895-1921.

Rabalais, N.N., R.E. Turner, and D. Scavia, 2002. Beyond science into policy: Gulf of Mexico hypoxia and the Mississippi River. BioScience, 52(2), 129-142.

Redfield, A.C., B.H. Ketchum, and F.A. Richards, 1963. The influence of organism on the composition of sea water. The Sea, 2, 26-77.

Reid, J.L., 1986. On the total geostrophic circulation of the South Pacific Ocean: Flow patterns, Tracers and Transports. Progress in Oceanography, 16, 1-61.

Reid, J.L., 1997. On the total geostrophic circulation of the South Pacific Ocean: Flow patterns, Tracers and Transports. Progress in Oceanography, 39, 263-352.

Robertson, L.A., and J.G. Kuenen, 1984a. Aerobic denitrification – old wine in new bottles?. Antonie van Leeuwenhoek, 50, 525-544.

Robertson, L.A., and J.G. Kuenen, 1984b. Aerobic denitrification: a controversy revived. Archives of Microbiology, 139, 351-354.

Robertson, L.A., R. Cornelisse, P. De Vos, R. Hadioetomo, and J.G. Kuenen, 1989. Aerobic denitrification in various heterotrophic nitrifiers. Antonie van Leeuwenhoek., 56, 289-299.

Robertson, L.A., T. Dalsgaard, N.-P. Revsbech, and J.G. Kuenen, 1995. Confirmation of 'aerobic denitrification' in batch cultures, using gas chromatography and ^{15}N mass spectrometry. FEMS Microbiology Ecology, 18, 113-120.

Schwartz, M.C., C. Woulds, and G.L. Cowie, 2009. Sedimentary denitrification rates across the Arabian Sea oxygen minimum zone. Deep-Sea Research II, 56, 324-332.

Seitzinger, S.P., and A.E. Giblin, 1996. Estimating denitrification in North Atlantic continental shelf sediments. Biogeochemistry, 35, 235-260.

Shanks, A.L., and M.L. Reeder, 1993. Reducing microzones and sulfide production in marine snow. Marine Ecology Progress Series, 96, 43-47.

Shim, J.H., S.R. Yang, and W.H. Lee, 1989. Phytohydrography and the vertical pattern of nitracline in the southern waters of the Korean East Sea in early spring. Journal of the Korean Society Oceanography, 24, 15-28.

Sohm, J.A., E.A. Webb, and D.G. Capone, 2011. Emerging patterns of marine nitrogen fixation. Nature Reviews Microbiology, 9, 499-508.

Stanton, B.R., 2002. Antarctic Intermediate Water variability in the northern New Zealand region. New Zealand Journal of Marine and Freshwater Research, 36, 645-654.

Su, J.-J., B.-Y. Liu, and C.-Y. Liu, 2001. Comparison of aerobic denitrification under high oxygen atmosphere by Thiosphaera pantotropha ATCC 35512 and Pseudo monas stutzeri SU2 newly isolated from the activated sludge of a piggery wastewater treatment system. Journal of Applied Microbiology, 90, 457-462.

Talley L.D., P.Ya. Tishchenko, G. Mitchell, D.-J. Kang, D.-H. Min, A. Nedashkovskii, D. Masten, and P. Robbins, 2001. Nitrite in a deep, oxygenated environment the Japan/East Sea and Ulleung Basin. CREAMS 2001, Honolulu.

Talley, L.D., 2008. Freshwater transport estimates and the global overturning circulation: Shallow, deep and throughflow components. Progress in Oceanography, 78, 257-303.

Talley, L.D., and T.M. Joyce, 1992. The double silica maximum in the North Pacific. Journal of Geophysical Research, 97, 5465-5480.

Talley, L.D., D.-H. Min, V.B. Lobanov, V.A. Luchin, V.I. Ponomarev, A.N. Salyuk, A.Y. Shcherbina, P.Y. Tishchenko, and I. Zhabin, 2006. Japan/East Sea water masses and their relation to the sea's circulation, Oceanography, 19(3), 32-49.

Talley, L.D., G.L. Pickard, W.J. Emery, and J.H. Swift, 2011. Descriptive Physical Oceanography: An Introduction (Sixth edition), Elsevier, Boston, 1-560.

Talley, L.D., P.Ya. Tischenko, V. Luchin, A. Nedashkovskiy, S. Sagalaev, D.-J. Kang, M. Warner, and D.-H. Min, 2004. Atlas of Japan (East) Sea hydrographic properties in summer, 1999. Progress in Oceanography, 61, 277-348.

Tanhua, T., D.W. Waugh, and D.W.R. Wallace, 2008. Use of SF6 to estimate anthropogenic CO_2 in the upper ocean. Journal of Geophysical Research, 113, C04037, doi:10.1029/2007JC004416.

Tishchenko, P.Ya., L.D. Talley, V.B. Labanov, A.P. Nedashkovskii, G.Yu. Pavlova, and S.G. Sagalaev, 2007. The influence of geochemical processes in the near-bottom layer on the hydrochemical characteristics of the waters of the Sea of Japan. Oceanology, 47(3), 350-359.

Tomczak, M., and D.G.B. Large, 1989. Optimum Multiparameter analysis of mixing in the thermocline of the Eastern Indian Ocean. Journal of Geophysical Research, 94, 16141-16149.

Tomczak, M., and J.S. Godfrey, 1994. Regional Oceanography: An Introduction. Pergamon Press, Oxford, UK, 1-422.

Tomczak, M., and S. Liefrink, 2005. Interannual variations of water mass volumes in the Southern Ocean. Journal of Atmospheric and Ocean Science, 10, 31-42.

Tsuchiya, M., and L.D. Talley, 1996. Water-property distributions along an eastern Pacific hydrographic section at 135W. Journal of Marine Research, 54, 541-564.

Van Heuven, S., D. Pierrot, E. Lewis, and D.W.R. Wallace, D.W.R. 2009. MATLAB program developed for CO2 system calculations. ORNL/CDIAC-105b, Carbon Dioxide Information Analysis Center, Oak Ridge National Laboratory, US Department of Energy, Oak Ridge, Tennessee.

Vidal, V.M.V., F.V. Vidal, A.F. Hernandez, E. Meza, and L. Zambrano, 1994. Winter water mass distributions in the Western Gulf of Mexico affected by a colliding anticyclonic ring. Journal of Oceanography, 50, 559-588.

Walker, J.T., C.A. Stow, and C. Geron, 2010. Nitrous oxide emissions from the Gulf of Mexico hypoxic zone. Environmental Science & Technology, 44, 1617-1623.

Waugh, D.W., T.M. Hall, and T.W.N. Haine, 2003. Relationship among tracer ages. Journal of Geophysical Research, 108 (C5), 3138, doi:10.1029/2002JC001325.

Waugh, D.W., T.M. Hall, B.I. McNeil, R. key, and R.J. Matear, 2006. Anthropogenic CO_2 in the oceans estimated using transit time distributions. Tellus, 58B, 376-389.

Waugh, D.W., T.W.N. Haine, and T.M. Hall, 2004. Transport times and anthropogenic carbon in the subpolar North Atlantic Ocean. Deep-Sea Research I, 51, 1475-1491.

Wijffels, S.E., J.M. Toole, and R. Davis, 2001. Revisiting the South Pacific subtropical circulation: A synthesis of World Ocean Circulation Experiment observations along 32°S. Journal of Geophysical Research, 106, 19481-19513.

Wiseman, Wm.J., and F.J. Kelly, 1994. Salinity variability within the Louisiana coastal current during the 1982 flood season. Estuaries, 17, 732-739.

Wiseman, Wm.J., N.N. Rabalais, R.E. Turner, S.P. Dinnel, and A. MacNaughton, 1997. Seasonal and interannual variability within the Louisiana coastal current: stratification and hypoxia. Journal of Marine Systems, 12, 237-248.

Wolgast, D.M., A.F. Carlucci, and J.E. Bauer, 1998. Nitrate respiration associated with detrital aggregates in aerobic bottom waters of the abyssal NE Pacific. Deep-Sea Research II 45, 881-892.

Yamagishi, H., N. Yoshida, S. Toyoda, B.N. Popp, M.B. Westley, and S. Watanabe, 2005. Contributions of denitrification and mixing on the distribution of nitrous oxide in the North Pacific. Geophysical Research Letters, 32, L04603, doi:10.1029/2004GL021458.

Yanagi, T., 2002. Water, salt, phosphorus and nitrogen budgets of the Japan Sea. Journal of Oceanography, 58, 797-804.

Yang, H.S., S.S. Kim, C.G. Kang, and K.D. Cho, 1991. A study on sea water and ocean current in the sea adjacent to Korea Peninsula. III. Chemical characteristics of water masses in the polar front area of the central Korean East Sea. Journal of the Korean Fisheries Society, 24(3), 185-192.

Zeebe, R.E., and D. Wolf-Gladrow, 2001. CO_2 in seawater: Equilibrium, kinetics, isotopes. Elsevier Oceanography Series, 65, 83.

Zehr, J.P., and R.M. Kudela, 2011. Nitrogen cycle of the open ocean: From genes to ecosystems. Annual Review of Marine Science, 3, 197-225.

Vita

IL NAM KIM was born on February 2, 1976, in Busan, Korea. In March, 1995, he entered Pusan National University in Busan, Korea. He received the degree of Bachelor of Science from Pusan National University in February, 1999. In March, 1999, he entered the Graduate School for master program at Pusan National University. He received the degree of Master of Science from Pusan National University in February, 2001. In September, 2007, he entered The University of Texas at Austin as a Ph.D. student in the Marine Science Department.

Permanent email: ilnamkim@utexas.edu

This dissertation was typed by IL NAM KIM.